TUM-HEP-727/09
MPP-2009-133

Anatomy and Phenomenology of FCNC and CPV Effects in SUSY Theories

Wolfgang Altmannshofer[1], Andrzej J. Buras[1,2], Stefania Gori[1,3], Paride Paradisi[1] and David M. Straub[1]

[1] *Physik-Department, Technische Universität München, D-85748 Garching, Germany*

[2] *TUM Institute for Advanced Study, Technische Universität München, D-80333 München, Germany*

[3] *Max-Planck-Institut für Physik (Werner-Heisenberg-Institut), D-80805 München, Germany*

Abstract

We perform an extensive study of FCNC and CP Violation within Supersymmetric (SUSY) theories with particular emphasis put on processes governed by $b \to s$ transitions and of their correlations with processes governed by $b \to d$ transitions, $s \to d$ transitions, $D^0 - \bar{D}^0$ oscillations, lepton flavour violating decays, electric dipole moments and $(g-2)_\mu$. We first perform a comprehensive model-independent analysis of $\Delta F = 2$ observables and we emphasize the usefulness of the $R_b - \gamma$ plane in exhibiting transparently various tensions in the present UT analyses. Secondly, we consider a number of SUSY models: the general MSSM, a flavour blind MSSM, the MSSM with Minimal Flavour Violation as well as SUSY flavour models based on abelian and non-abelian flavour symmetries that show representative flavour structures in the soft SUSY breaking terms. We show how the characteristic patterns of correlations among the considered flavour observables allow to distinguish between these different SUSY scenarios. Of particular importance are the correlations between the CP asymmetry $S_{\psi\phi}$ and $B_s \to \mu^+\mu^-$, between the anomalies in $S_{\phi K_S}$ and $S_{\psi\phi}$, between $S_{\phi K_S}$ and d_e, between $S_{\psi\phi}$ and $(g-2)_\mu$ and also those involving lepton flavour violating decays. In our analysis, the presence of right-handed currents and of the double Higgs penguin contributions to B_s mixing plays a very important role. We propose a "DNA-Flavour Test" of NP models including Supersymmetry, the Littlest Higgs model with T-parity and the Randall-Sundrum model with custodial protection, with the aim of showing a tool to distinguish between these NP scenarios, once additional data on flavour changing processes become available. As a byproduct, we present the SM prediction for $\mathrm{BR}(B^+ \to \tau^+\nu) = (0.80 \pm 0.12) \times 10^{-4}$ that follows solely from an analytical formula for this branching ratio in terms of $\Delta M_{s,d}$ and $S_{\psi K_S}$ asymmetry and which does not involve V_{ub} and F_B uncertainties.

Contents

1 Introduction and Motivation

The Standard Model (SM) of elementary particles has been very successfully tested at the loop level both in flavour-conserving electroweak (EW) physics at the LEP and the SLC and also in low-energy flavour physics.

On the other hand, it is a common belief that the SM has to be regarded as an effective field theory, valid up to some still undetermined cut-off scale Λ above the EW scale. Theoretical arguments based on a natural solution of the hierarchy problem suggest that Λ should not exceed a few TeV.

Besides the direct search for New Physics (NP) at the TeV scale (the so-called *high-energy frontier*) that will be performed at the upcoming LHC, a complementary and equally important tool to shed light on NP is provided by high-precision low-energy experiments (the so-called *high-intensity frontier*). In particular, the latter allows to indirectly probe very short distances even beyond those accessible by direct detection.

In the last years, the two B factories have established that the measured B_d flavour- and CP-violating processes are well described by the SM theory up to an accuracy of the $(10-20)\%$ level [1, 2]. Unfortunately, irreducible hadronic uncertainties and the overall good agreement of flavour data with the SM predictions still prevent any conclusive evidence for NP effects in the quark sector.

This immediately implies a tension between the solution of the hierarchy problem that requires NP at the TeV scale and the explanation of the Flavour Physics data in which this NP did not show up convincingly. An elegant way to avoid this tension is provided by the Minimal Flavour Violation (MFV) hypothesis [3, 4, 5, 6, 7], where flavour violation, even beyond the SM, is still entirely described by the CKM matrix. As a result, it turns out that a low energy NP scale at the level of few TeV is still fully compatible with the flavour data within this minimalistic scenario [8, 9].

In this context, the question we intend to address in this work is whether it is still possible (and to which extent) to expect NP phenomena to appear in the B_s system where the SM has not been experimentally tested at the same accuracy level as in the B_d system. In particular, it is well known that $b \to s$ transitions represent a special ground where to perform efficient tests of NP scenarios [10, 11, 12, 13, 14, 15, 16, 17, 18]. Indeed, CP violation in $b \to s$ transitions is predicted to be very small in the SM, thus, any experimental evidence for sizable CP violating effects in the B_s system would unambiguously point towards a NP evidence. Recent messages from the CDF and D0 experiments [19, 20] seem to indicate that this indeed could be the case [21, 22].

On the theoretical side, there exist many well motivated NP scenarios predicting large effects especially in $b \to s$ transitions. Among them are supersymmetric (SUSY) flavour models based on abelian [23, 24, 25, 26, 27, 28, 29, 30, 31, 32, 33, 34, 35, 36, 37] and non-abelian [38, 39, 40, 41, 42, 43, 44, 45, 46, 47, 48, 49, 50, 51, 52] flavour symmetries naturally leading to large NP contributions in $b \to s$ processes while maintaining, at the same time, the NP contributions occurring in $s \to d$ and (sometimes) $b \to d$ transitions, under control. Moreover, also Grand Unified Theories (GUTs) represent a suitable ground where large NP effects in $b \to s$ transitions can be generated [10, 11, 53, 54, 55, 56, 57]. In fact, GUTs link leptonic and hadronic sources of flavour and CP violation and the observed large atmospheric neutrino mixing is transmitted to a large flavour violation in $b \leftrightarrow s$ transitions [10, 11].

In the present work, we focus on the NP predictions for the CP violating and CP conserving $b \to s$ transitions within SUSY models and their correlations with other observables, measured

in coming years in dedicated flavour precision experiments in K, B, D and charged lepton decays. In particular, when we deal with specific models, the source of the flavour and CP violation for $b \to s$ transitions will simultaneously generate not only $\Delta B = 2$ and $\Delta B = 1$ processes that will turn out to be correlated, but will also have impact on observables outside the B meson system. The major aim of the present work is twofold:

i) to quantify the NP room left for $b \to s$ transitions compatible with all the available experimental data on $\Delta F = 2$ and $\Delta F = 1$ processes,

ii) to outline strategies to disentangle different NP scenarios by means of a correlated analysis of low energy observables, including also K and D systems as well as lepton flavour violation, electric dipole moments (EDMs) and the anomalous magnetic moment of the muon ($(g-2)_\mu$).

Since many analyses along this subject appeared in the literature [2, 12, 13, 58, 59, 60, 56, 61], we want to emphasize here the novelties of our study. In particular,

- We consider a very complete set of $\Delta F = 2$, $\Delta F = 1$ and $\Delta F = 0$ processes, i.e. the EDMs and the $(g-2)_\mu$. To best of our knowledge, the current analysis represents the most complete analysis present in the literature in this subject as for i) the number of processes considered and ii) the inclusion of all relevant SUSY contributions. We believe that the steps i) and ii) are extremely important in order to try to understand the pattern of deviations from the SM predictions that we could obtain by means of future experimental measurements.

- We perform an updated analysis of the bounds on the flavour violating terms in the SUSY soft sector, the so-called Mass Insertions (MIs), in the general MSSM, in the light of all the available experimental data in flavour physics.

- In addition to the general MSSM, we study several well motivated and predictive SUSY frameworks, such as the MSSM with MFV, a flavour blind MSSM (FBMSSM) and in particular SUSY flavour models based on abelian and non-abelian flavour symmetries and compare their predictions with those found in the Littlest Higgs Model with T-parity (LHT) and a Randall-Sundrum (RS) model with custodial protection.

- We outline a comprehensive set of strategies to disentangle among different NP scenarios by means of their predicted patterns of deviations from the SM expectations in many low energy processes. At the same time, we exploit the synergy and interplay of low energy flavour data with the high energy data, obtainable at the LHC, to unveil the kind of NP model that will emerge, if any.

Our paper is organized as follows. In sec. 2, we present a model independent analysis of B_d, K^0 and B_s mixing observables, analyzing in particular the existing tensions between the data and the SM in the $R_b - \gamma$ plane. We also investigate what room for NP is still present in the B_d and B_s systems.

In sec. 3, we list the formulae for $\Delta F = 0, 1, 2$ processes in a general MSSM that are most relevant for our purposes.

In sec. 4, we briefly review basic features of SUSY models with abelian and non-abelian flavour symmetries as well as models respecting the MFV principle. We also address the

question of the stability of the squark mass matrix textures, predicted by the flavour models, under RGE effects from the GUT scale to the EW scale.

As our paper involves many observables calculated in several supersymmetric models, we outline in sec. 5 our strategy for the numerical analysis that consists of five steps. The first step is a model independent analysis within the general MSSM framework resulting in the allowed ranges of the MIs. The next two steps deal with three specific supersymmetric flavour models in which right-handed currents play an important role: the abelian model by Agashe and Carone (AC) [36] based on a $U(1)$ flavour symmetry and the non-abelian models by Ross, Velasco-Sevilla and Vives (RVV) [51] (or, more precisely, a specific example of the RVV model, i.e. the RVV2 model [62]) and by Antusch, King and Malinsky (AKM) [52] based on the flavour symmetry $SU(3)$. These three models are then compared in the last two steps with a flavour model with left-handed (CKM-like) currents only [42, 63], with a flavour blind MSSM (FBMSSM) [64, 65, 66, 67, 68] and with the MFV MSSM with additional CP phases [69, 70, 71]. The numerical results of our strategy are presented systematically in sec. 6. The correlations between different observables, offering very powerful means to distinguish between various models, play an important role in this presentation.

In sec. 7, we review very briefly the patterns of flavour violation in the Littlest Higgs Model with T-Parity (LHT) [72, 17, 73, 74, 75, 76, 77] and a Randall-Sundrum (RS) model with custodial protection [15, 16] and compare them with the ones identified in supersymmetric models in sec. 6. The main result of this section is a table summarizing and comparing the sensitivity of various observables to NP effects present in each model. This table can be considered as a "DNA-Flavour Test" of the considered extensions of the SM.

In sec. 8, we exploit the complementarity and the synergy between flavour and LHC data in shedding light on the NP scenario that is at work.

Finally, in sec. 9, the main results of our paper are summarized and an outlook for coming years is given. A compendium of one loop functions can be found in appendix A and in appendix B some details on the convention of the MSSM parameters used throughout our paper are shown.

2 Model-independent Analysis of $\Delta F = 2$ Observables

2.1 The B_d System

The present unitarity triangle (UT) analyses are dominated by $\Delta F = 2$ processes. We begin by reviewing the status of the UT trying to outline transparently possible hints of NP and related tests to falsify or to confirm them.

We consider the following two sets of fundamental parameters related to the CKM matrix and to the unitarity triangle:

$$|V_{us}| \equiv \lambda\,, \quad |V_{cb}|\,, \quad R_b\,, \quad \gamma\,, \tag{2.1}$$

$$|V_{us}| \equiv \lambda\,, \quad |V_{cb}|\,, \quad R_t\,, \quad \beta\,. \tag{2.2}$$

Here,

$$R_b \equiv \frac{|V_{ud}V_{ub}^*|}{|V_{cd}V_{cb}^*|} = \sqrt{\bar\varrho^2+\bar\eta^2} = \left(1-\frac{\lambda^2}{2}\right)\frac{1}{\lambda}\left|\frac{V_{ub}}{V_{cb}}\right|\,, \tag{2.3}$$

$$R_t \equiv \frac{|V_{td}V_{tb}^*|}{|V_{cd}V_{cb}^*|} = \sqrt{(1-\bar\varrho)^2+\bar\eta^2} = \frac{1}{\lambda}\left|\frac{V_{td}}{V_{cb}}\right|\,, \tag{2.4}$$

are the length of the sides of the UT opposite to the angles β and γ, respectively. The latter are defined as follows

$$V_{td} = |V_{td}|e^{-i\beta} \ , \quad V_{ub} = |V_{ub}|e^{-i\gamma} \ , \tag{2.5}$$

and one has

$$\sin 2\beta = \frac{2\bar\eta(1-\bar\varrho)}{\bar\eta^2 + (1-\bar\varrho)^2} \ , \qquad \tan\gamma = \frac{\bar\eta}{\bar\varrho} \ . \tag{2.6}$$

The parameter set in (2.1) can be obtained entirely from tree level decays, hence, it should be unaffected by any significant NP pollution (see however [78]). The corresponding UT is known as the reference unitarity triangle (RUT) [79]. In contrast, R_t and β in the parameter set in (2.2) can only be extracted from loop-induced FCNC processes and hence are potentially sensitive to NP effects. Consequently, the corresponding UT, the universal unitarity triangle (UUT) [3] of models with constrained minimal flavour violation (CMFV) [4, 80], could differ from the RUT signaling NP effects beyond not only the SM but also beyond CMFV models. Thus a comparative UT analysis performed by means of these two independent sets of parameters may represent a powerful tool to unveil NP effects. The dictionary between these two sets of variables is given by

$$R_b = \sqrt{1 + R_t^2 - 2R_t\cos\beta} \ , \qquad \cot\gamma = \frac{1 - R_t\cos\beta}{R_t\sin\beta} \ , \tag{2.7}$$

$$R_t = \sqrt{1 + R_b^2 - 2R_b\cos\gamma} \ , \qquad \cot\beta = \frac{1 - R_b\cos\gamma}{R_b\sin\gamma} \ . \tag{2.8}$$

Assuming no NP, the parameters R_t and β can be related directly to observables

$$R_t = \xi\frac{1}{\lambda}\sqrt{\frac{m_{B_s}}{m_{B_d}}}\sqrt{\frac{\Delta M_d}{\Delta M_s}} \ , \qquad \sin 2\beta = S_{\psi K_S} \ , \tag{2.9}$$

where ΔM_d and ΔM_s are the mass differences in the neutral B_d and B_s systems, $S_{\psi K_S}$ represents the mixing-induced CP asymmetry in the decay $B_d \to \psi K_S$ and the value of the non-perturbative parameter ξ is given in tab. 3. In the presence of NP however, these relations are modified and one finds

$$R_t = \xi\frac{1}{\lambda}\sqrt{\frac{m_{B_s}}{m_{B_d}}}\sqrt{\frac{\Delta M_d}{\Delta M_s}}\sqrt{\frac{C_{B_s}}{C_{B_d}}} \ , \qquad \sin(2\beta + 2\phi_{B_d}) = S_{\psi K_S} \ , \tag{2.10}$$

where $\Delta M_q = \Delta M_q^{\rm SM} C_{B_q}$ and ϕ_{B_d} is a NP phase in B_d mixing defined analogously to (2.18) below.

The experimentally measured values of ΔM_d and $S_{\psi K_S}$ can be found in tab. 1 along with their SM predictions. While in ΔM_d, there is still room for a NP contribution at the 25% level, scenarios with large new CP violating phases are strongly constrained by the bound on $S_{\psi K_S}$. This is also illustrated by fig. 1, showing the experimental constraints in the complex M_{12}^d and the $S_{\psi K_S}$-$\Delta M_d/\Delta M_d^{\rm SM}$ plane, respectively.

2.2 The K System

In the K system the central role at present is played by ϵ_K, that represents another crucial ingredient of any UT analysis.

observable	experiment	SM prediction	exp./SM
ΔM_K	$(5.292 \pm 0.009) \times 10^{-3}\ \mathrm{ps}^{-1}$ [81]		
$\|\epsilon_K\|$	$(2.229 \pm 0.010) \times 10^{-3}$ [81]	$(1.91 \pm 0.30) \times 10^{-3}$	1.17 ± 0.18
ΔM_d	$(0.507 \pm 0.005)\ \mathrm{ps}^{-1}$ [1]	$(0.51 \pm 0.13)\ \mathrm{ps}^{-1}$	0.99 ± 0.25
$S_{\psi K_S}$	0.672 ± 0.023 [1]	0.734 ± 0.038	0.92 ± 0.06
ΔM_s	$(17.77 \pm 0.12)\ \mathrm{ps}^{-1}$ [82]	$(18.3 \pm 5.1)\ \mathrm{ps}^{-1}$	0.97 ± 0.27
$\Delta M_d/\Delta M_s$	$(2.85 \pm 0.03) \times 10^{-2}$	$(2.85 \pm 0.38) \times 10^{-2}$	1.00 ± 0.13

Table 1: Experimental values and SM predictions for $\Delta F = 2$ observables. The SM predictions are obtained using CKM parameters from the NP UTfit [83]. The last column shows the ratio of the measured value and the SM prediction, signaling the room left for NP effects in the corresponding observable. We do not give a SM prediction for ΔM_K because of unknown long distance contributions.

The CP-violating parameter ϵ_K can be written in the SM as follows

$$|\epsilon_K|^{\mathrm{SM}} = \kappa_\epsilon C_\epsilon \hat{B}_K |V_{cb}|^2 |V_{us}|^2 \left(\frac{1}{2}|V_{cb}|^2 R_t^2 \sin 2\beta \eta_{tt} S_0(x_t) + R_t \sin\beta (\eta_{ct} S_0(x_c, x_t) - \eta_{cc} x_c)\right) , \tag{2.11}$$

where C_ϵ is a numerical constant

$$C_\epsilon = \frac{G_F^2 M_W^2 F_K^2 m_{K^0}}{6\sqrt{2}\pi^2 \Delta M_K} \simeq 3.655 \times 10^4 \tag{2.12}$$

and the SM loop function S_0 depends on $x_i = m_i^2(m_i)/M_W^2$ (where $m_i(m_i)$ is the quark mass m_i computed at the scale m_i in the $\overline{\mathrm{MS}}$ scheme) and can be found in appendix A. The factors η_{tt}, η_{ct} and η_{cc} are QCD corrections known at the NLO level [84, 85, 86, 87], $\hat{B}_K$ is a non-perturbative parameter and κ_ϵ is explained below.

While ϵ_K has been dormant for some time due to a large error in the relevant nonperturbative parameter $\hat{B}_K$ and CKM parameter uncertainties, the improved value of $\hat{B}_K$, the improved determinations of the elements of the CKM matrix and in particular the inclusion of additional corrections to ϵ_K [88] that were neglected in the past enhanced the role of this CP-violating parameter in the search for NP.

Indeed it has been recently stressed [88] that the SM prediction of ϵ_K implied by the measured value of $\sin 2\beta$ may be too small to agree with experiment. The main reasons for this are on the one hand a decreased value of $\hat{B}_K = 0.724 \pm 0.008 \pm 0.028$ [89] (see also [90]), lower by 5–10% with respect to the values used in existing UT fits [83, 91], and on the other hand the decreased value of ϵ_K in the SM arising from a multiplicative factor, estimated as $\kappa_\epsilon = 0.92 \pm 0.02$ [88, 92].

Given that $\epsilon_K \propto \hat{B}_K \kappa_\epsilon$, the total suppression of ϵ_K compared to the commonly used formulae is typically of order 15%. Using directly (2.9) together with (2.11), one finds then [92][1]

$$|\epsilon_K|^{\mathrm{SM}} = (1.78 \pm 0.25) \times 10^{-3} , \tag{2.13}$$

to be compared with the experimental measurement [81]

$$|\epsilon_K|^{\mathrm{exp}} = (2.229 \pm 0.010) \times 10^{-3} . \tag{2.14}$$

[1]Using instead the values of $\bar{\varrho}$ and $\bar{\eta}$ from tab. 3 one finds the SM prediction in tab. 1.

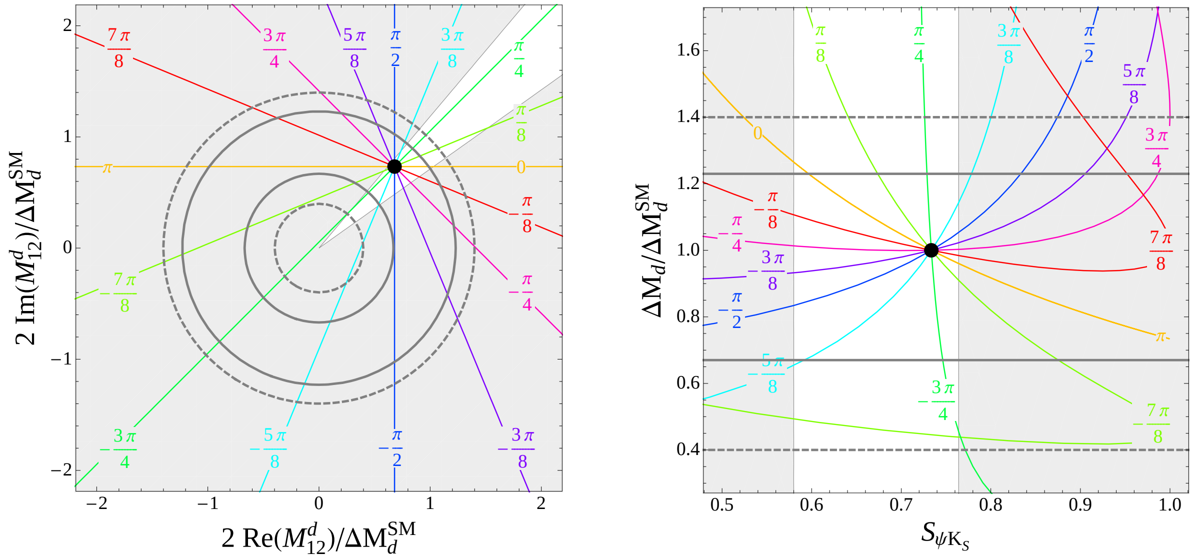

Figure 1: Left: The complex M_{12}^d plane. The thick solid circles show the constraint on the B_d mixing amplitude from the measurement of $\Delta M_d/\Delta M_s$ assuming no NP in ΔM_s, while the thick dashed circles correspond to the constraint coming from ΔM_d alone. The thin lines correspond to NP contributions to M_{12}^d with the indicated fixed phases θ_d, defined analogously to (2.18). The white region corresponds to the allowed region of $S_{\psi K_S}$ (see tab. 1) and the SM value corresponds to the black point. Right: Same as in the left panel, but now in the $S_{\psi K_S}$-$\Delta M_d/\Delta M_d^{SM}$ plane.

The 15% error in (2.13) arises from the three main sources of uncertainty that are still $\hat{B}_K$, $|V_{cb}|^4$ and R_t^2.

On general grounds, the agreement between (2.13) and (2.14) improves for higher values of $\hat{B}_K$, R_t or $|V_{cb}|$ and also the correlation between ϵ_K and $\sin 2\beta$ within the SM is highly sensitive to these parameters. Consequently improved determinations of all these parameters is very desirable in order to find out whether NP is at work in $S_{\psi K_S}$ or in ϵ_K or both. Some ideas can be found in [93, 88, 92, 94]. We will now have a closer look at possible tensions in the UT analysis in a somewhat different manner than done in the existing literature.

2.3 A New Look at Various Tensions: R_b-γ Plane

While the above tension can be fully analyzed by means of the standard UT analysis, we find it more transparent to use the $R_b - \gamma$ plane [95, 96] for this purpose. In fig. 2, in the upper left plot the *blue* (*green*) region corresponds to the 1σ allowed range for $\sin 2\beta$ (R_t) as calculated by means of (2.9). The *red* region corresponds to $|\epsilon_K|^{\rm SM}$ as given in (2.11). Finally the solid black line corresponds to $\alpha = 90^\circ$ that is close to the one favoured by UT fits and the determination from $B \to \rho\rho$ [97].

The numerical input parameter that we use to obtain this plot are collected in tabs. 1 and 3. It is evident that there is a tension between various regions as there are three different values of (R_b, γ), dependently which two constraints are simultaneously applied.

Possible solutions to this tension can be achieved by assuming NP contributions just in one of the three observables ϵ_K, $\sin 2\beta$, R_t:

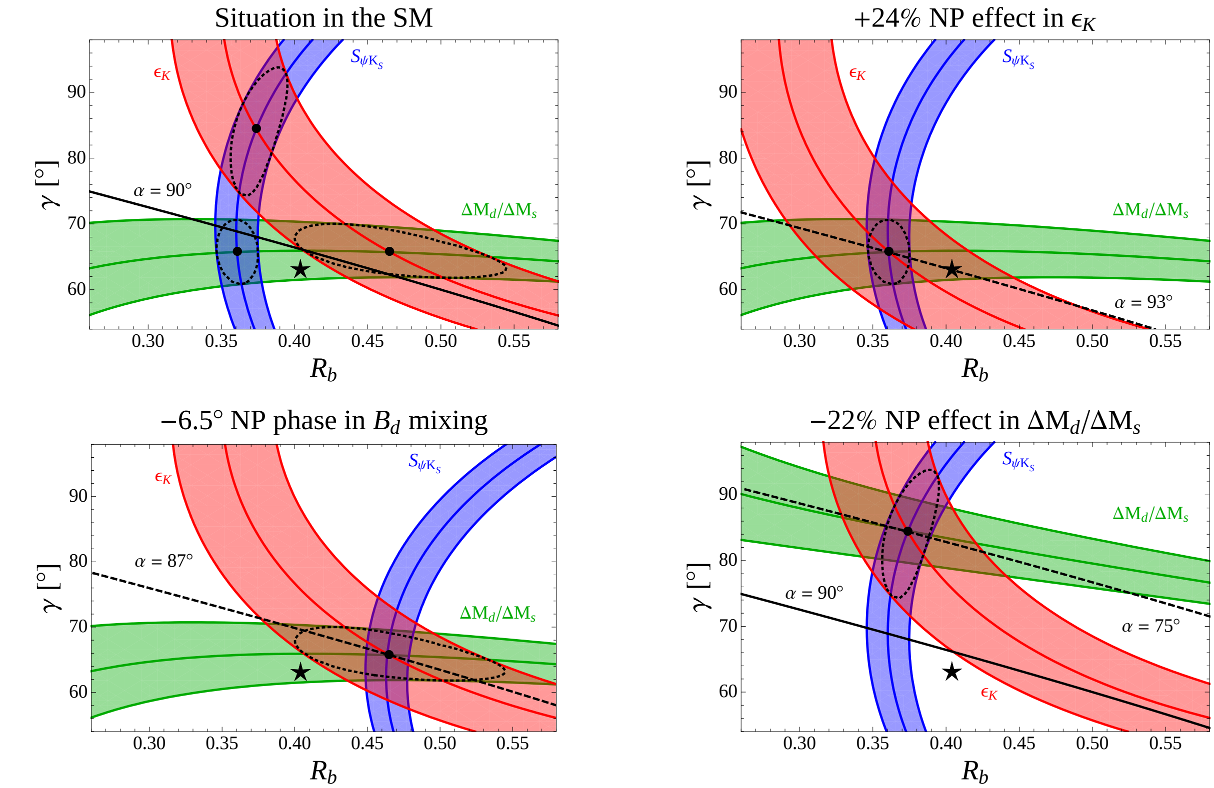

Figure 2: The $R_b - \gamma$ plane assuming: **i)** $\sin 2\beta$, R_t and ϵ_K not affected by NP effects (upper left), **ii)** $\sin 2\beta$ and R_t NP free while ϵ_K affected by a positive NP effect at the level of $+24\%$ compared to the SM contribution (upper right), **iii)** ϵ_K and R_t NP free while $\sin 2\beta$ affected by a NP phase in B_d mixing of $-6.5°$ (lower left), **iv)** ϵ_K and $\sin 2\beta$ NP free while $\Delta M_d/\Delta M_s$ affected by a negative NP effect at the level of -22% compared to the SM contribution (lower right). The black star indicates the values for R_b and γ obtained in the NP UT fit of [83].

1) a positive NP effect in ϵ_K (at the level of $+24\%$ compared to its SM value) while taking $\sin 2\beta$ and $\Delta M_d/\Delta M_s$ SM-like [88], as shown by the upper right plot of fig. 2. The required effect in ϵ_K could be for instance achieved within models with CMFV by a positive shift in the function $S_0(x_t)$ [92] which, while not modifying $(\sin 2\beta)_{\psi K_S}$ and $\Delta M_d/\Delta M_s$, would require the preferred values of $\sqrt{B_{d,s}}F_{B_{d,s}}$ to be by $\simeq 10\%$ lower than the present central values in order to fit ΔM_d and ΔM_s separately. Alternatively, new non-minimal sources of flavour violation relevant only for the K system could solve the problem.

2) ϵ_K and $\Delta M_d/\Delta M_s$ NP free while $S_{\psi K_S}$ affected by a NP phase in B_d mixing of $-6.5°$ as indicated in (2.10) and shown by the lower left plot of fig. 2. The predicted value for $\sin 2\beta$ is now $\sin 2\beta = 0.823^{+0.088}_{-0.090}$ [2]. This value is significantly larger than the measured $S_{\psi K_S}$ which allows to fit the experimental value of ϵ_K.

3) ϵ_K and $S_{\psi K_S}$ NP free while the determination of R_t through $\Delta M_d/\Delta M_s$ affected by NP as indicated in (2.10) and shown by the lower right plot of fig. 2. In that scenario one finds a very high value for $|V_{td}| \simeq 9.6 \times 10^{-3}$ that corresponds to $\Delta M_d^{\rm SM}/\Delta M_s^{\rm SM} =$

[2] The value we give here is slightly smaller than the one found in [93, 88, 94] performing comprehensive fits of the UT.

	$\bar{\rho}$	$\bar{\eta}$	$\alpha[^\circ]$	$\gamma[^\circ]$	R_b	$\lvert V_{ub}\rvert \times 10^3$
1)	$0.148^{+0.029}_{-0.029}$	$0.329^{+0.018}_{-0.017}$	$93.2^{+5.0}_{-5.0}$	$65.7^{+4.9}_{-4.9}$	$0.361^{+0.014}_{-0.014}$	$3.44^{+0.17}_{-0.16}$
2)	$0.191^{+0.059}_{-0.049}$	$0.424^{+0.063}_{-0.055}$	$86.6^{+4.2}_{-3.8}$	$65.7^{+4.3}_{-3.9}$	$0.465^{+0.080}_{-0.065}$	$4.44^{+0.77}_{-0.64}$
3)	$0.036^{+0.064}_{-0.062}$	$0.372^{+0.023}_{-0.019}$	$74.5^{+10.0}_{-9.0}$	$84.4^{+9.4}_{-10.2}$	$0.374^{+0.021}_{-0.018}$	$3.57^{+0.23}_{-0.19}$
UTfit	0.177 ± 0.044	0.360 ± 0.031	92 ± 7	63 ± 7	0.404 ± 0.025	3.87 ± 0.23

Table 2: Predictions of several CKM parameters in the three scenarios as discussed in the text. For comparison, in the last line results are also shown from a global NP fit of the UT [83].

$(3.66^{+0.52}_{-0.53}) \times 10^{-2}$, much higher than the actual measurement. In order to agree exactly with the experimental central value, one needs a NP contribution to $\Delta M_d/\Delta M_s$ at the level of -22%. Non-universal contributions suppressing ΔM_d ($C_{B_d} < 1$) and/or enhancing ΔM_s ($C_{B_s} > 1$) could be responsible for this shift as is evident from (2.10). The increased value of R_t that compensates the negative effect of NP in $\Delta M_d/\Delta M_s$ allows to fit the experimental value of ϵ_K.

Possibility 3) has not been discussed in [93, 88, 94]. Interestingly, there are concrete and well motivated SUSY extensions of the SM compatible with scenario 3) as, for instance, abelian flavour models (see the following sections) or SUSY GUTs with right-handed neutrinos. In such cases, if the $b \to s$ transition contains, in addition to a large mixing angle, also a natural $\mathcal{O}(1)$ CPV phase, then solution 3) also implies a non standard value for $S_{\psi\phi}$.

From fig. 2 it is clear that each of the solutions corresponds to particular values of R_b and γ. In tab. 2 we show the values of the relevant CKM parameters corresponding to each case, where the values of the two variables characteristic for a given scenario are assumed not to be affected by NP. We observe

- **Solution 1)** corresponds to $\gamma \simeq 66^\circ$, $R_b \simeq 0.36$ and $\alpha \simeq 93^\circ$ in accordance with the usual UT analysis.

- **Solution 2)** is characterized by a large value of $R_b \simeq 0.47$, that is significantly larger than its exclusive determinations but still compatible with the inclusive determinations. The angles $\gamma \simeq 66^\circ$ and $\alpha \simeq 87^\circ$ agree with the usual UT analysis.

- **Solution 3)** finally is characterized by a large value of $\gamma \simeq 84^\circ$ and α much below 90°. The latter fact could be problematic for this solution given the improving determinations of α.

As seen in tab. 2, these three NP scenarios characterized by black points in fig. 2 will be clearly distinguished from each other once the values of γ and R_b from tree level decays will be precisely known. Moreover, if the future measurements of (R_b, γ) will select a point in the $R_b - \gamma$ plane that differs from the black points in fig. 2, it is likely that NP will simultaneously enter ϵ_K, $S_{\psi K_S}$ and $\Delta M_d/\Delta M_s$.

We also note that the easiest way to solve the tensions in question is to require a particular sign in the NP contribution to a given observable: positive shift in $|\epsilon_K|$, $\phi_{B_d} \leq 0$ and negative shift in $\Delta M_d/\Delta M_s$, with the latter implying increased values of R_t and γ.

On the other hand, a negative NP contribution to ϵ_K would make the tensions in the $R_b - \gamma$ plane more pronounced, requiring stronger shifts in ϕ_{B_d} and R_t than in the examples

parameter	value	parameter	value
$\hat{B}_K$	$0.724 \pm 0.008 \pm 0.028$ [89]	$m_t(m_t)$	(163.5 ± 1.7) GeV [98, 99]
F_{Bs}	(245 ± 25) MeV [100]	$m_c(m_c)$	(1.279 ± 0.013) GeV [101]
F_B	(200 ± 20) MeV [100]	η_{cc}	1.44 ± 0.35 [85, 102]
F_K	(156.1 ± 0.8) MeV [103]	η_{tt}	0.57 ± 0.01 [84]
$\hat{B}_{B_d}$	1.22 ± 0.12 [100]	η_{ct}	0.47 ± 0.05 [86, 87, 102]
$\hat{B}_{B_s}$	1.22 ± 0.12 [100]	η_B	0.55 ± 0.01 [84, 104]
$F_{Bs}\sqrt{\hat{B}_{Bs}}$	(270 ± 30) MeV [100]	λ	0.2258 ± 0.0014 [8]
$F_B\sqrt{\hat{B}_{Bd}}$	(225 ± 25) MeV [100]	A	0.808 ± 0.014 [8]
ξ	1.21 ± 0.04 [100]	$\bar{\varrho}$	0.177 ± 0.044 [8]
V_{cb}	$(41.2 \pm 1.1) \times 10^{-3}$ [81]	$\bar{\eta}$	0.360 ± 0.031 [8]

Table 3: Input parameters used in the numerical analysis.

given above. This specific pattern of the tension in the first plot in fig. 2 points towards certain NP scenarios and rules out specific regions of their parameter space.

2.4 The B_s System

Since the B_s system is central for our investigations, let us recall some known formulae. First the time-dependent mixing induced CP asymmetry

$$A^s_{\rm CP}(\psi\phi, t) \equiv \frac{\Gamma(\bar{B}_s(t) \to \psi\phi) - \Gamma(B_s(t) \to \psi\phi)}{\Gamma(\bar{B}_s(t) \to \psi\phi) + \Gamma(B_s(t) \to \psi\phi)} \simeq S_{\psi\phi} \sin(\Delta M_s t) \ , \tag{2.15}$$

where the CP violation in the decay amplitude is set to zero. Next, the semileptonic asymmetry is given by

$$A^s_{\rm SL} \equiv \frac{\Gamma(\bar{B}_s \to l^+ X) - \Gamma(B_s \to l^- X)}{\Gamma(\bar{B}_s \to l^+ X) + \Gamma(B_s \to l^- X)} = {\rm Im}\left(\frac{\Gamma^s_{12}}{M^s_{12}}\right) \ , \tag{2.16}$$

where Γ^s_{12} represents the absorptive part of the B_s mixing amplitude. The theoretical prediction in the SM for the semileptonic asymmetry $A^s_{\rm SL}$ improved thanks to improvements in lattice studies of $\Delta B = 2$ four-fermion operators [105] and to the NLO perturbative calculations of the corresponding Wilson coefficients [106, 107].

Both asymmetries are very small in the SM where they turn out to be proportional to $\sin 2|\beta_s|$ with $\beta_s \simeq -1^\circ$. The latter phase enters the CKM matrix element V_{ts}

$$V_{ts} = -|V_{ts}| e^{-i\beta_s} \ . \tag{2.17}$$

As a consequence, both $A^s_{\rm SL}$ and $S_{\psi\phi}$ represent very promising grounds where to look for NP effects.

In order to study NP effects in $A^s_{\rm SL}$ and $S_{\psi\phi}$, let us recall possible parameterizations of the NP contributions entering the $\Delta F = 2$ mixing amplitudes [83, 108]

$$\begin{aligned} M^s_{12} &= \langle B_s | H^s_{\rm eff} | \bar{B}_s \rangle = (M^s_{12})^{\rm SM} + (M^s_{12})^{\rm NP} = |(M^s_{12})^{\rm SM}| e^{2i\beta_s} + |(M^s_{12})^{\rm NP}| e^{i\theta_s} \\ &\equiv C_{B_s} e^{2i\phi_{B_s}} (M^s_{12})^{\rm SM} \ . \end{aligned} \tag{2.18}$$

For the mass difference in the B_s meson system, one then has

$$\Delta M_s = 2|M_{12}^s| = C_{B_s} \Delta M_s^{\rm SM} \ . \tag{2.19}$$

In the case of the time-dependent CP asymmetry one finds [80]

$$S_{\psi\phi} = -\sin\left[\mathrm{Arg}(M_{12}^s)\right] = \sin(2|\beta_s| - 2\phi_{B_s}) \ , \tag{2.20}$$

where we took the CP parity of the $\psi\phi$ final state equal to $+1$.

Concerning $A_{\rm SL}^s$, we recall that, in the presence of NP, $A_{\rm SL}^s$ is correlated with $S_{\psi\phi}$ according to the following expression [108],

$$A_{\rm SL}^s = -\left|\mathrm{Re}\left(\frac{\Gamma_{12}^s}{M_{12}^s}\right)^{\rm SM}\right| \frac{1}{C_{B_s}} S_{\psi\phi} \ , \tag{2.21}$$

where we have neglected small contributions proportional to $\mathrm{Im}(\Gamma_{12}^s/M_{12}^s)^{\rm SM}$ and used [106]

$$|\mathrm{Re}(\Gamma_{12}^s/M_{12}^s)^{\rm SM}| = (2.6 \pm 1.0) \times 10^{-3} \, . \tag{2.22}$$

Note that even a rather small value of $S_{\psi\phi} \simeq 0.1$ would lead to an order of magnitude enhancement of $A_{\rm SL}^s$ relative to its SM expectation, since $A_{\rm SL}^s$ within the SM is predicted to be of order 10^{-5} [17, 22].

An alternative formula for the $A_{\rm SL}^s - S_{\psi\phi}$ model-independent correlation, pointed out recently in [109], uses only measurable quantities

$$A_{\rm SL}^s = -\frac{\Delta\Gamma_s}{\Delta M_s} \frac{S_{\psi\phi}}{\sqrt{1 - S_{\psi\phi}^2}} \ , \tag{2.23}$$

and can be used once the data on $\Delta\Gamma_s$ improves. In writing (2.23), we have assumed that $\Delta\Gamma_s > 0$, as obtained in the SM using lattice methods.

Concerning the experimental situation, HFAG gives the following value for the semileptonic asymmetry [1],

$$(A_{\rm SL}^s)_{\rm exp} = (-3.7 \pm 9.4) \times 10^{-3} \ . \tag{2.24}$$

In the case of $S_{\psi\phi}$, there have been several analyses of the data from CDF [19, 110] and D0 [20] on the $B_s \to \psi\phi$ decay. Taking into account additional constraints coming e.g. from the flavour-specific B_s lifetime and the semileptonic asymmetry, tensions with the tiny SM prediction $S_{\psi\phi}^{\rm SM} = \sin 2|\beta_s| \simeq 0.036$ at the level of $(2-3)\sigma$ are found [21, 111, 112, 1]. In the following we will use the results given by HFAG [1]. For the B_s mixing phase, they quote

$$|\beta_s| - \phi_{B_s} = 0.47^{+0.13}_{-0.21} \vee 1.09^{+0.21}_{-0.13} \ , \tag{2.25}$$

and give the following range at the 90% C.L.

$$|\beta_s| - \phi_{B_s} \in [0.10, 0.68] \cup [0.89, 1.47] \ . \tag{2.26}$$

This corresponds to

$$S_{\psi\phi} = 0.81^{+0.12}_{-0.32} \quad \text{and} \quad S_{\psi\phi} \in [0.20, 0.98] \ , \tag{2.27}$$

respectively.

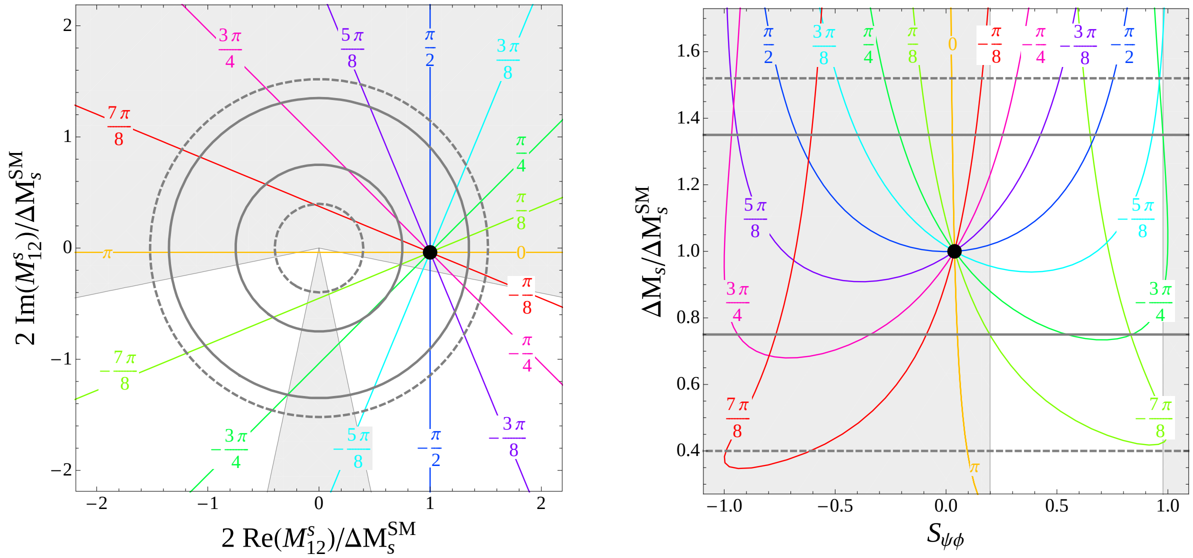

Figure 3: Left: The complex M_{12}^s plane. The thick solid circles show the constraint on the B_s mixing amplitude from the measurement of $\Delta M_d/\Delta M_s$ assuming no NP in ΔM_d, while the thick dashed circles correspond to the constraint coming from ΔM_s alone. The thin lines correspond to NP contributions to M_{12}^s with the indicated fixed phases θ_s, see (2.18). The white regions correspond to the 90% C.L. range for $S_{\psi\phi}$ in (2.27). The SM value corresponds to the black point. Right: Same as in the left panel, but now in the $S_{\psi\phi}$-$\Delta M_s/\Delta M_s^{\rm SM}$ plane.

In fig. 3, we show the experimental constraints in the complex M_{12}^s plane and the $S_{\psi\phi}$-$\Delta M_s/\Delta M_s^{\rm SM}$ plane, analogous to fig. 1 in the B_d case. Interestingly enough, they show that the scenario with maximum CP violation, in which the phase of $(M_{12}^s)_{\rm NP}$ is $-\pi/2$, is perfectly allowed and it would imply $S_{\psi\phi} \leq 0.7$ after imposing the constraint on $R_{\Delta M} = (\Delta M_d/\Delta M_s)/(\Delta M_d^{\rm SM}/\Delta M_s^{\rm SM})$ given in tab. 1. If we do not fix the phase of $(M_{12}^s)_{\rm NP}$ then all values for $S_{\psi\phi}$ in the interval $[-1, 1]$ are obviously possible, still being consistent with the constraint on $R_{\Delta M}$.

3 $\Delta F = 0, 1, 2$ Transitions in a General MSSM

In this section, we discuss NP effects arising in general SUSY scenarios both in flavour violating and flavour conserving processes. In the former case, we consider $\Delta F = 2$ and $\Delta F = 1$ transitions both in the K and in the B systems, in the latter, $\Delta F = 0$ transitions such as the electron and the neutron EDMs $d_{e,n}$ are discussed.

Concerning the $\Delta F = 2$ transitions, we present the SUSY contributions to the $B_{s,d}$ and K^0 mixing amplitudes that enter the predictions of CP conserving quantities such as the mass differences $\Delta M_{s,d}$ and ΔM_K and CP violating ones such as the time-dependent CP asymmetries $S_{\psi K_S}$, $S_{\psi\phi}$ and ϵ_K. We also investigate the constraints coming from $D^0 - \bar{D}^0$ mixing.

Regarding $\Delta F = 1$ transitions, we give expressions for the CP asymmetries in $b \to s\gamma$, $B \to \phi(\eta')K_S$, the rare decays $B_{s,d} \to \mu^+\mu^-$ and $B^+ \to \tau^+\nu$ and discuss the three T-odd CP asymmetries in $B \to K^*\mu^+\mu^-$.

In a general MSSM framework, there are various NP contributions to the FCNC processes that we consider. In particular, in the case of flavour changing processes in the down quark sector, one has contributions arising from one loop diagrams involving charged Higgs bosons and the top quark, charginos and up squarks, neutralinos and down squarks and also gluinos and down squarks.

Gluino loops typically give the dominant contributions if flavour off-diagonal entries in the soft SUSY breaking terms are present. Such off-diagonal entries can be conveniently parameterized in terms of Mass Insertions. Throughout the paper, we will adopt the following convention for the MIs

$$\mathcal{M}_D^2 = \mathrm{diag}(\tilde{m}^2) + \tilde{m}^2 \delta_d \ , \ \ \mathcal{M}_U^2 = \mathrm{diag}(\tilde{m}^2) + \tilde{m}^2 \delta_u \ , \tag{3.1}$$

where $\mathcal{M}_Q^2$ are the full 6×6 squark mass matrices in the super CKM (SCKM) basis in the convention of [113] (see also appendix B for the convention used) and $\tilde{m}^2$ is an average squark mass. The MIs are then further decomposed according to the "chirality" of the squarks

$$\delta_q = \begin{pmatrix} \delta_q^{LL} & \delta_q^{LR} \\ \delta_q^{RL} & \delta_q^{RR} \end{pmatrix} \ . \tag{3.2}$$

Our convention for the trilinear couplings A_u and A_d follows also [113] and is such that

$$\tilde{m}^2 (\delta_u^{LR})_{33} = -m_t \left(A_t + \mu^*/t_\beta\right) \ , \ \ \tilde{m}^2 (\delta_d^{LR})_{33} = -m_b \left(A_b + \mu^* t_\beta\right) \ , \tag{3.3}$$

with $m_t A_t = \frac{v_2}{\sqrt{2}} \left(A_u\right)_{33}$ and $m_b A_b = \frac{v_1}{\sqrt{2}} \left(A_d\right)_{33}$.

In the remainder of this section, we will report expressions in the Mass Insertion Approximation (MIA) for the SUSY contributions entering in the processes we consider, since they are more suitable to understand the physical results [3].

In our numerical analysis instead, we work with mass eigenstates and we do not make use of the MIA as the latter cannot be applied when the flavour violating mixing angles are $\mathcal{O}(1)$, as it is predicted by many flavour models.

3.1 $\Delta F = 2$ Processes

We begin our presentation with $\Delta F = 2$ transitions induced in the MSSM. To this end, let us briefly recall, as already stated for the B_s system in (2.18), that the meson-antimeson oscillations are described by the mixing amplitudes $M_{12}^{(M)} \equiv \langle M | \mathcal{H}_{\rm eff}^{\Delta F=2} | \overline{M} \rangle$, with $M = K^0$, $B_{d,s}$. Within the MSSM, the effective Hamiltonian has the form

$$\mathcal{H}_{\rm eff}^{\Delta F=2} = \sum_{i=1}^{5} C_i Q_i + \sum_{i=1}^{3} \tilde{C}_i \tilde{Q}_i \ + \mathrm{h.c.} \ , \tag{3.4}$$

[3] All the expressions we quote are relative to the MIA assuming a scenario with degenerate sfermion families. The phenomenological implications in flavour physics arising from a hierarchical sfermion scenario have been recently addressed in [114].

with the operators Q_i given, in the case of B_s mixing[4], by

$$
\begin{aligned}
Q_1 &= (\bar{s}^\alpha \gamma_\mu P_L\, b^\alpha)\,(\bar{s}^\beta \gamma^\mu P_L\, b^\beta)\ , \\
Q_2 &= (\bar{s}^\alpha P_L\, b^\alpha)\,(\bar{s}^\beta P_L\, b^\beta)\ , \\
Q_3 &= (\bar{s}^\alpha P_L\, b^\beta)\,(\bar{s}^\beta P_L\, b^\alpha)\ , \\
Q_4 &= (\bar{s}^\alpha P_L\, b^\alpha)\,(\bar{s}^\beta P_R\, b^\beta)\ , \\
Q_5 &= (\bar{s}^\alpha P_L\, b^\beta)\,(\bar{s}^\beta P_R\, b^\alpha)\ ,
\end{aligned} \tag{3.5}
$$

where $P_{R,L} = \frac{1}{2}(1 \pm \gamma_5)$ and α, β are colour indices. The operators $\tilde{Q}_{1,2,3}$ are obtained from $Q_{1,2,3}$ by the replacement $L \leftrightarrow R$. In the SM only the operator Q_1 is generated, because of the $(V-A)$ structure of the SM charged currents. On the other hand, within the MSSM, all operators typically arise.

In a MFV MSSM, the NP effects to the mixing amplitudes are quite small both in the low $\tan\beta$ regime [96] and also at large $\tan\beta$ [115, 116].

In the former case, the largest contributions to the amplitude $M_{12}^{(M)}$ arise from the chargino and charged Higgs effects by means of C_1 and $\tilde{C}_3$. All the other Wilson coefficients (WCs) involve couplings that are highly suppressed by light quark Yukawa couplings. Moreover, it turns out that the chargino box contributions to $\tilde{C}_3$ are the only non-negligible contributions sensitive to flavour diagonal phases. In particular

$$
C_1^{\tilde{\chi}^\pm} \simeq -\frac{g_2^4}{16\pi^2}(V_{tb}V_{ts}^\star)^2\left[\frac{m_t^4}{8M_W^4}\frac{1}{\tilde{m}^2}f_1(x_\mu)\right] + \mathcal{O}\left(\frac{v^2}{\tilde{m}^2}\right), \tag{3.6}
$$

$$
\tilde{C}_3^{\tilde{\chi}^\pm} \simeq -\frac{g_2^4}{16\pi^2}(V_{tb}V_{ts}^\star)^2\frac{m_b^2 t_\beta^2}{(1+\epsilon t_\beta)^2}\left[\frac{m_t^4}{8M_W^4}\frac{\mu^2 A_t^2}{\tilde{m}^8}f_3(x_\mu)\right], \tag{3.7}
$$

where $x_\mu = |\mu|^2/\tilde{m}^2$, $t_\beta = \tan\beta$, the loop functions are such that $f_1(1) = -1/12$, $f_3(1) = 1/20$ and ϵ is the well known resummation factor arising from non-holomorphic (t_β enhanced) threshold corrections [117, 118, 119, 115, 120, 121]. The dominant gluino contributions read

$$
\epsilon \simeq \frac{2\alpha_s}{3\pi}\frac{\mu M_{\tilde{g}}}{\tilde{m}^2}f(x_g)\ , \tag{3.8}
$$

with $x_g = M_{\tilde{g}}^2/\tilde{m}^2$ and the loop function f given in the appendix. One has $f(1) = 1/2$ such that $\epsilon \simeq \alpha_s/3\pi$ for a degenerate SUSY spectrum.

As anticipated, (3.6) clearly shows that C_1 is not sensitive to flavour conserving phases, while $\tilde{C}_3$ can be complex for complex μA_t. In (3.7) we have omitted contributions sensitive to the phases of the combinations $\mu^2 M_2^2$ and $\mu^2 A_t M_2$, as they vanish in the limit of degenerate (left-handed) squark generations as a result of the super-GIM mechanism.

Moreover, we note that ϵ_K can receive sizable effects only through C_1, as the contributions to ϵ_K from $\tilde{C}_3$ are suppressed by m_s^2/m_b^2 and thus safely negligible. We find that the Wilson coefficient C_1 in (3.6) has the same sign as the SM contribution, thus we conclude that for flavour diagonal soft terms one has $|\epsilon_K| > |\epsilon_K^{\rm SM}|$.

Within a MFV framework at large $\tan\beta$, there are additional contributions to $\Delta F = 2$ transitions stemming from the neutral Higgs sector [122, 116, 115, 123, 124, 120]. However,

[4] Analogous formulae hold for the B_d and K^0 systems, with the appropriate replacements of the quarks involved in the transition.

at least for $\mu > 0$, these contributions turn out to be highly constrained by the experimental limits on $\mathrm{BR}(B_s \to \mu^+\mu^-)$, hence, they can be safely neglected.

In the following, we therefore focus on the effects that arise in the presence of non-MFV structures in the soft SUSY breaking sector. In such a setup, the leading contributions to the K^0, B_d and B_s mixing amplitudes come from gluino boxes[5]. The relevant Wilson coefficients in the MIA read [61][6]

$$
\begin{aligned}
C_1^{\tilde g} &\simeq -\frac{\alpha_s^2}{\tilde m^2}\left[(\delta_d^{LL})_{32}\right]^2 g_1^{(1)}(x_g)\ , && (3.9)\\
\tilde C_1^{\tilde g} &\simeq -\frac{\alpha_s^2}{\tilde m^2}\left[(\delta_d^{RR})_{32}\right]^2 g_1^{(1)}(x_g)\ , && (3.10)\\
C_4^{\tilde g} &\simeq -\frac{\alpha_s^2}{\tilde m^2}\left[(\delta_d^{LL})_{32}(\delta_d^{RR})_{32}\right] g_4^{(1)}(x_g)\ , && (3.11)\\
C_5^{\tilde g} &\simeq -\frac{\alpha_s^2}{\tilde m^2}\left[(\delta_d^{LL})_{32}(\delta_d^{RR})_{32}\right] g_5^{(1)}(x_g)\ , && (3.12)
\end{aligned}
$$

where $x_g = M_{\tilde g}^2/\tilde m^2$ and the analytic expressions for the loop functions $g_1^{(1)}$, $g_4^{(1)}$ and $g_5^{(1)}$ can be found in appendix A. For the limiting case of degenerate masses we find $g_1^{(1)}(1) = -1/216$, $g_4^{(1)}(1) = 23/180$ and $g_5^{(1)}(1) = -7/540$.

In the above expressions, we omitted the contributions arising from the LR and RL MI because, as we will see in sec. 3.2.1, they are tightly constrained by $\mathrm{BR}(b \to s\gamma)$.

The same argument does not apply to the $s \to d$ and $b \to d$ transitions as there is no $\mathrm{BR}(B \to X_s\gamma)$ analog here [7]. However, in the concrete flavour models we are dealing with, it turns out that the contributions from $(\delta_d^{LL})_{ij}(\delta_d^{RR})_{ij}$ are always dominant compared to those from $(\delta_d^{LR})_{ij}$ and $(\delta_d^{RL})_{ij}$, hence, the above expressions are accurate enough for all the $\Delta F = 2$ transitions [8] .

An important observation comes directly from the Wilson coefficients (3.9)–(3.12): we expect large NP contributions in the mixing amplitudes from models that predict both nonzero $(\delta_d^{LL})_{32}$ and $(\delta_d^{RR})_{32}$ MIs, since in this way the operators Q_4 and Q_5, that are strongly enhanced through QCD renormalization group effects [127, 128], have non-vanishing Wilson coefficients. We note in addition that especially the loop function $g_4^{(1)}$ entering the Wilson coefficient $C_4^{\tilde g}$ is roughly a factor 30 larger than the one entering $C_1^{\tilde g}$.

Expressions (3.9)-(3.12) are valid for the B_s mixing amplitude, while the corresponding expressions for B_d and K^0 mixing can be obtained by replacing the indices (32) with (31) or (21), respectively. Similarly, the corresponding expressions for $D^0 - \bar D^0$ mixing are easily obtained from those relative to $K^0 - \bar K^0$ making the replacement $(\delta_d)_{21} \to (\delta_u)_{21}$.

In the case of K^0 mixing, it is important for our analysis to consider also the additional contribution coming from effective $(2 \to 1)$ mass insertions generated by a double flavour flip $(2 \to 3) \times (3 \to 1)$. Results for the Wilson coefficients with one effective $(2 \to 1)$ transition

[5]In our numerical analysis we include the full set of contributions that can be found e.g. in [96].

[6]The NLO Wilson coefficients in the MIA are given in [125] and in [126, 121] in the mass eigenstate basis.

[7]although, as a future perspective, LR and RL MIs relative to the $b \to d$ transition will be probed by $\mathrm{BR}(B \to \rho\gamma)$.

[8]Clearly the contributions of the MIs $(\delta_d^{LR})_{ij}$ and $(\delta_d^{RL})_{ij}$ are taken into account in our model independent analysis of sec. 5.

are obtained in the third order of the MIA. We find

$$C_1^{\tilde g} \simeq -\frac{\alpha_s^2}{\tilde m^2}\left[(\delta_d^{LL})_{21}(\delta_d^{LL})_{23}(\delta_d^{LL})_{31}\right] g_1^{(2)}(x_g) , \tag{3.13}$$

$$\tilde C_1^{\tilde g} \simeq -\frac{\alpha_s^2}{\tilde m^2}\left[(\delta_d^{RR})_{21}(\delta_d^{RR})_{23}(\delta_d^{RR})_{31}\right] g_1^{(2)}(x_g) , \tag{3.14}$$

$$C_4^{\tilde g} \simeq -\frac{\alpha_s^2}{\tilde m^2}\frac{1}{2}\left[(\delta_d^{LL})_{21}(\delta_d^{RR})_{23}(\delta_d^{RR})_{31}+(\delta_d^{LL})_{23}(\delta_d^{LL})_{31}(\delta_d^{RR})_{21}\right] g_4^{(2)}(x_g) , \tag{3.15}$$

$$C_5^{\tilde g} \simeq -\frac{\alpha_s^2}{\tilde m^2}\frac{1}{2}\left[(\delta_d^{LL})_{21}(\delta_d^{RR})_{23}(\delta_d^{RR})_{31}+(\delta_d^{LL})_{23}(\delta_d^{LL})_{31}(\delta_d^{RR})_{21}\right] g_5^{(2)}(x_g) . \tag{3.16}$$

The loop functions are again given in appendix A and for degenerate masses we find $g_1^{(2)}(1) = 1/360$, $g_4^{(2)}(1) = -1/6$ and $g_5^{(2)}(1) = 1/90$.

Finally we also have to consider the case where the $(2 \to 1)$ flavour transition is entirely generated by $(2 \to 3)$ and $(3 \to 1)$ transitions. We find

$$C_1^{\tilde g} \simeq -\frac{\alpha_s^2}{\tilde m^2}\left[(\delta_d^{LL})_{23}(\delta_d^{LL})_{31}\right]^2 g_1^{(3)}(x_g) , \tag{3.17}$$

$$\tilde C_1^{\tilde g} \simeq -\frac{\alpha_s^2}{\tilde m^2}\left[(\delta_d^{RR})_{23}(\delta_d^{RR})_{31}\right]^2 g_1^{(3)}(x_g) , \tag{3.18}$$

$$C_4^{\tilde g} \simeq -\frac{\alpha_s^2}{\tilde m^2}\left[(\delta_d^{LL})_{23}(\delta_d^{LL})_{31}(\delta_d^{RR})_{23}(\delta_d^{RR})_{31}\right] g_4^{(3)}(x_g) , \tag{3.19}$$

$$C_5^{\tilde g} \simeq -\frac{\alpha_s^2}{\tilde m^2}\left[(\delta_d^{LL})_{23}(\delta_d^{LL})_{31}(\delta_d^{RR})_{23}(\delta_d^{RR})_{31}\right] g_5^{(3)}(x_g) , \tag{3.20}$$

with $g_1^{(3)}(1) = -1/3780$, $g_4^{(3)}(1) = 37/630$ and $g_5^{(3)}(1) = -1/378$. The analytic expressions for these loop functions can again be found in appendix A.

In the large $\tan\beta$ regime, the gluino box contributions are not the dominant ones anymore but they have to compete with double Higgs penguin contributions, see the Feynman diagrams of fig. 4, that are enhanced by $\tan^4\beta$ as in the MFV case [122, 116, 115]. Taking into account both gluino and chargino loops and generalizing the formulae of [122, 116, 115] to non-MFV contributions we find in the case of the B_s system[9]

$$\begin{aligned}(C_4^H)_B \simeq\; & -\frac{\alpha_s^2\alpha_2}{4\pi}\frac{m_b^2}{2M_W^2}\frac{t_\beta^4}{(1+\epsilon t_\beta)^4}\frac{|\mu|^2 M_{\tilde g}^2}{M_A^2\tilde m^4}(\delta_d^{LL})_{32}(\delta_d^{RR})_{32}\left[h_1(x_g)\right]^2 + \\ & + \frac{\alpha_2^2\alpha_s}{4\pi}\frac{m_b^2}{2M_W^2}\frac{t_\beta^4}{(1+\epsilon t_\beta)^4}\frac{|\mu|^2}{M_A^2\tilde m^2}\times\left[\frac{m_t^2}{M_W^2}\frac{A_t M_{\tilde g}}{\tilde m^2}h_1(x_g)h_3(x_\mu)(\delta_d^{RR})_{32}V_{tb}V_{ts}^* + \right. \\ & \left. + \frac{M_2 M_{\tilde g}}{\tilde m^2}(\delta_u^{LL})_{32}(\delta_d^{RR})_{32}h_1(x_g)h_4(x_2,x_\mu)\right] ,\end{aligned} \tag{3.21}$$

with the mass ratios $x_\mu = |\mu|^2/\tilde m^2$, $x_2 = |M_2|^2/\tilde m^2$ and the loop functions, reported in appendix A, satisfying $h_1(1) = 4/9$, $h_3(1) = -1/4$ and $h_4(1,1) = 1/6$. We stress that, due to the presence of the RR MIs, these contributions are neither suppressed by m_s/m_b nor by other suppression factors, as it happens in contrast in the MFV framework [122, 116, 115, 124].

In the case of K^0 mixing, the most relevant effect from the neutral Higgses arises only at the fourth order in the MI expansion and we find the following expression

$$(C_4^H)_K \simeq -\frac{\alpha_s^2\alpha_2}{4\pi}\frac{m_b^2}{2M_W^2}\frac{t_\beta^4}{(1+\epsilon t_\beta)^4}\frac{|\mu|^2 M_{\tilde g}^2}{M_A^2\tilde m^4}(\delta_d^{LL})_{23}(\delta_d^{LL})_{31}(\delta_d^{RR})_{23}(\delta_d^{RR})_{31}h_2(x_g)^2 , \tag{3.22}$$

[9]The Wilson coefficient for B_d mixing can be obtained by replacing (32) with (31) and V_{ts} by V_{td}.

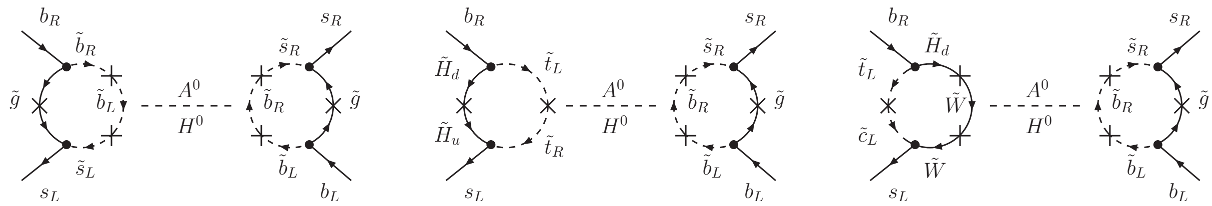

Figure 4: Feynman diagrams for the dominant Higgs mediated contributions to $\Delta B = 2$ transitions. The leading contribution proportional to $\tan^4\beta$ comes from the self-energy corrections in diagrams where the Higgs propagators are attached to the external quark legs.

with h_2 given in appendix A and $h_2(1) = -2/9$.

In contrast to the case with gluino box contributions, now there are no analogous Higgs mediated contributions for $D^0 - \bar{D}^0$ mixing; in fact, the non-holomorphic ($\tan\beta$ enhanced) threshold corrections lead to important FCNC couplings only among down-type fermions with the Higges.

3.2 $\Delta F = 1$ Processes

3.2.1 Wilson Coefficients of the Dipole Operator

The part of the $\Delta F = 1$ effective Hamiltonian relevant for the $b \to s\gamma$ transition that is most sensitive to NP effects reads

$$\mathcal{H}_{\rm eff} \supset -\frac{4G_F}{\sqrt{2}} V_{tb}V_{ts}^* \left(C_7 O_7 + C_8 O_8 + \tilde{C}_7 \tilde{O}_7 + \tilde{C}_8 \tilde{O}_8 \right) \ , \tag{3.23}$$

with the magnetic and chromomagnetic operators

$$O_7 = \frac{e}{16\pi^2} m_b (\bar{s}\sigma^{\mu\nu} P_R b) F_{\mu\nu} \ , \quad O_8 = \frac{g_s}{16\pi^2} m_b (\bar{s}\sigma^{\mu\nu} T^A P_R b) G^A_{\mu\nu} \ . \tag{3.24}$$

Here, $\sigma^{\mu\nu} = \frac{i}{2}[\gamma^\mu, \gamma^\nu]$ and T^A are the $SU(3)_c$ generators. The operators $\tilde{O}_i$ are obtained by the corresponding operators O_i by means of the replacement $L \leftrightarrow R$.

The dominant SUSY contributions to $C_{7,8}$ arise from the one-loop charged Higgs, chargino and gluino amplitudes $C_{7,8}^{\rm NP} = C_{7,8}^{H^\pm} + C_{7,8}^{\tilde{\chi}^\pm} + C_{7,8}^{\tilde{g}}$.

The charged Higgs contribution reads

$$C_{7,8}^{H^\pm} \simeq \left(\frac{1 - \epsilon t_\beta}{1 + \epsilon t_\beta} \right) \frac{1}{2} h_{7,8}(y_t) \ , \tag{3.25}$$

where $y_t = m_t^2 / M_{H^\pm}^2$, $\epsilon \sim 10^{-2}$ for a degenerate SUSY spectrum and the loop functions can be found in appendix A.

The corresponding expressions for the chargino contributions to C_7 and C_8 read

$$\frac{4G_F}{\sqrt{2}}\ C_{7,8}^{\tilde{\chi}^\pm} \simeq \frac{g_2^2}{\tilde{m}^2} \left[\frac{(\delta_u^{LL})_{32}}{V_{tb}V_{ts}^*} \frac{\mu M_2}{\tilde{m}^2} f_{7,8}^{(1)}(x_2, x_\mu) + \frac{m_t^2}{M_W^2} \frac{A_t \mu}{\tilde{m}^2} f_{7,8}^{(2)}(x_\mu) \right] \frac{t_\beta}{(1 + \epsilon t_\beta)} \ . \tag{3.26}$$

The relevant loop functions are again defined in appendix A.

Within a MFV SUSY framework, charged Higgs effects unambiguously increase the $b \to s\gamma$ branching ratio relative to the SM expectation, while the chargino ones (mostly from the

Higgsinos) can have either sign depending mainly on the sign and phase of μA_t. Since in SUGRA inspired models the sign of A_t is set (in almost the entire SUSY parameter space) by the large (CP-conserving) RGE induced effects driven by the $SU(3)$ interactions, the final MFV chargino effects will depend on the sign of the μ term that we assume to be real and positive which is preferred by the $(g-2)_\mu$ constraint (see also sec. 3.3.2). Then, the MFV contributions from the charged Higgs bosons and Higgsinos interfere destructively in BR$(b \to s\gamma)$.

At the LO, both the charged Higgs and the chargino contributions to $\tilde{C}_{7,8}$ are suppressed by m_s/m_b. However, this m_s/m_b suppression can be avoided in non-MFV scenarios at the NLO in the presence of RH currents by means of threshold corrections to the Yukawa interactions that are induced by $\tan\beta$-enhanced non-holomorphic effects [129]. For simplicity, we do not present these last contributions here, although they are systematically included in our numerical analysis.

In the presence of non-CKM flavour structures, gluino mediated FCNC contributions also arise and the corresponding Wilson coefficients governing the $b \to s\gamma$ transition read [10]

$$\frac{4G_F}{\sqrt{2}}\; C^{\tilde{g}}_{7,8} \simeq \frac{g_s^2}{\tilde{m}^2}\left[\frac{M_{\tilde{g}}}{m_b}\frac{(\delta_d^{RL})_{32}}{V_{tb}V_{ts}^*}g^{(1)}_{7,8}(x_g) + \frac{M_{\tilde{g}}\mu}{\tilde{m}^2}\frac{t_\beta}{(1+\epsilon t_\beta)}\frac{(\delta_d^{LL})_{32}}{V_{tb}V_{ts}^*}g^{(2)}_{7,8}(x_g)\right] , \tag{3.27}$$

$$\frac{4G_F}{\sqrt{2}}\; \tilde{C}^{\tilde{g}}_{7,8} \simeq \frac{g_s^2}{\tilde{m}^2}\left[\frac{M_{\tilde{g}}}{m_b}\frac{(\delta_d^{LR})_{32}}{V_{tb}V_{ts}^*}g^{(2)}_{7,8}(x_g) + \frac{M_{\tilde{g}}\mu^*}{\tilde{m}^2}\frac{t_\beta}{(1+\epsilon t_\beta)}\frac{(\delta_d^{RR})_{32}}{V_{tb}V_{ts}^*}g^{(3)}_{7,8}(x_g)\right] . \tag{3.28}$$

The functions $g^{(i)}_{7,8}$ $(i=1,2)$ are given in appendix A. As is evident from (3.27) and (3.28), $b \to s\gamma$ puts very strong constraints on the helicity flipping mass insertions $(\delta_d^{RL})_{32}$ and $(\delta_d^{LR})_{32}$ because the corresponding terms are chirally enhanced by a factor $M_{\tilde{g}}/m_b$.

In fact, once the constraint from BR$(b \to s\gamma)$ is imposed, these helicity flipping MIs cannot generate large effects in $\Delta B = 2$ observables, in particular in $S_{\psi\phi}$, anymore.

3.2.2 Direct CP Asymmetry in $b \to s\gamma$

A very sensitive observable to NP CP violating effects is represented by the direct CP asymmetry in $b \to s\gamma$, i.e. $A_{\rm CP}(b \to s\gamma)$ [133]. If NP effects dominate over the tiny SM contribution $A^{\rm SM}_{\rm CP}(b \to s\gamma) \simeq -0.5\%$, the following expression for $A_{\rm CP}(b \to s\gamma)$ holds [134, 135]

$$\begin{aligned} A_{\rm CP}(b \to s\gamma) &\equiv \frac{\Gamma(B \to X_{\bar{s}}\gamma) - \Gamma(\overline{B} \to X_s\gamma)}{\Gamma(B \to X_{\bar{s}}\gamma) + \Gamma(\overline{B} \to X_s\gamma)} \simeq \\ &\simeq -\frac{1}{|C_7|^2}\left(1.23\;{\rm Im}[C_2C_7^*] - 9.52\;{\rm Im}[C_8C_7^*] + 0.10\;{\rm Im}[C_2C_8^*]\right) - 0.5 \quad (\text{in }\%) , \end{aligned} \tag{3.29}$$

where we assumed a cut for the photon energy at $E_\gamma \simeq 1.8$ GeV (see [134, 135] for details). In (3.29), the Wilson coefficients C_i are evaluated at the scale m_b and they refer to the sum of SM plus NP contributions, i.e. $C_i = C_i^{\rm SM} + C_i^{\rm NP}$ (with $C_i^{\rm SM}$ real).

In order to take into account effects from the Wilson coefficients $\tilde{C}_i$ related to the operators $\tilde{O}_i$, (3.29) has to be modified according to $C_iC_j \to C_iC_j + \tilde{C}_i\tilde{C}_j$. Within a MFV scenario, $\tilde{C}_i$ are completely negligible, being suppressed by a factor of m_s/m_b compared to the corresponding

[10] Gluino contributions can also arise in the framework of the general MFV ansatz [5], see e.g. [130, 131, 132].

Wilson coefficients C_i. This statement is no longer valid in the presence of NP in the right-handed currents, as is the case in some of the scenarios we are going to discuss.

Still, as $\tilde{C}_2$ is negligibly small and the phases of $\tilde{C}_7$ and $\tilde{C}_8$ are the same to a very good approximation in all the frameworks that we consider, $A_{\rm CP}(b \to s\gamma)$ receives NP contributions only through the imaginary parts of $C_{7,8}^{\rm NP}$.

3.2.3 Time-Dependent CP Asymmetries in $B_d \to \phi(\eta')K_S$

The time-dependent CP asymmetries in the decays of neutral B mesons into final CP eigenstates f can be written as

$$\mathcal{A}_f(t) = S_f \sin(\Delta M t) - C_f \cos(\Delta M t) \ . \tag{3.30}$$

Within the SM, it is predicted with good accuracy that the $|S_f|$ and C_f parameters are universal for all the transitions $\bar{b} \to \bar{q}' q' \bar{s}$ ($q' = c, s, d, u$). In particular, the SM predicts that $-\eta_f S_f \simeq \sin 2\beta$ and $C_f \simeq 0$ where $\eta_f = \pm 1$ is the CP eigenvalue of the final state f. NP effects can contribute to[11]

i) the B_d mixing amplitude [81];

ii) the decay amplitudes $\bar{b} \to \bar{q} q \bar{s}$ ($q = s, d, u$) [81, 136].

In case i), the NP contribution shifts all S_f's from $\sin 2\beta$ in a universal way while the C_f's will still vanish. In case ii), the various S_f's and also the C_f's are, in general, not the same as in the SM.

The CP asymmetries S_f and C_f in $B_d \to f$ decays are calculated as follows. One defines a complex quantity λ_f,

$$\lambda_f = e^{-2i(\beta+\phi_{B_d})}(\overline{A}_f/A_f) \ , \tag{3.31}$$

where ϕ_{B_d} is the NP phase of the B_d mixing amplitude, M_{12}^d, and A_f ($\overline{A}_f$) is the decay amplitude for $B_d(\overline{B_d}) \to f$. A_f and $\overline{A}_f$ can be calculated from the effective Hamiltonian relevant for $\Delta B = 1$ decays [137], in the following way

$$A_f = \langle f|\mathcal{H}_{\rm eff}|B_d\rangle \ , \quad \overline{A}_f = \langle f|\mathcal{H}_{\rm eff}|\overline{B_d}\rangle \ , \tag{3.32}$$

where the Wilson coefficients of the effective Hamiltonian depend on the electroweak theory while the matrix elements $\langle f|O_i|B_d(\overline{B_d})\rangle$ can be evaluated, for instance, by means of QCD factorization [138]. We then have

$$S_f = \frac{2{\rm Im}(\lambda_f)}{1+|\lambda_f|^2} \ , \quad C_f = \frac{1-|\lambda_f|^2}{1+|\lambda_f|^2} \ . \tag{3.33}$$

The SM contribution to the decay amplitudes, related to $\bar{b} \to \bar{q}' q' \bar{s}$ transitions, can always be written as a sum of two terms, $A_f^{\rm SM} = A_f^c + A_f^u$, with $A_f^c \propto V_{cb}^* V_{cs}$ and $A_f^u \propto V_{ub}^* V_{us}$. Defining the ratio $a_f^u \equiv e^{-i\gamma}(A_f^u/A_f^c)$, we have

$$A_f^{\rm SM} = A_f^c \left(1 + a_f^u e^{i\gamma}\right) \ , \tag{3.34}$$

where the a_f^u parameters have been evaluated in the QCD factorization approach at the leading order and to zeroth order in Λ/m_b in [138]. Within the SM, it turns out that $S_{\phi K_S} \simeq S_{\eta' K_S} \simeq$

[11] We assume that the asymmetry in the tree level transition $\bar{b} \to \bar{c} c \bar{s}$ is not significantly affected by NP.

$S_{\psi K_S} \simeq \sin 2\beta$ with precise predictions given in tabs. 1 and 6. The a_f^u term provides only a negligible contribution to $B_d \to \psi K_S$, thus $\lambda_{\psi K_S}^{\rm SM} = -e^{-2i\beta}$. Also for charmless modes, the effects induced by a_f^u are small (at the percent level), being proportional to $|(V_{ub}V_{us}^*)/(V_{cb}V_{cs}^*)|$.

The modification of A_f from the SM expression (3.34) due to NP contributions can always be written as follows [12]

$$A_f = A_f^c \left[1 + a_f^u e^{i\gamma} + \sum_i \left(b_{fi}^c + b_{fi}^u e^{i\gamma} \right) \left(C_i^{\rm NP*}(M_W) + \zeta \tilde{C}_i^{\rm NP*}(M_W) \right) \right] , \tag{3.35}$$

where $C_i^{\rm NP}(M_W)$ and $\tilde{C}_i^{\rm NP}(M_W)$ are the NP contributions to the Wilson coefficients evaluated at the scale M_W, the parameters b_{fi}^u and b_{fi}^c calculated in [138] and $\zeta = \pm 1$ depending on the parity of the final state; for instance $\zeta = 1$ for ϕK_S and $\zeta = -1$ for $\eta' K_S$ [139].

The generalization of this formalism to B_s decays is straightforward.

3.2.4 CP Asymmetries in $B \to K^* \mu^+ \mu^-$

The rare decay $B \to K^*(\to K\pi)\mu^+\mu^-$ represents a very promising channel to look for NP in the B system, since its angular decay distribution is sensitive to the polarization of the K^* and gives access to many observables probing NP effects. Furthermore, for the neutral B^0 decay, the CP parity of the initial state can be unambiguously determined by measuring the charges of the kaon and pion in the final state. This "self-tagging" property allows a very clean access to CP-violating observables.

In this paper, we focus on those CP-violating observables with relatively small dependence on hadronic quantities and large sensitivity to NP, following closely the analysis of [140]; other recent analyses can be found in [141, 142]. In particular

- all the observables are evaluated in the dilepton mass range $1\,\mathrm{GeV}^2 < q^2 < 6\,\mathrm{GeV}^2$;
- power-suppressed corrections are accounted for by means of the full QCD form factors in the naively factorized amplitude, and the "soft" form factors $\xi_{\perp,\parallel}$ in the QCD factorization corrections;
- we focus on those observables which only depend on the ratios of form factors;
- we assume NP effects in $C_{7,9,10,S,P}$ and $\tilde{C}_{7,9,10,S,P}$ but not in the other C_i.

In our analysis, we consider the T-odd CP asymmetries A_7, A_8 and A_9 which are not suppressed by small strong phases and can thus be sizable in the presence of new sources of CP violation (CPV) [141, 140]. We use the conventions of [140] to which we refer for the full expressions of the asymmetries.

In tab. 4, we just recall the main sensitivities of A_7, A_8 and A_9 to the relevant WCs of the $\Delta F = 1$ effective Hamiltonian. Notice that $\langle A_9 \rangle$ is only sensitive to $\tilde{C}_7$, $\tilde{C}_9$ and $\tilde{C}_{10}$ hence it represents, in principle, a golden channel to probe *right-handed* currents. However, as we will discuss in sec. 6, within the SUSY flavour models we are dealing with, the attained values for $\langle A_9 \rangle$ seem to be far below the expected future experimental resolutions. This also implies that any potential signal of NP in $\langle A_9 \rangle$ would disfavour the flavour models under study pointing towards different scenarios.

[12] We thank Dominik Scherer for pointing out the correct expression for A_f [120].

process	CP asymmetry	sensitivity to the WCs
$B \to K^* \mu^+ \mu^-$	A_7	C_7, $\tilde{C}_7$, C_{10}, $\tilde{C}_{10}$
$B \to K^* \mu^+ \mu^-$	A_8	C_7, $\tilde{C}_7$, C_9, $\tilde{C}_9$, $\tilde{C}_{10}$
$B \to K^* \mu^+ \mu^-$	A_9	$\tilde{C}_7$, $\tilde{C}_9$, $\tilde{C}_{10}$
$b \to s\gamma$	$A_{\rm CP}(b \to s\gamma)$	C_7, C_8
$B_d \to \phi K_S$	$S_{\phi K_S}$	C_8, $\tilde{C}_8$
$B_d \to \eta' K_S$	$S_{\eta' K_S}$	C_8, $\tilde{C}_8$

Table 4: CP asymmetries of various $\Delta F = 1$ channels and the Wilson coefficients they are most sensitive to.

We would also like to emphasize that $\langle A_9 \rangle$ is peculiar from an experimental point of view since, in contrast to $\langle A_7 \rangle$ and $\langle A_8 \rangle$, it can be obtained from a one-dimensional angular distribution and should thus be accessible at current B factories. In the conventions of [140], the CP-averaged differential decay distribution in the angle ϕ reads

$$\frac{1}{\Gamma + \bar{\Gamma}} \frac{d(\Gamma + \bar{\Gamma})}{d\phi} = \frac{1}{2\pi} \left[\langle S_2^c \rangle + \langle S_3 \rangle \cos(2\phi) + \langle A_9 \rangle \sin(2\phi) \right] \ , \tag{3.36}$$

where $\langle S_2^c \rangle = -F_L$ has already been measured by BaBar [143] and Belle [144] and $\langle S_3 \rangle$ is a sensitive probe of new CP conserving physics in right-handed currents [145, 142, 140].

3.2.5 $B_s \to \mu^+\mu^-$

The SM prediction for the branching ratio of the decay $B_s \to \mu^+\mu^-$ is (using the results in [80] with updated input parameters)

$$\text{BR}(B_s \to \mu^+\mu^-)_{\rm SM} = (3.60 \pm 0.37) \times 10^{-9} \ . \tag{3.37}$$

This value should be compared to the present 95% C.L. upper bound from CDF [146]

$$\text{BR}(B_s \to \mu^+\mu^-)_{\rm exp} \lesssim 5.8 \times 10^{-8} \ , \tag{3.38}$$

that still leaves a large room for NP contributions [13]. In particular, the MSSM with large $\tan\beta$ allows, in a natural way, large departures of $\text{BR}(B_s \to \mu^+\mu^-)$ from its SM expectation [149, 150, 151].

The most relevant NP effects in the MSSM are encoded in the effective Hamiltonian

$$\mathcal{H}_{\rm eff} = -C_S Q_S - C_P Q_P - \tilde{C}_S \tilde{Q}_S - \tilde{C}_P \tilde{Q}_P \ , \tag{3.39}$$

with the scalar and pseudoscalar operators

$$Q_S = m_b \left(\bar{s} P_R b\right) \left(\bar{\ell}\ell\right) \ , \quad Q_P = m_b \left(\bar{s} P_R b\right) \left(\bar{\ell}\gamma_5 \ell\right) \ , \tag{3.40}$$

as well as the corresponding operators $\tilde{Q}_S$ and $\tilde{Q}_P$ that are obtained by the exchange $L \leftrightarrow R$. For the corresponding Wilson coefficients in the MSSM, one has to a very good approximation

$$C_P \simeq -C_S \ , \quad \tilde{C}_P \simeq \tilde{C}_S \ , \tag{3.41}$$

[13] An unofficial Tevatron combination with D0 data [147] yields an upper bound of 4.5×10^{-8} [148].

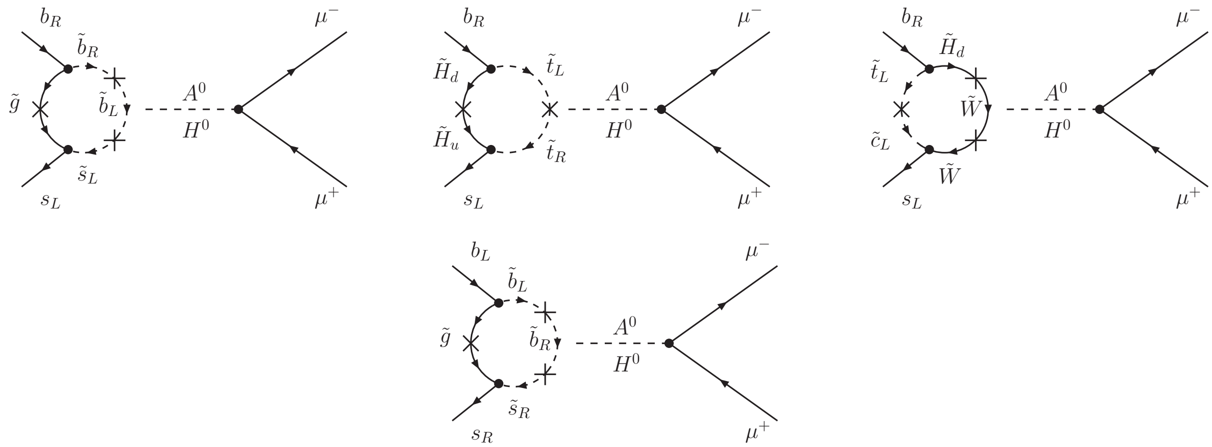

Figure 5: Feynman diagrams for the dominant Higgs mediated contributions to $B_s \to \mu^+\mu^-$. The leading contribution to the decay amplitude proportional to $\tan^3\beta$ comes from the self-energy corrections in diagrams where the Higgs propagators are attached to the external quark legs. The diagrams in the first row correspond to (3.42), the one in the second row to (3.43).

with

$$\begin{aligned} C_S &= -\frac{\alpha_2^2}{M_A^2}\frac{m_\ell}{4M_W^2}\frac{t_\beta^3}{(1+\epsilon t_\beta)^2(1+\epsilon_\ell t_\beta)}\left[\frac{m_t^2}{M_W^2}\frac{A_t\mu}{\tilde{m}^2}V_{tb}V_{ts}^* h_3(x_\mu) + \frac{M_2\mu}{\tilde{m}^2}(\delta_u^{LL})_{32}h_4(x_2,x_\mu)\right] \\ &\quad +\frac{\alpha_2\alpha_s}{M_A^2}\frac{m_\ell}{4M_W^2}\frac{t_\beta^3}{(1+\epsilon t_\beta)^2(1+\epsilon_\ell t_\beta)}\frac{M_{\tilde{g}}\mu}{\tilde{m}^2}(\delta_d^{LL})_{32}h_1(x_g)\ , \end{aligned} \tag{3.42}$$

$$\tilde{C}_S = \frac{\alpha_2\alpha_s}{M_A^2}\frac{m_\ell}{4M_W^2}\frac{t_\beta^3}{(1+\epsilon t_\beta)^2(1+\epsilon_\ell t_\beta)}\frac{M_{\tilde{g}}\mu^*}{\tilde{m}^2}(\delta_d^{RR})_{32}h_1(x_g)\ . \tag{3.43}$$

The loop functions h_1, h_3 and h_4 already appeared in the discussion of the double Higgs penguin contributions to B_s mixing. This hints to correlations between NP effects in B_s mixing and $B_s \to \mu^+\mu^-$ identified within the MSSM with MFV at large $\tan\beta$ in [116, 115].

In fig. 5, we show the relevant SUSY Feynman diagrams for $B_s \to \mu^+\mu^-$ in the presence of new flavour structures.

The branching ratio for $B_s \to \mu^+\mu^-$ can be expressed in the following way

$$\mathrm{BR}(B_s \to \mu^+\mu^-) = \frac{\tau_{B_s}F_{B_s}^2 m_{B_s}^3}{32\pi}\sqrt{1-4\frac{m_\mu^2}{m_{B_s}^2}}\left(|B|^2\left(1-4\frac{m_\mu^2}{m_{B_s}^2}\right)+|A|^2\right)\ , \tag{3.44}$$

where the expressions A and B are given by the two linear combinations of the Wilson coefficients

$$A = 2\frac{m_\mu}{m_{B_s}}C_{10}^{\mathrm{SM}} + m_{B_s}\left(C_P - \tilde{C}_P\right)\ , \quad B = m_{B_s}\left(C_S - \tilde{C}_S\right)\ , \tag{3.45}$$

where we assumed C_{10} free of NP, which is approximately true in all the scenarios that we consider. At leading order, the SM value for the Wilson coefficient C_{10} is given by

$$C_{10}^{\mathrm{SM}} = \frac{g_2^2}{16\pi^2}\frac{4G_F}{\sqrt{2}}V_{tb}V_{ts}^* Y_0(x_t)\ , \tag{3.46}$$

and the loop function Y_0 can be found in appendix A. The NLO QCD corrections to Y_0 have been calculated in [152] and found very small when $m_t(m_t)$ has been used, which we do also in our analysis.

3.2.6 $B^+ \to \tau^+\nu$

The SM expression for the branching ratio of the tree-level decay $B^+ \to \tau^+\nu$ is given by

$$\mathrm{BR}(B^+ \to \tau^+\nu)_{\mathrm{SM}} = \frac{G_F^2 m_{B^+} m_\tau^2}{8\pi}\left(1-\frac{m_\tau^2}{m_{B^+}^2}\right)^2 F_{B^+}^2 |V_{ub}|^2 \tau_{B^+} \ . \tag{3.47}$$

Its numerical value suffers from sizable parametrical uncertainties induced by F_{B^+} and V_{ub}.

On the theoretical side, the $B \to \tau\nu$ process is one of the cleanest probes of the large $\tan\beta$ scenario due to its enhanced sensitivity to tree-level charged-Higgs exchange [153, 154, 155]. In particular, a scalar charged current induced by NP theories with extended Higgs sectors, leads to the following modification of the branching ratio

$$R_{B\tau\nu} = \frac{\mathrm{BR}(B^+ \to \tau^+\nu)}{\mathrm{BR}(B^+ \to \tau^+\nu)_{\mathrm{SM}}} = \left[1 - \frac{m_{B^+}^2}{M_{H^+}^2}\frac{t_\beta^2}{(1+\epsilon t_\beta)(1+\epsilon_\ell t_\beta)}\right]^2 , \tag{3.48}$$

where we have included the $\tan\beta$ enhanced non-holomorphic corrections for the quark and lepton Yukawas. In the limit of degenerate SUSY particles, it turns out that $\epsilon \simeq \alpha_s/3\pi$ [115] and $\epsilon_\ell \simeq -3\alpha_2/16\pi$ [129].

Concerning the experimental situation, the HFAG collaboration [1] quotes

$$\mathrm{BR}(B^+ \to \tau^+\nu)_{\mathrm{exp}} = (1.43 \pm 0.37) \times 10^{-4} \ , \tag{3.49}$$

which is based on results by BaBar [156] and Belle [157, 158]. Including additional preliminary results from BaBar [159], one finds the following new World Average [112]

$$\mathrm{BR}(B^+ \to \tau^+\nu)_{\mathrm{exp}} = (1.73 \pm 0.35) \times 10^{-4} \ , \tag{3.50}$$

that is considerably higher than (3.49).

Using the value for $|V_{ub}|$ quoted by the PDG [81], $|V_{ub}| = (3.95\pm0.35)\times10^{-3}$ and $F_{B^+} \simeq F_B$ given in tab. 3, we find the SM branching ratio given in tab. 6, corresponding to

$$(R_{B\tau\nu})_{\mathrm{exp}} = 1.57 \pm 0.53\,. \tag{3.51}$$

In view of the parametric uncertainties induced in (3.47) by F_{B^+} and V_{ub}, in order to find the SM prediction for this branching ratio one can also use ΔM_d to find

$$\mathrm{BR}(B^+ \to \tau^+\nu)_{\mathrm{SM}} \;=\; \frac{3\pi}{4\,\eta_B\, S_0(x_t)\, \hat{B}_{B_d}}\frac{m_\tau^2}{M_W^2}\left(1-\frac{m_\tau^2}{m_{B^+}^2}\right)^2 \left|\frac{V_{ub}}{V_{td}}\right|^2 \tau_{B^+}\, \Delta M_d \ . \tag{3.52}$$

Here ΔM_d is supposed to be taken from experiment and $|V_{ub}/V_{td}|^2$ is found using the formulae (2.3), (2.4) and (2.7)

$$\left|\frac{V_{ub}}{V_{td}}\right|^2 = \left(\frac{1}{1-\lambda^2/2}\right)^2 \frac{1+R_t^2-2R_t\cos\beta}{R_t^2} \ , \tag{3.53}$$

with R_t and β determined by means of (2.9). In writing (3.52), we used $F_B \simeq F_{B^+}$ and $m_{B_d} \simeq m_{B^+}$. We then find

$$\mathrm{BR}(B^+ \to \tau^+\nu)_{\mathrm{SM}} = (0.80 \pm 0.12) \times 10^{-4} \tag{3.54}$$

that is by roughly a factor of two below the data in (3.50). This result agrees well with a recent result presented by the UTfit collaboration [160].

It should be noted that the value of $|V_{ub}|$ used effectively in this procedure turns out to be 3.50×10^{-3}, which is close to $|V_{ub}| = (3.38 \pm 0.36) \times 10^{-3}$ obtained from exclusive decays [161]. On the other hand, it is significantly lower than the one quoted by the PDG and obtained from tree level decays.

For $|V_{ub}|$ even higher than the PDG value, the experimental value for $\mathrm{BR}(B^+ \to \tau^+\nu)$ can be reproduced, simultaneously making the appearance of a new phase in $B_d^0 - \bar{B}_d^0$ likely as discussed in sec. 2.3. In fact, the solution 2) to the UT tensions presented there would imply the central value $\mathrm{BR}(B^+ \to \tau^+\nu) = 1.32 \times 10^{-4}$ in the SM and be fully compatible with the experimental data, assuming no NP contributions to the latter decay.

This discussion highlights the importance of accurate determinations of $|V_{ub}|$ and of $\mathrm{BR}(B^+ \to \tau^+\nu)$ in the future in order to be able to decide whether NP is at work here or not. In particular, for low $|V_{ub}|$ values (exclusive determination) there is a clear tension between the SM prediction for $\mathrm{BR}(B^+ \to \tau^+\nu)$ and the data and an even larger tension exists in the presence of charged Higgs contributions.

In our numerical analysis of NP contributions to various observables, we will use, to be conservative, (3.51) as the constraint coming from this decay.

One could contemplate whether the charged Higgs correction in (3.48) could be so large that $R_{B\tau\nu}$ becomes larger than unity improving the agreement of theory with the data. Such a possibility, that would necessarily imply a light charged Higgs and large $\tan\beta$ values, seems to be quite unlikely, even if not excluded yet [14], in view of the constraints from other observables [163].

This discussion is at first sight independent of the values of the weak decay constants that cancel in the ratio (3.52). Yet, the increase of the weak decay constants as suggested by recent non-quenched lattice calculations would certainly bring the SM value for $\mathrm{BR}(B^+ \to \tau^+\nu)$ to agree better with the data. In (3.52), this effect is seen through the decreased value of $|V_{td}|$ in order to agree with the experimental value of ΔM_d when the value of the relevant weak decay constant is increased.

Another potentially interesting channel where to look for the presence of scalar charged currents is represented by the purely leptonic Kaon decays. In particular, the NP effect on $R_{K\mu\nu} = \Gamma^{\mathrm{SUSY}}(K \to \mu\nu)/\Gamma^{\mathrm{SM}}(K \to \mu\nu)$ is obtained from (3.48) with the replacement $m_B^2 \to m_K^2$ [155]. Although the charged Higgs contributions are now suppressed by a factor $m_K^2/m_B^2 \simeq 1/100$, this is well compensated by the excellent experimental resolution [103] and the good theoretical control. The best strategy to fully exploit the NP sensitivity of $K_{\ell 2}$ systems is to consider the ratio $R^{'} = R_{K\mu\nu}/R_{\pi\mu\nu}$ [155, 103] instead of $R_{K\mu\nu}$. In fact, while $R^{'}$ and $R_{K\mu\nu}$ have the same NP content (as $R_{\pi\mu\nu}$ is not sizably affected by NP), $R^{'}$ depends on $(F_K/F_\pi)^2$ instead of F_K^2 with F_K/F_π determined more precisely than F_K by unquenched calculations in lattice QCD. However, given that the resolution on F_K/F_π is at the % level, the same level of NP sensitivity of $K \to \ell\nu$, we prefer to not include the constraints from $K \to \ell\nu$

[14]For a detailed analysis on the viability of NP scenarios with a heavy-light extended Higgs sector, we refer the reader to Ref. [162].

Process	Present Bounds	Expected Future Bounds	Future Experiments
$\mathrm{BR}(\mu \to e\,\gamma)$	1.2×10^{-11}	$\mathcal{O}(10^{-13} - 10^{-14})$	MEG, PSI
$\mathrm{BR}(\mu \to e\,e\,e)$	1.1×10^{-12}	$\mathcal{O}(10^{-13} - 10^{-14})$	?
$\mathrm{BR}(\mu \to e$ in Nuclei (Ti))	1.1×10^{-12}	$\mathcal{O}(10^{-18})$	J-PARC
$\mathrm{BR}(\tau \to e\,\gamma)$	1.1×10^{-7}	$\mathcal{O}(10^{-8})$	SuperB
$\mathrm{BR}(\tau \to e\,e\,e)$	2.7×10^{-7}	$\mathcal{O}(10^{-8})$	SuperB
$\mathrm{BR}(\tau \to e\,\mu\,\mu)$	$2. \times 10^{-7}$	$\mathcal{O}(10^{-8})$	SuperB
$\mathrm{BR}(\tau \to \mu\,\gamma)$	6.8×10^{-8}	$\mathcal{O}(10^{-8})$	SuperB
$\mathrm{BR}(\tau \to \mu\,\mu\,\mu)$	2×10^{-7}	$\mathcal{O}(10^{-8})$	LHCb
$\mathrm{BR}(\tau \to \mu\,e\,e)$	2.4×10^{-7}	$\mathcal{O}(10^{-8})$	SuperB

Table 5: Present [81] and upcoming experimental limits on various leptonic processes at 90% C.L.

in the present analysis. The above argument for $K \to \ell\nu$ does not apply to $B^+ \to \tau^+\nu$. In fact, even if the hadronic uncertainties related to F_B and V_{ub} are much larger that those for F_K/F_π and V_{us}, they cannot hide in any way the huge NP effects that can affect $\mathrm{BR}(B^+ \to \tau^+\nu)$.

3.2.7 $K \to \pi\nu\bar{\nu}$ and $b \to s\nu\bar{\nu}$

Within the MSSM with R-parity conservation, sizable non-standard contributions to $K \to \pi\nu\bar{\nu}$ decays can be generated only if the soft-breaking terms have a non-MFV structure. The leading amplitudes giving rise to large effects are induced by: i) chargino/up-squark loops [164, 165, 166, 167] and ii) charged Higgs/top quark loops [168]. In the first case, large effects are generated if the trilinear couplings of the up-squarks have a non-MFV structure. In the second case, deviations from the SM are induced by non-MFV terms in the right-right down sector, provided $\tan\beta$ is large (30 to 50).

In the case of $b \to s\nu\bar{\nu}$ transitions like $B \to K\nu\bar{\nu}$, $B \to K^*\nu\bar{\nu}$ or $B \to X_s\nu\bar{\nu}$, the second case above is prevented by the constraint on $\mathrm{BR}(B_s \to \mu^+\mu^-)$, while chargino/up-squark loops with non-MFV trilinear couplings in the up-squark sector can also generate sizable effects [169, 170].

However, since the SUSY models we consider in sec. 6 feature neither sizeable off-diagonal entries in the trilinear couplings nor simultaneously large enough $(\delta_d^{RR})_{13}$ and $(\delta_d^{RR})_{23}$ mass insertions, both $K \to \pi\nu\bar{\nu}$ and $b \to s\nu\bar{\nu}$ decays turn out to be SM-like.

3.2.8 $\ell_i \to \ell_j\gamma$

Within SUSY models, LFV effects relevant to charged leptons originate from any misalignment between fermion and sfermion mass eigenstates. Once non-vanishing LFV entries in the slepton mass matrices are generated, irrespective of the underlying mechanism accounting for them, LFV rare decays like $\ell_i \to \ell_j\gamma$ are naturally induced by one-loop diagrams with the exchange of gauginos and sleptons. The present and projected bounds on these processes are summarized in tab. 5 [15].

[15] The 2008 data from MEG are already close ($\mathrm{BR}(\mu \to \mathrm{e}\,\gamma) < 3 \times 10^{-11}$ [171]) to the present upper bound from MEGA so that the 2009 data should be able to provide a new improved bound.

The decay $\ell_i \to \ell_j\gamma$ is described by the dipole operator and the corresponding amplitude reads

$$T = m_{\ell_i}\epsilon^\lambda \overline{u}_j(p-q)[iq^\nu\sigma_{\lambda\nu}(A_L P_L + A_R P_R)]u_i(p)\,, \tag{3.55}$$

where p and q are momenta of the leptons ℓ_k and of the photon respectively and $A_{L,R}$ are the two possible amplitudes entering the process. The lepton mass factor m_{ℓ_i} is associated to the chirality flip present in this transition. The branching ratio of $\ell_i \to \ell_j\gamma$ can be written as

$$\frac{\mathrm{BR}(\ell_i\to\ell_j\gamma)}{\mathrm{BR}(\ell_i\to\ell_j\nu_i\bar{\nu}_j)} = \frac{48\pi^3\alpha}{G_F^2}(|A_L^{ij}|^2+|A_R^{ij}|^2)\,.$$

In the MI approximation it is found that [172]

$$\begin{aligned} A_L^{ij} &\simeq \frac{\alpha_2}{4\pi}\frac{\left(\delta_\ell^{LL}\right)_{ij}}{m_{\tilde{\ell}}^2}t_\beta\left[\frac{\mu M_2}{(M_2^2-\mu^2)}\Big(f_{2n}(x_2,x_\mu)+f_{2c}(x_2,x_\mu)\Big)\right.\\ &+ \left.\tan^2\theta_W\,\mu M_1\left(\frac{f_{3n}(x_1)}{m_{\tilde{\ell}}^2}+\frac{f_{2n}(x_1,x_\mu)}{(\mu^2-M_1^2)}\right)\right]\\ &+ \frac{\alpha_1}{4\pi}\frac{\left(\delta_\ell^{RL}\right)_{ij}}{m_{\tilde{\ell}}^2}\left(\frac{M_1}{m_{\ell_i}}\right)\;2\;f_{2n}(x_1)\;, \end{aligned} \tag{3.56}$$

$$A_R^{ij} \simeq \frac{\alpha_1}{4\pi}\left[\frac{\left(\delta_e^{RR}\right)_{ij}}{m_{\tilde{\ell}}^2}\mu M_1 t_\beta\left(\frac{f_{3n}(x_1)}{m_{\tilde{\ell}}^2}-\frac{2f_{2n}(x_1,x_\mu)}{(\mu^2-M_1^2)}\right)+2\frac{\left(\delta_e^{LR}\right)_{ij}}{m_{\tilde{\ell}}^2}\left(\frac{M_1}{m_{\ell_i}}\right)\;f_{2n}(x_1)\right]\;, \tag{3.57}$$

where θ_W is the weak mixing angle, $m_{\tilde{\ell}}$ is an average slepton mass, $x_{1,2} = M_{1,2}^2/m_{\tilde{\ell}}^2$, $x_\mu = \mu^2/m_{\tilde{\ell}}^2$ and $f_{i(c,n)}(x,y) = f_{i(c,n)}(x) - f_{i(c,n)}(y)$. The loop functions f_i are given in appendix A.

In the case of $\mu \to e\gamma$, one has to consider also the contributions arising from double MIs $\delta_{23}\delta_{31}$ as they can compete with the single MI contributions when $\delta_{21} \approx \delta_{23}\delta_{31}$; in particular, this will turn out to be the case for the flavour models we will analyze. A particularly important effect is provided by the following amplitude

$$A_L^{21} \simeq \frac{\alpha_1}{4\pi}\left(\frac{m_\tau}{m_\mu}\right)\frac{\mu M_1 t_\beta}{m_{\tilde{\ell}}^4}f_{4n}(x_1)(\delta_e^{RR})_{23}(\delta_\ell^{LL})_{31} \tag{3.58}$$

because of the enhancement factor m_τ/m_μ. The analog expression for A_R^{21} is obtained by $A_R^{21} = A_L^{21}(L \leftrightarrow R)$. In (3.58), the loop function is such that $f_{4n}(x) = f_0^{(3)}(x)/2$ with $f_0^{(3)}(1) = -1/15$ and $f_0^{(3)}(x)$ defined in appendix A. Other contributions, generated by the double MIs $(\delta_\ell^{LL})_{23}(\delta_\ell^{LL})_{31}$ and $(\delta_e^{RR})_{23}(\delta_e^{RR})_{31}$ and not enhanced by m_τ/m_μ, can be still relevant; however, for simplicity, we do not report them here although they are systematically included in our numerical analysis. In (3.56), (3.57), (3.58), as well as in the remainder of sec. 3, we assume the μ term, the trilinear couplings and the gaugino masses to be real and the latter also positive.

In the illustrative case of a degenerate SUSY spectrum with a common mass $m_{\tilde{\ell}}$, we find

that

$$
\begin{aligned}
A_L^{21} &\simeq \frac{\alpha_2}{60\pi}\frac{t_\beta}{m_{\tilde\ell}^2}(\delta_\ell^{LL})_{21} + \frac{\alpha_1}{48\pi}\frac{(\delta_\ell^{RL})_{21}}{m_{\tilde\ell}^2}\left(\frac{m_{\tilde\ell}}{m_\mu}\right) - \frac{\alpha_1}{120\pi}\frac{m_\tau}{m_\mu}\frac{t_\beta}{m_{\tilde\ell}^2}(\delta_e^{RR})_{23}(\delta_\ell^{LL})_{31}\,, && (3.59)\\
A_L^{32} &\simeq \frac{\alpha_2}{60\pi}\frac{t_\beta}{m_{\tilde\ell}^2}(\delta_\ell^{LL})_{32} + \frac{\alpha_1}{48\pi}\frac{(\delta_\ell^{RL})_{32}}{m_{\tilde\ell}^2}\left(\frac{m_{\tilde\ell}}{m_\tau}\right)\,, && (3.60)\\
A_R^{21} &\simeq -\frac{\alpha_1}{4\pi}\frac{t_\beta}{m_{\tilde\ell}^2}\left[\frac{(\delta_e^{RR})_{21}}{60} + \frac{m_\tau}{m_\mu}\frac{(\delta_\ell^{LL})_{23}(\delta_e^{RR})_{31}}{30}\right] + \frac{\alpha_1}{48\pi}\frac{(\delta_e^{LR})_{21}}{m_{\tilde\ell}^2}\left(\frac{m_{\tilde\ell}}{m_\mu}\right)\,, && (3.61)\\
A_R^{32} &\simeq -\frac{\alpha_1}{4\pi}\frac{t_\beta}{m_{\tilde\ell}^2}\frac{(\delta_e^{RR})_{32}}{60} + \frac{\alpha_1}{48\pi}\frac{(\delta_\ell^{RL})_{32}}{m_{\tilde\ell}^2}\left(\frac{m_{\tilde\ell}}{m_\tau}\right)\,. && (3.62)
\end{aligned}
$$

Besides $\ell_i \to \ell_j\gamma$, there are also other promising LFV channels, such as $\ell_i \to \ell_j\ell_k\ell_k$ and μ-e conversion in nuclei, that could be measured with the upcoming experimental sensitivities. However, within SUSY models, these processes are typically dominated by the dipole transition $\ell_i \to \ell_j\gamma^*$ leading to the unambiguous prediction,

$$
\begin{aligned}
\frac{\mathrm{BR}(\ell_i \to \ell_j\ell_k\bar\ell_k)}{\mathrm{BR}(\ell_i \to \ell_j\bar\nu_j\nu_i)} &\simeq \frac{\alpha_{el}}{3\pi}\left(\log\frac{m_{\ell_i}^2}{m_{\ell_k}^2} - 3\right)\frac{\mathrm{BR}(\ell_i \to \ell_j\gamma)}{\mathrm{BR}(\ell_i \to \ell_j\bar\nu_j\nu_i)}\,,\\
\mathrm{CR}(\mu \to e \text{ in N}) &\simeq \alpha_{\rm em} \times \mathrm{BR}(\mu \to e\gamma)\,. && (3.63)
\end{aligned}
$$

Thus, an experimental confirmation of the above relations would be crucial to prove the dipole nature of the LFV transitions. This would provide a powerful tool to discriminate between different NP scenarios as, for instance, SUSY and LHT models, as the latter do not predict a dipole dominance for $\ell_i \to \ell_j\ell_k\ell_k$ [73].

Additional and sizable contributions to LFV decays may arise from the Higgs sector by means of the effective LFV Yukawa interactions induced by non-holomorphic terms [173]; hence, in general, the expectations of (3.63) can be violated [174, 175, 176, 177, 178, 179, 180]. However, these effects become relevant only if $\tan\beta = \mathcal{O}(40-50)$ and if the Higgs masses are roughly one order of magnitude lighter then the slepton masses [174, 175, 176, 177, 178, 179, 180]. The last condition never occurs in our scenarios, hence Higgs mediated LFV effects are safely negligible in our analysis.

3.3 $\Delta F = 0$ Processes

3.3.1 Electric Dipole Moments

As the SM predictions for the electric dipole moments are very far from the present experimental resolutions, the EDMs represent very clean probes of NP effects. Given that the EDMs are CP-violating but flavour conserving observables, they do not require in principle any source of flavour violation, hence, we refer to them as $\Delta F = 0$ processes. Yet, they can also be generated by two $\Delta F = 1$ transitions, in which case one refers to *"flavoured"* EDMs.

Indeed, within a MSSM framework with flavour violating soft terms, large and potentially visible effects in the *"flavoured"* EDMs are typically expected [181, 129, 182]. In particular, when NP sources of flavour violation generating $b \to s$ transitions are assumed, the chromo-EDM (CEDM) and the EDM of the strange quark are unambiguously predicted. Unfortunately, an issue which is still unclear at present is the impact of the strange quark CEDM and EDM on the EDMs of physical systems like the neutron or heavy atoms like the

Thallium or the Mercury. The main source of uncertainty comes from the evaluation of the relevant hadronic matrix elements that should be ultimately evaluated by means of lattice QCD techniques. As a result, it is not possible at present to correlate or to constrain CPV processes in B-physics by means of the EDMs of physical systems that are induced by the strange quark (C)EDM. Therefore, in our analysis, we only monitor the predictions for the strange quark (C)EDM generated by sizable CP violating effects in the flavour observables.

If in the future there will be theoretical improvements enabling us to relate in a reliable way the strange quark (C)EDM to physical quantities, we could make use of additional observables, i.e. the EDMs of several systems, to test the NP theory that is at work, provided some NP signals in CPV B_s systems would appear.

In the following, we report the relevant expressions for the *"flavoured"* EDMs including the dominant beyond-leading-order (BLO) effects [181, 129, 182]. In fact, as shown in [181, 129, 182] BLO effects dominate over the leading-order (LO) ones in a large region of the parameter space, hence, their inclusion in the evaluation of the hadronic EDMs is essential.

Although our numerical results have been obtained including the full set of contributions, for simplicity, we report the dominant contributions to the hadronic EDMs.

The dominant gluino/squark contribution to the down-quark (C)EDMs is

$$\left\{\frac{d_{d_i}}{e},\ d^c_{d_i}\right\}_{\tilde g} = -\frac{\alpha_s}{4\pi}\frac{m_b}{\tilde m^2}\frac{M_{\tilde g}\mu}{\tilde m^2}t_\beta\frac{f^d_{\tilde g}(x_g)}{1+\epsilon t_\beta}\mathrm{Im}\left[(\delta^{LL}_d)_{i3}(\delta^{RR}_d)_{3i}\right]\,, \tag{3.64}$$

where the loop functions satisfy $f^d_{\tilde g}(1) = \{4/135,\ 11/180\}$.

Similarly, the corresponding prediction for the up-quark (C)EDMs is

$$\left\{\frac{d_u}{e},\ d^c_u\right\}_{\tilde g} = -\frac{\alpha_s}{4\pi}\frac{m_{u_k}}{\tilde m^2}\frac{M_{\tilde g}A_{u_k}}{\tilde m^2}f^u_{\tilde g}(x_g)\mathrm{Im}\left[(\delta^{LL}_u)_{1k}(\delta^{RR}_u)_{k1}\right]\,, \tag{3.65}$$

where $k = 2,3$, $A_{u_2,u_3} = A_{c,t}$ and $f^u_{\tilde g}(1) = \{-8/135,\ 11/180\}$.

The first $H^\pm$ effects to the (C)EDMs appear at the BLO [182, 181, 129] and they are well approximated by

$$\left\{\frac{d_{d_i}}{e},\ d^c_{d_i}\right\}_{H^\pm} = -\frac{\alpha_2}{16\pi}\frac{m_b}{M^2_{H^\pm}}\frac{m_t^2}{M_W^2}\frac{(1-\epsilon t_\beta)\epsilon_R t_\beta}{3(1+\epsilon t_\beta)^2}\mathrm{Im}\left[V^*_{3i}(\delta^{RR}_d)_{3i}\right]f_{H^\pm}(y_t)\,, \tag{3.66}$$

where $f_{H^\pm}(1) = \{-7/9, -2/3\}$.

Charginos contribute to the EDMs already at the LO but the corresponding (C)EDMs are suppressed by the light quark masses m_{d_i}. At the BLO, a new effect proportional to m_b is generated by the charged-Higgsino/squark diagrams leading to [182, 181, 129]

$$\left\{\frac{d_{d_i}}{e},\ d^c_{d_i}\right\}_{\tilde H^\pm} = \frac{\alpha_2}{16\pi}\frac{m_b}{\tilde m^2}\frac{m_t^2}{M_W^2}\frac{A_t\mu}{\tilde m^2}t_\beta\frac{\epsilon_R t_\beta}{3(1+\epsilon t_\beta)^2}\mathrm{Im}\left[V^*_{3i}(\delta^{RR}_d)_{3i}\right]f_{\tilde H^\pm}(x_\mu)\,, \tag{3.67}$$

where $x_\mu = \mu^2/\tilde m^2$ and $f_{\tilde H^\pm}(1) = \{-5/18, -1/6\}$. The full expressions of the loop functions $f_{\tilde g}(x_g)$, $f_{H^\pm}(x)$ and $f_{\tilde H^\pm}(x)$ are listed in appendix A. For equal SUSY masses and $\mu > 0$, it turns out that $\epsilon_R = \epsilon/3 = \alpha_s/9\pi$.

So far, we have presented the dominant contributions to the quark (C)EDMs assuming the presence of right-handed currents, hence of RR MIs. Since in the present work we are also

interested in models with purely left-handed currents, it is useful to show also the dominant (one loop induced) contributions to the (C)EDMs arising within this scenario. They read

$$\left\{\frac{d_{d_i}}{e},\ d^c_{d_i}\right\}_{\tilde{H}^\pm} = \frac{\alpha_2}{16\pi}\frac{m_{d_i}}{\tilde{m}^2}\frac{m_t^2}{m_W^2}\frac{A_t\mu}{\tilde{m}^2}\frac{t_\beta}{(1+\epsilon t_\beta)}\ \mathrm{Im}\left[V^*_{3i}(\delta_d^{LL})_{3i}\right] g_{\tilde{H}^\pm}(x_\mu)\,, \tag{3.68}$$

where $g_{\tilde{H}^\pm}(1) = \{2/15,\ 1/10\}$, with its complete expressions given in appendix A. Eq. (3.68) shows that, in this case, the (C)EDMs are suppressed by the external light quark masses, in contrast to the case where also RR MIs are non-vanishing. The analogous expression for up-type quarks, namely $d^{(c)}_{u_i}$, is of order $d^{(c)}_d/d^{(c)}_u \sim [m_t^2/(m_b^2 t_\beta^2)]\times[A_t\mu/\mu^2]\times t_\beta$ and thus safely negligible.

Passing to the leptonic sector, the dominant contribution to the electron EDM arises from the one-loop exchange of binos/sleptons, and the corresponding EDM is given as

$$\begin{aligned}\frac{d_e}{e} = -\frac{\alpha_1}{4\pi}\frac{M_1}{m^2_{\tilde{\ell}}}\Big\{ & \mathrm{Im}[(\delta_\ell^{LR})_{1k}(\delta_e^{RR})_{k1} + (\delta_\ell^{LL})_{1k}(\delta_\ell^{LR})_{k1}]\, f_{3n}(x_1) + \mathrm{Im}[(\delta_\ell^{LL})_{1k}(\delta_\ell^{LR})_{kl}(\delta_e^{RR})_{l1} \\ & + (\delta_\ell^{LR})_{1k}(\delta_e^{RR})_{kl}(\delta_e^{RR})_{l1} + (\delta_\ell^{LL})_{1k}(\delta_\ell^{LL})_{kl}(\delta_\ell^{LR})_{l1}]\, f_{4n}(x_1)\Big\}\,,\end{aligned} \tag{3.69}$$

where $k,l = 2,3$, $(\delta_\ell^{LR})_{33} = -m_\tau(A_\tau + \mu t_\beta)/m^2_{\tilde{\ell}}$ and $f_{3n}(1) = -1/12$.

One of the most peculiar features of the *flavoured* EDMs is that they might be proportional to the heaviest fermionic masses m_t, m_b and m_τ instead of the lightest ones, as it happens in the case of flavour *blind* phases. This huge enhancement factor can bring the (C)EDMs close to the current and future experimental sensitivities, providing a splendid opportunity to probe the flavour structure of the MSSM.

The main obstacles to fully exploit the NP sensitivity of the EDMs is that experimentally, one measures the EDMs of composite systems, as heavy atoms, molecules or the neutron EDM while the theoretical predictions are relative to the EDMs of constituent particles, *i.e.* quarks and leptons, thus a matching between quarks and leptons EDMs into physical EDMs is necessary and this induces sizable uncertainties related to QCD, nuclear and atomic interactions.

The quark (C)EDMs and lepton EDMs can be obtained starting from the effective CP-odd Lagrangian

$$\mathcal{L}_{\rm eff} = -\sum_{i=u,d,s,e,\mu} i\frac{d_f}{2}\bar{\psi}_i(F\cdot\sigma)\gamma_5\psi_i - \sum_{i=u,d,s} i\frac{d^c_f}{2}g_s\bar{\psi}_i(G\cdot\sigma)\gamma_5\psi_i + \sum_{i,j} C_{ij}\,(\bar{\psi}_i\psi_i)(\bar{\psi}_j i\gamma_5\psi_j) + \ldots\,, \tag{3.70}$$

where the first and the second terms of (3.70) are the fermion EDMs and CEDMs, respectively, while the coefficients C_{ij} are relative to the dimension-six CP-odd four-Fermi interaction operators.

Among the various atomic and hadronic EDMs, a particularly important role is played by the thallium EDM ($d_{\rm Tl}$) and the neutron EDM (d_n). They can be estimated as [183, 184, 185, 186, 187]

$$d_{\rm Tl} = -585\, d_e - e\, 43\,\mathrm{GeV}\, C_S^{(0)}\,, \tag{3.71}$$

$$d_n = (1\pm 0.5)\Big[1.4\,(d_d - 0.25\,d_u) + 1.1\,e\,(d^c_d + 0.5\,d^c_u)\Big]\,, \tag{3.72}$$

where $C_s^{(0)}$ is given by a combination of the coefficients C_{ij} [186, 187]. However, when $d_{\rm Tl}$ and d_n are generated by flavour effects, as in our case, the contributions they receive from $C_s^{(0)}$ are always very suppressed hence, safely negligible [129].

3.3.2 The Anomalous Magnetic Moment of the Muon

The possibility that the anomalous magnetic moment of the muon (we define $a_\mu = (g-2)_\mu/2$), which has been measured very precisely in the last few years [188], provides a first hint of physics beyond the SM has been widely discussed in the literature. Despite substantial progress both on the experimental and on the theoretical sides, the situation is not completely clear yet (see [189] for an updated discussion).

Most recent analyses based on e^+e^- data converge towards a 3σ discrepancy [16] in the 10^{-9} range [189]:

$$\Delta a_\mu = a_\mu^{\rm exp} - a_\mu^{\rm SM} \approx (3 \pm 1) \times 10^{-9} \ . \tag{3.73}$$

The possibility that the present discrepancy may arise from errors in the determination of the hadronic leading-order contribution to Δa_μ seems to be unlikely, as recently stressed in [191].

The main SUSY contribution to $a_\mu^{\rm MSSM}$ is usually provided by the loop exchange of charginos and sneutrinos [192]. The supersymmetric contributions to a_μ are correctly reproduced by the following approximate expression

$$\begin{aligned} a_\mu^{\rm MSSM} &= \frac{\alpha_2}{4\pi}\frac{m_\mu^2}{m_{\tilde\ell}^2} t_\beta \left[\frac{\mu M_2}{(M_2^2-\mu^2)}\left(\frac{1}{2} f_{2n}(x_2,x_\mu) - f_{2c}(x_2,x_\mu)\right)\right. \\ &+ \left. \tan^2\theta_W \left(\frac{\mu M_1}{m_{\tilde\ell}^2} f_{3n}(x_1) + \frac{1}{2}\frac{\mu M_1}{(M_1^2-\mu^2)} f_{2n}(x_1,x_\mu)\right)\right] . \end{aligned} \tag{3.74}$$

In the limit of degenerate SUSY masses one can easily find that

$$\frac{a_\mu^{\rm MSSM}}{1\times 10^{-9}} \approx 1.5 \left(\frac{\tan\beta}{10}\right)\left(\frac{300\ \text{GeV}}{m_{\tilde\ell}}\right)^2 \text{sgn}\,\mu\,. \tag{3.75}$$

The most relevant feature of (3.75) is that the sign of $a_\mu^{\rm MSSM}$ is fixed by the sign of the μ term (given $M_2 > 0$) so that the solution $\mu > 0$ is strongly favoured.

3.4 Correlations between $\Delta F = 0$ and $\Delta F = 1$ Processes in the Leptonic Sector

In the following, we discuss the implications of a potential evidence or improved upper bound of $\text{BR}(\mu \to e\gamma)$ at the expected sensitivities of MEG, namely at the level of $\text{BR}(\mu \to e\gamma) \gtrsim 10^{-13}$ [204]. In particular, we will exploit the correlations among $\text{BR}(\mu \to e\gamma)$, the leptonic electric dipole moments (EDMs) and the SUSY contributions to $(g-2)_\mu$ [205]. Finally, we discuss the prospects for the observation of LFV signals in τ decays [205]. The corresponding numerical analysis in a concrete model will be performed in sec. 6.

3.4.1 $(g-2)_\mu$ vs. $\text{BR}(\ell_i \to \ell_j\gamma)$

An observation of $\mu \to e\gamma$ would provide an unambiguous evidence of NP but, unfortunately, not a direct test of the LFV source, as $\text{BR}(\mu \to e\gamma)$ depends also on other SUSY parameters like the particle masses and $\tan\beta$. While the latter parameters should be ultimately determined at the LHC/linear collider experiments, it would be desirable to access them by

[16] The most recent τ-based estimate of the muon magnetic anomaly is found to be 1.9 standard deviations lower than the SM prediction [190], coming closer to the e^+e^- value.

observable	SM prediction	exp. current	exp. future
$S_{\psi\phi}$	$\simeq 0.036$ [81]	$0.81^{+0.12}_{-0.32}$ [1]	$\simeq 0.02$ [193]
$S_{\phi K_S}$	$\sin 2\beta + 0.02 \pm 0.01$ [2]	0.44 ± 0.17 [1]	$(2-3)\%$ [194]
$S_{\eta' K_S}$	$\sin 2\beta + 0.01 \pm 0.01$ [2]	0.59 ± 0.07 [1]	$(1-2)\%$ [194]
$A_{\rm CP}(b \to s\gamma)$	$\left(-0.44^{+0.14}_{-0.24}\right)\%$ [195]	$(-0.4 \pm 3.6)\%$ [1]	$(0.4-0.5)\%$ [194]
$\langle A_7 \rangle$	$(3.4^{+0.4}_{-0.5})10^{-3}$ [140]		
$\langle A_8 \rangle$	$(-2.6^{+0.4}_{-0.3})10^{-3}$ [140]		
$\langle A_9 \rangle$	$(0.1^{+0.1}_{-0.1})10^{-3}$ [140]		
$\lvert d_e \rvert$ $(e\,{\rm cm})$	$\simeq 10^{-38}$ [196]	$< 1.6 \times 10^{-27}$ [197]	$\simeq 10^{-31}$ [196]
$\lvert d_n \rvert$ $(e\,{\rm cm})$	$\simeq 10^{-32}$ [196]	$< 2.9 \times 10^{-26}$ [198]	$\simeq 10^{-28}$ [196]
${\rm BR}(B_s \to \mu^+\mu^-)$	$(3.60 \pm 0.37)10^{-9}$	$< 5.8 \times 10^{-8}$ [146]	$\simeq 10^{-9}$ [199]
${\rm BR}(B_d \to \mu^+\mu^-)$	$(1.08 \pm 0.11)10^{-10}$	$< 1.8 \times 10^{-8}$ [146]	
${\rm BR}(B \to X_s\gamma)$	$(3.15 \pm 0.23)10^{-4}$ [200]	$(3.52 \pm 0.25)10^{-4}$ [1]	
${\rm BR}(B \to X_s\ell^+\ell^-)$	$(1.59 \pm 0.11)10^{-6}$ [201]	$(1.59 \pm 0.49)10^{-6}$ [202, 203]	
${\rm BR}(B \to \tau\nu)$	$(1.10 \pm 0.29)10^{-4}$	$(1.73 \pm 0.35)10^{-4}$ [112]	

Table 6: SM predictions and current/expected experimental sensitivities for the observables most relevant for our analysis. The branching ratio of $B \to X_s\ell^+\ell^-$ refers to the low dilepton invariant mass region, $q^2_{\ell^+\ell^-} \in [1,6]\,{\rm GeV}^2$. For the SM prediction of ${\rm BR}(B \to \tau\nu)$, see also (3.54): ${\rm BR}(B \to \tau\nu) = (0.80 \pm 0.12) \times 10^{-4}$.

exploiting the NP sensitivity of additional low energy observables. In particular, since both $(g-2)_\mu$ and ${\rm BR}(\ell_i \to \ell_j\gamma)$ are governed by dipole transitions, the SUSY contributions to these observables are well correlated and their combined analysis provides a powerful tool to get access to the related LFV source.

For a natural choice of the SUSY parameters, $t_\beta = 10$ and a degenerate SUSY spectrum at $\tilde m = 300\,{\rm GeV}$, it turns out that $\Delta a_\mu^{\rm SUSY} \simeq 1.5 \times 10^{-9}$ and the current observed anomaly can be easily explained. Assuming a degenerate SUSY spectrum, it is straightforward to find the correlation between $\Delta a_\mu^{\rm SUSY}$ and the branching ratios of $\ell_i \to \ell_j\gamma$

$$
\begin{aligned}
{\rm BR}(\mu \to e\gamma) &\approx 2 \times 10^{-12} \left[\frac{\Delta a_\mu^{\rm SUSY}}{3 \times 10^{-9}}\right]^2 \left|\frac{(\delta_\ell^{LL})_{21}}{10^{-4}}\right|^2 , \\
{\rm BR}(\tau \to \mu\gamma) &\approx 8 \times 10^{-8} \left[\frac{\Delta a_\mu^{\rm SUSY}}{3 \times 10^{-9}}\right]^2 \left|\frac{(\delta_\ell^{LL})_{32}}{10^{-2}}\right|^2 ,
\end{aligned}
\tag{3.76}
$$

where we have assumed that the MIs $(\delta_\ell^{LL})_{ij}$ provide the dominant contributions to ${\rm BR}(\ell_i \to \ell_j\gamma)$.

Eq. (3.76) tell us that, as long as the $(g-2)_\mu$ anomaly finds an explanation in SUSY theories, ${\rm BR}(\ell_i \to \ell_j\gamma)$ are predicted once we specify the LFV sources.

We emphasize that the extraordinary experimental sensitivities of the MEG experiment

Observable	Exp. bound on $(\delta_\ell^{LL})_{ij}$	$(\delta_\ell^{LL})_{ij}$ in RVV
$\mathrm{BR}(\mu \to e\gamma)$	$\lvert(\delta_\ell^{LL})_{21}\rvert < 3 \times 10^{-4}$	$\sim (0.3-1) \times 10^{-4}$
$\mathrm{BR}(\tau \to e\gamma)$	$\lvert(\delta_\ell^{LL})_{31}\rvert < 6 \times 10^{-2}$	$\sim (2-6) \times 10^{-3}$
$\mathrm{BR}(\tau \to \mu\gamma)$	$\lvert(\delta_\ell^{LL})_{32}\rvert < 4 \times 10^{-2}$	$\sim (0.3-1) \times 10^{-1}$

Table 7: Bounds on the effective LFV couplings $(\delta_\ell^{LL})_{ij}$ from the current experimental bounds on the radiative LFV decays of τ and μ leptons (see tab. 5) by setting $\Delta a_\mu^{\mathrm{SUSY}} = 3 \times 10^{-9}$. The expectations for the $(\delta_\ell^{LL})_{ij}$'s within the RVV2 model [51, 206, 62] are reported in the last column. The bound on $(\delta_\ell^{LL})_{21}$ scales as $[\mathrm{BR}(\mu \to e\gamma)_{exp}/1.2 \times 10^{-11}]^{1/2}$. The scaling properties for the other flavour transitions are obtained analogously.

looking for $\mu \to e\gamma$ offer a unique chance to obtain the first evidence for NP in low-energy flavour processes. Should this be the case, several leptonic observables related to $\mu \to e\gamma$ are also likely to show NP signals, i.e. the $(g-2)_\mu$, the electron EDM d_e but also other LFV processes like $\mu \to eee$ and $\mu - e$ conversion in nuclei.

In order to get a more concrete idea of where we stand, in tab. 7, we report the bounds on the MIs $(\delta_\ell^{LL})_{ij}$ arising from the current experimental bounds on $\mathrm{BR}(\ell_i \to \ell_j\gamma)$ imposing $\Delta a_\mu^{\mathrm{SUSY}} = 3 \times 10^{-9}$, corresponding to the central value of the $(g-2)_\mu$ anomaly. Moreover, in the last column of tab. 7, we also show the expectations for the MIs $(\delta_\ell^{LL})_{ij}$ within a *non-abelian* $SU(3)$ model that we will analyze in detail in following sections: the RVV2 model [51, 206, 62]. Interestingly enough, the expected experimental reaches of MEG (for $\mu \to e\gamma$) and of a SuperB factory (for $\tau \to \mu\gamma$) would most likely probe the RVV model, provided we assume the explanation of the $(g-2)_\mu$ anomaly in terms of SUSY effects.

3.4.2 Leptonic EDMs vs. $\mathrm{BR}(\ell_i \to \ell_j\gamma)$

Within a SUSY framework, CP-violating sources are naturally induced by the soft SUSY breaking terms through *i)* flavour blind F-terms [196, 207] and *ii)* flavour dependent terms [181]. It seems quite likely that the two categories *i)* and *ii)* of CP violation are controlled by different physical mechanisms, thus, they may be distinguished and discussed independently.

In the case *i)*, the corresponding CP-violating phases generally lead to large electron and neutron EDMs as they arise already at the one-loop level. For example, when $t_\beta = 10$ and $m_{\tilde{\ell}} = 300\,\mathrm{GeV}$ it turns out that

$$d_e \sim 6 \times 10^{-25}(\sin\theta_\mu + 10^{-2}\sin\theta_A)\, e\,\mathrm{cm}\,, \tag{3.77}$$

while in the case *ii)* the leptonic EDMs, induced by *flavour dependent* phases (flavoured EDMs), read

$$d_e \sim 10^{-22} \times \mathrm{Im}((\delta_e^{RR})_{13}(\delta_\ell^{LL})_{31})\, e\,\mathrm{cm}\,. \tag{3.78}$$

One of the most peculiar features disentangling the EDMs as induced by *flavour blind* or *flavour dependent* phases regards their ratios. In particular,

$$\begin{aligned}
\frac{d_e}{d_\mu} &= \frac{m_e}{m_\mu} && \textit{flavour blind}\text{ phases,}\\
\frac{d_e}{d_\mu} &= \frac{\Sigma_{k=2,3}\mathrm{Im}((\delta_e^{RR})_{1k}(\delta_\ell^{LL})_{k1})}{\mathrm{Im}((\delta_e^{RR})_{23}(\delta_\ell^{LL})_{32})} && \textit{flavour dependent}\text{ phases}\,.
\end{aligned} \tag{3.79}$$

In the case of *flavour blind* phases, the current bound $d_e < 1.7 \times 10^{-27}\, e\,\mathrm{cm}$ [81] implies that $d_\mu \lesssim 3.5 \times 10^{-25}\, e\,\mathrm{cm}$. On the contrary, in the presence of *flavour dependent* phases, the leptonic EDMs typically violate the naive scaling and values for $d_\mu > 2 \times 10^{-25}\, e\,\mathrm{cm}$ are still allowed.

Moreover, when the EDMs are generated by *flavour blind* phases, they are typically unrelated to flavour violating transitions [17]. On the contrary, the *flavoured* EDMs are closely related to LFV processes as they both arise from LFV effects and their correlated study would help to reconstruct the flavour structure responsible for LFV transitions.

We recall that the predictions for the leptonic EDMs within a pure SUSY see-saw model are highly suppressed [208, 209, 210], at a level well below any future (realistic) experimental resolution.

After imposing the current experimental bound on $\mathrm{BR}(\mu \to e\gamma)$, it turns out that $d_e \lesssim 10^{-34}$ $e$cm, irrespective of the details of the heavy/light neutrino sectors. On the contrary, when the see-saw mechanism is embedded in a SUSY GUT scheme, as $SU(5)_{\mathrm{RN}}$, d_e may naturally saturate its current experimental upper bound. As we will show in sec.6, also the RVV model naturally predicts large (observable) values for d_e.

Hence, any experimental evidence for the leptonic EDMs at the upcoming experiments would point towards an underlying theory with either new sources of *flavour blind* phases or new CP and flavour violating structures beyond those predicted by a MFV scenario. In fact, as shown by (3.69), a crucial ingredient to generate non-vanishing EDMs is the presence of right-handed mixing angles and hence of right-handed currents. The latter are unavoidably generated in SUSY GUT scenarios as $SU(5)_{\mathrm{RN}}$ or $SU(10)$ through the CKM matrix and also in a broad class of abelian and non-abelian flavour models.

A simultaneous evidence for the electronic EDM d_e and of $\mu \to e\gamma$ at the MEG experiment, could most likely suggest the presence of *flavoured* CP violating phases.

Noteworthily enough, the synergy of low-energy experiments, as the leptonic EDMs and LFV processes (like $\mu \to e\gamma$), that are in principle unrelated, provides an important tool to unveil the anatomy of the soft SUSY sector.

4 Soft SUSY Breaking and FCNC Phenomena

4.1 Preliminaries

The still elusive explanation of the pattern of SM fermion masses and mixing angles constitutes one of the main issues of the SM: the so-called *"SM flavour problem"*. In addition, if nature is supersymmetric, the *"flavour problem"* acquires a new aspect: whenever fermions and corresponding sfermions have mass matrices which are not diagonalized by the same rotation, new flavour mixings occur at the gaugino-fermion-sfermion vertices, generally leading to unacceptably large contributions to FCNC and/or CP-violating observables, of which K^0 mixing, ϵ_K and $\mu \to e\gamma$ are the most problematic.

The most popular protection mechanisms to suppress such unwanted contributions are

- *Decoupling.* The sfermion mass scale is taken to be very high. Still, such a scenario may be probed at the LHC through non-decoupling effects such as the super-oblique parameters [211].

[17] A relevant exception is represented by the FBMSSM where it has been shown that there exist correlations among CP and flavour violating transitions in the B-meson systems and the EDMs [68].

- *Degeneracy*. The sfermion masses are degenerate to a large extent, leading to a strong GIM suppression. Such degeneracy could naturally arise from models with gauge-mediated supersymmetry breaking (GMSB) – or with some other flavour-blind mechanism of SUSY breaking mediation – if the mediation scale is low.[18]

- *Alignment*. The quark and squark mass matrices are aligned, so that the flavour-changing gaugino-sfermion-fermion couplings are suppressed [23].

- *MFV*. Flavour violation is assumed to be entirely described by the CKM matrix even in theories beyond the SM [5].

We recall here that the MFV symmetry principle in itself does not forbid the presence of *flavour blind* CP violating sources [64, 65, 66, 67, 69, 68, 70, 214, 215], hence a MFV MSSM suffers, in general, from the same SUSY CP problem as the ordinary MSSM. Either an extra assumption or a mechanism accounting for a natural suppression of these CPV phases is desirable. The authors of [5] proposed the extreme situation where the SM Yukawa couplings are the only source of CPV. In contrast, in [71], such a strong assumption has been relaxed and the following generalized MFV ansatz has been proposed: the SUSY breaking mechanism is *flavour blind* and CP conserving and the breaking of CP only arises through the MFV compatible terms breaking the *flavour blindness*. That is, CP is preserved by the sector responsible for SUSY breaking, while it is broken in the flavour sector. While the generalized MFV ansatz still accounts for a natural solution of the SUSY CP problem, it also leads to peculiar and testable predictions in low energy CP violating processes [71].

As discussed in the previous section, in the general SUSY framework it is useful to parameterize non-MFV interactions in terms of the MIs $(\delta^{AB}_{d,u})_{ij}$ with $(A, B) = (L, R)$ and $(i, j = 1, 2, 3)$ on which the present data on FCNC processes put quite severe constraints [61, 53, 172]. Large departures from SM expectations are obviously still allowed in such a model-independent approach.

While a model-independent analysis gives a global picture of still allowed deviations from the SM, its weakness lies in the fact that the suppression of FCNC processes is not achieved by some symmetry principle but basically by fine tuning the MIs so that existing experimental bounds are kept under control. Moreover, such an approach does not address the question of the hierarchies of the quark mixings in the CKM matrix nor the hierarchies of the quark masses. Analogous comments apply to the lepton sector.

Much more ambitious in this respect are supersymmetric models containing flavour symmetries that relate the structure of fermion and sfermion mass matrices. Such symmetries, while being at the origin of the pattern of fermion masses and mixings, can at the same time provide the sufficient suppression of FCNC and CP-violating phenomena by means of the *degeneracy* or *alignment* protection mechanisms discussed above. Moreover, as we will see in the context of our numerical analysis, SUSY flavour models imply certain characteristic patterns of flavour and CP violation that can be confirmed or falsified with the upcoming experimental sensitivities.

Supersymmetric models with flavour symmetries have been considered extensively in the literature. They can be naturally divided into two broad classes depending on whether they are based on abelian or *non-abelian* flavour symmetries. They can be considered as generalizations of the Froggatt-Nielsen mechanism [216]: the flavour symmetry is spontaneously

[18]In GMSB models with a high messenger scale, gravity-mediated contributions cannot be neglected. The phenomenology of such gauge-gravity "hybrid" models is discussed in [212, 213].

broken by the vacuum expectation value of one or more "flavon" fields Φ_i and the hierarchical patterns in the fermion mass matrices can then be generated by means of the suppression factors $(\langle\Phi_i\rangle/M)^n$, where M is the scale of the breaking of the flavour symmetry and the power n depends on the group charges of the fermions involved in the Yukawa couplings, generating the mass terms.

4.2 Abelian Flavour Models

There is a rich literature on models based on abelian flavour symmetries [23, 24, 25, 26, 27, 28, 29, 30, 31, 32, 33, 34, 35, 36, 37]. While the simplest case, where a single $U(1)_F$ group is employed, is disfavoured since it leads to unacceptably large contributions to FCNC processes as ϵ_K and ΔM_K [23, 37], more successful models are realized through the abelian flavour group $U(1)_{F1} \times U(1)_{F2}$ [23]. In this last case, the tight FCNC constraints are naturally accounted for thanks to a precise alignment of the down-quark and down-squark mass matrices [23].

On the other hand, the most prominent signature of this class of models are typically large effects in $D^0 - \bar{D}^0$ mixing. In fact, abelian flavour symmetries do not impose any restriction on the mass splittings between squarks of different generations therefore they are expected to be non-degenerate with natural order one mass splittings.

In particular, a mass splitting between the first two generations of left-handed squarks unavoidably implies a $(1 \leftrightarrow 2)$ flavour transition in the up-squark sector of order $(\delta_u^{LL})_{21} \sim \lambda$.

This can be easily understood by recalling that the $SU(2)_L$ gauge symmetry relates the left-left blocks of up and down squark matrices, i.e. $(M_u^2)^{LL}$ and $(M_d^2)^{LL}$ respectively, in such a way that $(M_u^2)^{LL} = V^*(M_d^2)^{LL}V^{\mathrm{T}}$. In turn, the expansion of this relation at the first order in λ implies that

$$(M_u^2)_{21}^{LL} = \left[V^*(M_d^2)^{LL}V^{\mathrm{T}}\right]_{21} \simeq (M_d^2)_{21}^{LL} + \lambda\left(\tilde{m}_2^2 - \tilde{m}_1^2\right) \ . \tag{4.1}$$

Thus, even for $(M_d^2)_{21}^{LL} = 0$, which is approximately satisfied in alignment models, there are irreducible flavour violating terms in the up squark sector driven by the CKM as long as the left-handed squarks are splitted in mass. This is opposite to the case of non abelian flavour symmetries which we discuss now.

4.3 Non-abelian Flavour Models

In contrast to abelian models, where there is a lot of freedom in fixing the charges of the SM fermions under the flavour symmetry, non-abelian models [38, 39, 40, 41, 42, 43, 44, 45, 46, 47, 48, 49, 50, 51, 52] are quite predictive for fermion mass matrices once the pattern of symmetry breaking is specified.

Moreover, non-abelian flavour models predict very small NP contributions for $(1 \leftrightarrow 2)$ flavour transitions, since, if the non-abelian symmetry was an exact symmetry, then at least the first two generations of squarks are degenerate, which would lead to a vanishing NP contribution to $K^0 - \bar{K}^0$ and $D^0 - \bar{D}^0$ mixings. However, as we will find in sec. 6.3, the violation of the symmetry is strong enough to produce large effects in the observable ϵ_K.

There are many candidates for the flavour symmetry group G_F, each having distinct symmetry breaking patters. In general, G_F must be contained in the full global $U(3)^5$ symmetry group of the SM in the limit of vanishing Yukawa couplings. In particular, a lot of attention is received by models with a $U(2)$ symmetry [47, 48] motivated by the large top mass, and also models with $SU(3)$ symmetry [49, 50] which are additionally able to naturally predict an

almost maximal atmospheric neutrino mixing angle $\theta_{23} \approx 45°$ and to suggest a near maximal solar mixing angle $\theta_{12} \approx 30°$.

4.4 Running Effects in Flavour Models

Since the flavour models discussed in the previous subsections predict the pattern of off-diagonal elements of the squark mass matrices at the GUT scale while for the calculation of physical observables, their values at low energies are relevant, we now discuss the renormalization group (RG) evolution of these elements. In particular, crucial questions are whether these off-diagonal elements are strongly reduced or enhanced in the running, whether they mix with each other and whether they are generated if they vanish at the initial scale. In short, the question is whether the textures of the squark mass matrices predicted by the flavour models are RG stable. We will disregard off-diagonalities in the trilinear couplings, i.e. LR and RL MIs, as well as the slepton sector in the following discussion.

Studies of these running effects in the context of the MSSM with Minimal Flavour Violation have been performed in [217, 69].

A close inspection of the relevant RG equations (RGEs) [218] shows that for $\mathbf{m}_U^2$ and $\mathbf{m}_D^2$, i.e. the RR MIs [19], all mixing terms are suppressed by 1st or 2nd generation Yukawa couplings and can therefore be safely neglected. In fact, neglecting 1st and 2nd generation Yukawa couplings, the RGEs for the off-diagonal elements of $\mathbf{m}_{U,D}^2$ read at the one-loop level

$$16\pi^2 \frac{d}{dt}(\mathbf{m}_U^2)_{ij} \overset{i\neq j}{=} 2\left(y_t^2\right)(\mathbf{m}_U^2)_{ij}(\delta_{i3}+\delta_{j3}) + 4(h_u h_u^\dagger)_{ij}\,, \tag{4.2}$$

$$16\pi^2 \frac{d}{dt}(\mathbf{m}_D^2)_{ij} \overset{i\neq j}{=} 2\left(y_b^2\right)(\mathbf{m}_D^2)_{ij}(\delta_{i3}+\delta_{j3}) + 4(h_d h_d^\dagger)_{ij}\,, \tag{4.3}$$

where $t = \log(\mu/\mu_0)$. As can be easily seen, $(\mathbf{m}_{U,D}^2)_{12}$ are RG invariant in this approximation; we have checked that this holds numerically to an excellent approximation even if light generation Yukawas and two-loop effects are taken into account.

Concerning the remaining entries, we find that their values at low energies are well approximated by

$$\left(\mathbf{m}_U^2\right)_{13} \simeq 0.87\left(\mathbf{m}_U^2\right)_{13}^0\,, \qquad \left(\mathbf{m}_U^2\right)_{23} \simeq 0.82\left(\mathbf{m}_U^2\right)_{23}^0\,, \tag{4.4}$$

$$\left(\mathbf{m}_D^2\right)_{13} \simeq (1 - 0.10\,\tilde{t}^2 - 0.05\,\tilde{t}^4)\left(\mathbf{m}_D^2\right)_{13}^0\,, \tag{4.5}$$

$$\left(\mathbf{m}_D^2\right)_{23} \simeq (1 - 0.10\,\tilde{t}^2 - 0.05\,\tilde{t}^4)\left(\mathbf{m}_D^2\right)_{23}^0\,, \tag{4.6}$$

where we have defined $\tilde{t} = \tan\beta/50$, and where quantities with superscript 0 on the right-hand side denote the values at the GUT scale predicted by the particular flavour model considered, while those on the left-hand side are meant to be evaluated at the weak scale.

To summarize, the off-diagonal squark mass matrix elements in the RR sector are reduced by at most 15%, they do not mix among each other or with LL MIs, and they are not generated by the running once they vanish at the GUT scale.

The situation in the LL sector is different; there, also mixing takes place, and the elements can be generated by RG effects even if they vanish at the GUT scale. Of course, both these

[19] The trilinear coupling matrices $h_{u,d}$ and the soft masses $\mathbf{m}_{Q,U,D}^2$ used in this section correspond to the conventions of Martin and Vaughn [218] and are related to the trilinear couplings and to the soft masses in the convention of [113] through the relations $h_{u,d} = -A_{u,d}^T$ and $\mathbf{m}_Q^2 = m_Q^2$, $\mathbf{m}_{U,D}^2 = (m_{U,D}^2)^T$. See also appendix B for additional details.

effects are suppressed by combinations of CKM elements, since they would be absent if the CKM matrix were diagonal. The RG equation for the off-diagonal elements of $\mathbf{m}_Q^2$ reads

$$16\pi^2 \frac{d}{dt}(\mathbf{m}_Q^2)_{ij} \overset{i\neq j}{=} 2\left(y_{d,i}\, y_{d,j}\right)(\mathbf{m}_D^2)_{ij} + \left(y_b^2\right)(\mathbf{m}_Q^2)_{ij}(\delta_{i3}+\delta_{j3}) + y_t^2(\mathbf{m}_Q^2)_{ik}\lambda_{kj} + y_t^2(\mathbf{m}_Q^2)_{kj}\lambda_{ik} + \\ + y_t^2 2m_{H_u}^2\lambda_{ij} + 2y_t^2(\mathbf{m}_U^2)_{33}\lambda_{ij} + 2(h_u^\dagger h_u)_{ij} + 2(h_d^\dagger h_d)_{ij}\,, \tag{4.7}$$

where $\lambda_{ij} = V_{ti}^* V_{tj}$ and we have again neglected light generation Yukawas, except in the first term, which in the case of $(ij) = (23)$ is only suppressed by y_s/y_b, but unsuppressed by CKM angles and can therefore be comparable in size to the remaining terms.

Consequently we find that, numerically, the low-energy values of the $(\mathbf{m}_Q^2)_{ij}$ are well approximated by the following formulae,

$$\left(\mathbf{m}_Q^2\right)_{13} \simeq (0.91 - 0.05\,\tilde{t}^2)\left(\mathbf{m}_Q^2\right)_{13}^0 - \Delta m_{13}^2 - 0.09\left[\lambda_{12}\left(\mathbf{m}_Q^2\right)_{23}^0 + \lambda_{23}\left(\mathbf{m}_Q^2\right)_{12}^0\right]\,, \tag{4.8}$$

$$\left(\mathbf{m}_Q^2\right)_{23} \simeq (0.91 - 0.05\,\tilde{t}^2)\left(\mathbf{m}_Q^2\right)_{23}^0 - \Delta m_{23}^2 - 0.09\left[\lambda_{21}\left(\mathbf{m}_Q^2\right)_{13}^0 + \lambda_{13}\left(\mathbf{m}_Q^2\right)_{21}^0 + 0.02\tilde{t}^2\left(\mathbf{m}_D^2\right)_{23}^0\right]\,, \tag{4.9}$$

$$\left(\mathbf{m}_Q^2\right)_{12} \simeq \left(\mathbf{m}_Q^2\right)_{12}^0 - \Delta m_{12}^2 - 0.09\left[\lambda_{13}\left(\mathbf{m}_Q^2\right)_{32}^0 + \lambda_{32}\left(\mathbf{m}_Q^2\right)_{13}^0\right]\,, \tag{4.10}$$

where

$$\Delta m_{ij}^2 = \lambda_{ij}\left(0.33\, m_0^2 + 0.89\, M_{1/2}^2 + 0.03\, A_0^2 - 0.14\, M_{1/2}A_0\right)\,, \tag{4.11}$$

assuming CMSSM-like boundary conditions for the gaugino masses, trilinear couplings and the diagonal elements of sfermion mass matrices.

As in the RR sector, the Yukawa-induced reduction of the elements, cf. the first terms in (4.7) and (4.8)–(4.10), is only sizable in the $(13, 23)$ sectors. The terms in square brackets describe the mixing among the LL elements, while Δm_{ij}^2 describes the CKM-induced generation of LL MIs, which takes place even in a completely flavour blind situation at the GUT scale, such as in the CMSSM.

To summarize, the off-diagonal squark mass matrix elements in the LL sector mix among each other and they can be generated even if vanishing at the GUT scale; however, these effects are suppressed by combinations of CKM elements. Mixing of RR elements into LL elements only takes place in the 23-sector and is suppressed by a factor $y_s y_b/y_t^2$.

Finally, let us also remind that the attained values for the MIs δ_{ij} are renormalization scale dependent as the diagonal elements are strongly affected by RGE effects.

5 Strategy

One of our main goals in the subsequent sections is to investigate the patterns of flavour violation in flavour models, putting particular emphasis on $b \to s$ transitions. To this end, we select specific flavour models showing representative flavour structures in the soft masses. As we will see in sec. 6, in order to generate large NP effects in $S_{\psi\phi}$, sizable – at least CKM-like – right-handed currents (driven by non-vanishing RR MIs) are unavoidable. The main reasons for this are twofold: 1) right-handed currents are less constrained than left-handed currents by low energy $b \to s$ transitions, especially $b \to s\gamma$ and 2) since LL MIs (and hence left-handed currents) even if not present at the GUT scale, are RGE generated at the low scale via

the CKM and the top Yukawa coupling (see sec. 4.4), non-vanishing right-handed currents guarantee the presence of the large NP contributions provided by the left-right $\Delta F = 2$ operators (Q_4 and Q_5 in (3.5)) that are strongly enhanced by QCD RGE effects and by a large loop function.

Therefore, we consider scenarios with

i) large $\mathcal{O}(1)$ RR mass insertions,

ii) comparable LL and RR mass insertions that are CKM-like,

iii) only CKM-like LL mass insertions.

In sec. 6 we present their predictions for both CP violating and CP conserving effects occurring in $b \to s$ transitions requiring at the same time that the models we consider satisfy the FCNC and CP violation bounds set by the experimental values of ϵ_K, ΔM_K, ΔM_D, d_e, d_n, etc. It will also be useful to compare the results of such an analysis with the results of the model-independent analysis discussed in sec. 2.

To the best of our knowledge, the current analysis represents the most complete analysis present in the literature in this subject as for the number of processes considered and the inclusion of all relevant SUSY contributions. In particular,

- We perform a full diagonalization of the sfermion mass matrices so that we do not make use of the MI approximation method. In fact, the latter method cannot be trusted when the flavour violating mixing angles are $\mathcal{O}(1)$, as is predicted by many flavour models.

- We systematically include the full set of one loop contributions to the FCNC processes, namely not only the gluino contributions, but also the charged Higgs, the chargino and the neutralino contributions.

- We systematically include the beyond-leading-order threshold corrections arising from $\tan\beta$-enhanced non-holomorphic corrections in the presence of new sources of flavour and CP violation hence, accounting also for FCNC effects driven by the neutral Higgs sector.

- All the above contributions have been systematically included for a very complete set of $\Delta F = 2$, $\Delta F = 1$ and $\Delta F = 0$ processes.

We believe that the inclusion of all these contributions and observables is crucial in order to try to understand the pattern of deviations from the SM prediction that may be found in future measurements.

In order to increase the transparency of our presentation, we will now outline the strategy for our numerics that will proceed in five steps.

Step 1: Bounds on Mass Insertions

In order to get an idea of the size of departures from the SM expectations that are still allowed in the supersymmetric framework, we will perform a model-independent analysis by calculating the allowed ranges for the mass insertions $(\delta^{AB}_{d,u})_{ij}$. In this approach, as usual, only one MI of a given "chirality" AB and relative to a given family transition ij will be switched on at a time. Consequently, the bounds so obtained are valid barring accidental cancellations among different contributions.

Step 2: An Abelian Flavour Model

In this step, we analyse an abelian flavour model by Agashe and Carone (AC) with a $U(1)$ flavour symmetry [36] which predicts large right-handed currents with order one CPV phases in the $b \to s$ sector.

As discussed previously, flavour models with a single $U(1)$ are typically disfavoured by the ϵ_K and ΔM_K constraints [23, 37]. However, this is no longer true in the case of the AC model, where a high degree of quark-squark alignment is realized by means of a particular localization of fermions in extra dimensions, suppressing unwanted FCNC effects.

In particular, the pattern of the relevant flavour off-diagonal MIs at the GUT scale, as function of the Cabibbo angle λ, is given by

$$\delta_d^{LL} \simeq \begin{pmatrix} \star & 0 & 0 \\ 0 & \star & \lambda^2 \\ 0 & \lambda^2 & \star \end{pmatrix} \;,\quad \delta_d^{RR} \simeq \begin{pmatrix} \star & 0 & 0 \\ 0 & \star & e^{i\phi_R} \\ 0 & e^{-i\phi_R} & \star \end{pmatrix} \;, \tag{5.12}$$

$$(\delta_u^{LL})_{12} \simeq \lambda, \;\; (\delta_u^{RR})_{12} \simeq \lambda^3 \;, \tag{5.13}$$

where we have suppressed the $\mathcal{O}(1)$ coefficients which multiply the individual elements of the matrices and ϕ_R is a free parameter.

In our analysis, the correlations between various observables will play the crucial role. We will show that in the AC model the most interesting correlations involve the CP asymmetry $S_{\psi\phi}$ that can be much larger than in the SM so that this model can accommodate the recent data from CDF and D0. Indeed, in this context it is important to ask whether the desire to explain the latter data automatically implies other departures from SM expectations. We will therefore calculate $\mathrm{BR}(B_s \to \mu^+\mu^-)$, $S_{\phi K_S}$, Δa_μ and A^s_{SL} as functions of $S_{\psi\phi}$.

The first correlation in our list is of particular interest as the upper bound on $\mathrm{BR}(B_s \to \mu^+\mu^-)$ should soon be improved by CDF, D0 and LHCb, possibly even finding first events for this decay. Next, the dependence of $S_{\phi K_S}$ on $S_{\psi\phi}$ will tell us whether large values of the latter asymmetry are compatible with $S_{\phi K_S}$ significantly lower than $S_{\psi K_S}$ as signalled by BaBar [1]. Similar comments apply to the $(g-2)_\mu$ anomaly Δa_μ. In addition, we investigate the ratios $\mathrm{BR}(B_s \to \mu^+\mu^-)/\Delta M_s$ and $\mathrm{BR}(B_s \to \mu^+\mu^-)/\mathrm{BR}(B_d \to \mu^+\mu^-)$ emphasizing the powerful tool they offer to unveil non-MFV structures of the model. We will also analyze the CP asymmetries in $B \to K^*\mu^+\mu^-$ and the impact of the $D^0 - \bar{D}^0$ mixing constraint on the correlations listed above. Finally, we will address the question how this model faces the current UT tension discussed in sec. 2.3.

Step 3: Non-Abelian $SU(3)$ Models

We next analyse a non-abelian model by Ross et al. (RVV) based on an $SU(3)$ flavour symmetry [51]. First, we recall that the observed structure in the Yukawa couplings does not fix uniquely the Kähler potential hence, the soft sector is not unambiguously determined. In the following, we analyse a particular case of the RVV model to which we refer to as RVV2 model [62]. Similarly to the abelian AC model, also the RVV2 model predicts large right-handed currents. More explicitly, at the GUT scale, again suppressing the $\mathcal{O}(1)$ coefficients, the expressions for the flavour off-diagonal entries in the soft mass matrices in the SCKM

basis read [62] [20]

$$\delta_d^{RR} \simeq \begin{pmatrix} \star & -\bar{\varepsilon}^3\, e^{i\omega_{us}} & -\bar{\varepsilon}^2\, y_b^{0.5} e^{i(\omega_{us}-\chi+\beta_3)} \\ -\bar{\varepsilon}^3\, e^{-i\omega_{us}} & \star & \bar{\varepsilon}\, y_b^{0.5} e^{-i(\chi-\beta_3)} \\ -\bar{\varepsilon}^2\, y_b^{0.5} e^{-i(\omega_{us}-\chi+\beta_3)} & \bar{\varepsilon}\, y_b^{0.5} e^{i(\chi-\beta_3)} & \star \end{pmatrix}, \tag{5.14}$$

$$\delta_d^{LL} \simeq \begin{pmatrix} \star & -\varepsilon^2 \bar{\varepsilon}\, e^{i\omega_{us}} & \varepsilon\bar{\varepsilon}\, y_t^{0.5} e^{i(\omega_{us}-2\chi+\beta_3)} \\ -\varepsilon^2 \bar{\varepsilon}\, e^{-i\omega_{us}} & \star & \varepsilon\, y_t^{0.5} e^{-i(2\chi-\beta_3)} \\ \varepsilon\bar{\varepsilon}\, y_t^{0.5} e^{-i(\omega_{us}-2\chi+\beta_3)} & \varepsilon\, y_t^{0.5} e^{i(2\chi-\beta_3)} & \star \end{pmatrix}, \tag{5.15}$$

where the parameters $\varepsilon \simeq 0.05$ and $\bar{\varepsilon} \simeq 0.15$ are defined, after the flavour symmetry breaking, in order to reproduce the observed values for fermion masses and mixing angles. Moreover, the phases ω_{us}, χ and β_3 are set, to a large extent, by the requirement of reproducing the CKM phase; in particular, it turns out that $\omega_{us} \approx -\lambda$ [62] and $(\chi, \beta_3) \approx (20^\circ, -20^\circ)$ (or any other values obtained by adding 180° to each) [62]. Additionally, it is found that [62]

$$(\delta_u^{LL})_{12} \simeq \lambda^4, \;\; (\delta_u^{RR})_{12} \simeq \lambda^6\,. \tag{5.16}$$

The trilinear couplings follow the same symmetries as the Yukawas. In the SCKM basis, after rephasing the fields, the trilinears lead to the following flavour off-diagonal LR MIs [62]

$$\delta_d^{LR} \simeq \begin{pmatrix} \star & \bar{\varepsilon}^3\, e^{-i\omega_{us}} & \bar{\varepsilon}^3\, e^{-i\omega_{us}} \\ \bar{\varepsilon}^3\, e^{-i\omega_{us}} & \star & \bar{\varepsilon}^2 \\ \bar{\varepsilon}^3\, e^{i(\omega_{us}+2\beta_3-2\chi)} & \bar{\varepsilon}^2\, e^{2i(\beta_3-\chi)} & \star \end{pmatrix} \frac{A_0}{m_0^2}\, m_b\,. \tag{5.17}$$

Similarly to the flavour model considered in step 2, $S_{\psi\phi}$ can be large so that the analysis can be done along the lines of the one done for the AC model making the comparison of both models very transparent. In particular, as is already evident from the structure of the MIs, NP enters $D^0 - \bar{D}^0$ mixing and ϵ_K in a profoundly different manner in these two models.

As the RVV model is embedded in a $SO(10)$ SUSY GUT model, correlations between flavour violating processes in the lepton and quark sectors naturally occur making additional tests of this model possible.

In particular, in the following, we list the flavour off-diagonal soft breaking terms of the leptonic sector arising in the RVV2 model [62]

$$\delta_e^{RR} \simeq \begin{pmatrix} \star & -\frac{1}{3}\bar{\varepsilon}^3 & -\frac{1}{3}\bar{\varepsilon}^2\, y_b^{0.5} e^{i(-\chi+\beta_3)} \\ -\frac{1}{3}\bar{\varepsilon}^3 & \star & \bar{\varepsilon}\, y_b^{0.5} e^{-i(\chi-\beta_3)} \\ -\frac{1}{3}\bar{\varepsilon}^2\, y_b^{0.5} e^{i(\chi-\beta_3)} & \bar{\varepsilon}\, y_\tau^{0.5} e^{i(\chi-\beta_3)} & \star \end{pmatrix}, \tag{5.18}$$

$$\delta_\ell^{LL} \simeq \begin{pmatrix} \star & -\frac{1}{3}\varepsilon^2\bar{\varepsilon} & \frac{1}{3}\varepsilon\bar{\varepsilon}\, y_t^{0.5} e^{i(-2\chi+\beta_3)} \\ -\frac{1}{3}\varepsilon^2\bar{\varepsilon} & \star & \varepsilon\, y_t^{0.5} e^{-i(2\chi-\beta_3)} \\ \frac{1}{3}\varepsilon\bar{\varepsilon}\, y_t^{0.5} e^{i(2\chi-\beta_3)} & \varepsilon\, y_t^{0.5} e^{i(2\chi-\beta_3)} & \star \end{pmatrix}, \tag{5.19}$$

while the leptonic off-diagonal LR MIs have the following structure [62]

$$\delta_e^{LR} \simeq \begin{pmatrix} \star & \bar{\varepsilon}^3 & \bar{\varepsilon}^3 \\ \bar{\varepsilon}^3 & \star & 3\bar{\varepsilon}^2 \\ \bar{\varepsilon}^3\, e^{i(2\beta_3-2\chi)} & 3\bar{\varepsilon}^2\, e^{2i(\beta_3-\chi)} & \star \end{pmatrix} \frac{A_0}{m_0^2}\, m_\tau\,. \tag{5.20}$$

[20]In (5.14), (5.15), in order to avoid accidental cancellations among different phases, we have set to zero an extra CPV phase, β_2' [62], that is not constrained by the requirement of reproducing a correct CKM matrix.

Finally, we consider a second example of *non-abelian* $SU(3)$ flavour model analyzed by Antusch et al. [52] to which we refer to as AKM model. In the AKM model, in contrast to the RVV2 model, there is the freedom to suppress arbitrarily the flavour changing soft terms $(\delta_d^{LL})_{ij}$, hence we take the limit where $(\delta_d^{LL})_{ij} = 0$ at the high scale. Therefore, our results have to be regarded as irreducible predictions of the AKM model, barring accidental cancellations among different contributions to physical observables. In the following, we report the flavour structure for the soft sector of the AKM model, in the SCKM basis, suppressing the $\mathcal{O}(1)$ coefficients [52]

$$\delta_d^{RR} \simeq \begin{pmatrix} \star & \bar{\varepsilon}^3 & \bar{\varepsilon}^3 \\ \bar{\varepsilon}^3 & \star & \bar{\varepsilon}^2 e^{i\Psi_f} \\ \bar{\varepsilon}^3 & \bar{\varepsilon}^2 e^{-i\Psi_f} & \star \end{pmatrix} . \tag{5.21}$$

The trilinear couplings lead to the following flavour off-diagonal LR MIs [52]

$$\delta_d^{LR} \simeq \begin{pmatrix} \star & \bar{\varepsilon}^3 & \bar{\varepsilon}^3 \\ \bar{\varepsilon}^3 & \star & \bar{\varepsilon}^2 \\ \bar{\varepsilon}^3 & \bar{\varepsilon}^2 & \star \end{pmatrix} \frac{A_0 v}{m_0^2 \tan\beta} , \tag{5.22}$$

where the above expressions are the same both for the down squark and the slepton sectors, modulo the unknown $\mathcal{O}(1)$ coefficients. Concerning the up squark sector, the relevant flavour mixing angle generating $D^0 - \bar{D}^0$ mixing is $(\delta_u^{RR})_{12} \simeq \lambda^5$, hence, we conclude that the $D^0 - \bar{D}^0$ constraints are safely under control also in the AKM model.

An interesting feature of the AKM model is the presence of a leading $\mathcal{O}(1)$ CPV phase in the 23 RR sector but not in the 12 and 13 sectors. This will turn out to be crucial to generate CPV effects in the B_s mixing amplitude. Moreover, we notice that, while the RVV2 model predicts that $(\delta_d^{RR})_{23} \simeq \bar{\varepsilon}$, the AKM model predicts that $(\delta_d^{RR})_{23} \simeq \bar{\varepsilon}^2$ with $\bar{\varepsilon} \simeq 0.15$. Even if we expect that the CPV effects in the AKM model are smaller than in the RVV2 model, the indirect constraints (mainly coming from ϵ_K, $b \to s\gamma$ and $\Delta M_s/\Delta M_d$), that are different in the two models, can play a crucial role to establish the allowed NP room for CPV effects in B_s systems. Hence, in order to distinguish between the RVV2 and the AKM model, by means of their footprints in low energy processes, a careful and comparative analysis is necessary.

Step 4: Flavour Model with Purely Left-handed Currents

We will next turn to the predictions for various low-energy processes induced by $b \to s$ transitions within flavour models predicting pure, CKM-like, left-handed currents, i.e. $\delta_d^{LL} \neq 0$ and $\delta_d^{RR} = 0$ (or better $\delta_d^{RR} \ll \delta_d^{LL}$), with a CPV phase in the $b \to s$ sector[21].

This study will give us general predictions for a broad class of abelian [63] and non-abelian [42] flavour models not containing RH currents. Concerning the low energy predictions for the abelian case, we can draw clear cut conclusions immediately: the marriage of the tight constraints from $D^0 - \overline{D}^0$ mixing (typical of abelian flavour models) with the absence of RH currents (preventing large CP violating effects in $\Delta F = 2$ observables in the down sector) allows non-standard and testable effects to occur only in CPV observables related to $D^0 - \overline{D}^0$ mixing.

[21] We will refer to this model as δLL model in the following.

A non-abelian scenario has very different low energy predictions. In sec. 6, we will analyse a non-abelian model based on the following LL MIs

$$\delta_d^{LL} \simeq \begin{pmatrix} \star & \lambda^5 & \lambda^3 \\ \lambda^5 & \star & \lambda^2 e^{i\phi_L} \\ \lambda^3 & \lambda^2 e^{-i\phi_L} & \star \end{pmatrix} , \tag{5.23}$$

and all other MIs put to zero. Within that framework we will confirm our general statement of sec. 3.1 that $S_{\psi\phi}$ does not receive large NP contributions in this context. As the NP effects in $\Delta F = 2$ processes in such models are relatively small and a large asymmetry $S_{\psi\phi}$ cannot be easily generated, this asymmetry is not an interesting variable in this scenario.

In contrast, large non-standard effects can be generated in $\Delta F = 1$ observables like $S_{\phi K_S}$, $A_{\rm CP}(b \to s\gamma)$ and the CP asymmetries in $B \to K^*\mu^+\mu^-$. In particular, as we will see, $S_{\phi K_S}$ can attain values low enough to explain the related anomaly. We will therefore calculate this time Δa_μ, $A_{\rm CP}(b \to s\gamma)$, $S_{\eta' K_S}$ and the CP asymmetries in $B \to K^*\mu^+\mu^-$ as functions of $S_{\phi K_S}$. The predictions of models with purely left-handed currents will be systematically compared with those of somewhat similar models, i.e. the FBMSSM and the MFV MSSM, considered in step 5.

Step 5: Comparison with the FBMSSM and the MFV MSSM

Finally we comment on the predictions for CP violating effects arising within MFV MSSM models. This issue was recently addressed in [68] in the context of the so-called *flavour blind* MSSM (FBMSSM) [64, 65, 66, 67, 68], where the CKM matrix is the only source of flavour violation and where additional CP violating phases in the soft sector are allowed.

In the FBMSSM, universal soft masses for different squark generations are assumed. Such a strong assumption gets somewhat relaxed in the framework of the general MFV ansatz [5] where the scalar soft masses receive additional corrections. The most general expressions for the low-energy soft-breaking terms compatible with the MFV principle and relevant for our analysis read [5, 69]

$$m_Q^2 = \tilde{m}^2 \left[\mathbf{1} + b_1 \mathbf{Y}_u^\dagger \mathbf{Y}_u + b_2 \mathbf{Y}_d^\dagger \mathbf{Y}_d + (b_3 \mathbf{Y}_d^\dagger \mathbf{Y}_d \mathbf{Y}_u^\dagger \mathbf{Y}_u + \text{h.c.}) \right] , \tag{5.24}$$

where $\tilde{m}$ sets the mass scale of the left-left soft mass, while b_i are unknown, order one, numerical coefficients. The small departures from a complete flavour blindness of the soft terms generate additional FCNC contributions by means of gluino and squark loops. The latter effects were neglected in the context of the FBMSSM [68] since, in principle, they can be very small if the parameters b_i are small and/or if the gluino mass is significantly larger than the chargino/up-squark masses. In this respect, the contributions to FCNC processes discussed in [68] can be regarded as irreducible effects arising in MFV scenarios.

The natural question that arises is whether the findings of [68], remain valid in the general MFV framework. Actually, within a general MFV framework, there are even new CPV effects to both $\Delta F = 2$ and $\Delta F = 1$ transitions, hence, potential departures from the FBMSSM predictions could in principle be expected. In particular in (5.24) the SM Yukawa couplings are not necessarily the only source of CPV. While b_1 and b_2 must be real, the parameter b_3 is generally allowed to be complex [69].

However, our analysis in sec. 6.5 will confirm the general finding of [68] that within SUSY MFV scenarios, large NP contributions can only be expected in $\Delta F = 1$ and $\Delta F = 0$ transitions.

We will also see that the FBMSSM and the MFV MSSM bear similarities to the models with left-handed CKM-like currents discussed in step 4.

6 Numerical Analysis

In this section, we present the numerical analysis of our study following the five steps described in the previous section. To this end, we list a number of constraints we impose throughout the analysis:

i) the data on flavour physics observables (see tabs. 1 and 6),

ii) mass bounds from direct SUSY searches,

iii) requirement of a neutral lightest SUSY particle,

iv) requirement of correct electroweak symmetry breaking and vacuum stability,

v) constraints from electroweak precision observables (EWPO) .

We further assume a CMSSM spectrum where, in the case of the model-independent analysis (Step 1) we take at the EW scale only one non-vanishing MI at a time. Hence our bounds are valid barring accidental cancellations among amplitudes from different MIs. On the contrary, when we analyze abelian and non-abelian flavour models, we impose the flavour structures of the soft terms at the GUT scale where we assume the flavour models are defined. We then run the SUSY spectrum down to the EW scale by means of the MSSM RGEs at the 2-loop level [218], consistently taking into account all the effects discussed in sec. 4.4.

The usual CMSSM contains (assuming vanishing flavour blind phases) five parameters: $M_{1/2}$, m_0, A_0, $\tan\beta$ and the sign of μ. However, we take a positive μ as is preferred by both the $b \to s\gamma$ and muon anomalous magnetic moment constraints. Consequently only four parameters are involved.

6.1 Step 1: Bounds on Mass Insertions

Starting with the model-independent analysis, we derive the allowed ranges for the MIs $(\delta^{AB}_{d,u})_{ij}$ (with $A, B = L, R$ and $i \neq j = 1, 2, 3$) under the constraints listed above. We scan the values of the CMSSM parameters in the following ranges: $M_{1/2} \leq 200$ GeV, $m_0 \leq 300$ GeV, $|A_0| \leq 3m_0$ and $5 < \tan\beta < 15$, where the bound on A_0 is set to avoid charge and/or colour breaking minima [219]. This choice for the input parameters would correspond to squark and gluino masses of order $m_{\tilde{Q}}, M_{\tilde{g}} \lesssim 600$ GeV, both possibly observable at the LHC.

6.1.1 1-2 Sector

The measurements of ΔM_K and ϵ_K are used to constrain the $\left(\delta^{AB}_d\right)_{21}$, as shown in fig. 6. ΔM_K and ϵ_K constrain the real and imaginary parts of the product $\left(\delta^{AB}_d\right)_{21}\left(\delta^{AB}_d\right)_{21}$, respectively. In the case of ΔM_K, given the uncertainty coming from the long-distance SM contribution, we use the range $-\Delta M^{\rm exp}_K \leq (\Delta M_K)^{\rm SM}_{\rm SD} + (\Delta M_K)^{\rm SUSY} \leq \Delta M^{\rm exp}_K$ where $(\Delta M_K)^{\rm SM}_{\rm SD}$ refers to the short-distance SM contribution. The measurement of ϵ'/ϵ could put an additional bound on $\mathrm{Im}[(\delta^{AB}_d)_{21}]$ that is effective in the case of the LR MI only. However, given the large hadronic uncertainties in the SM calculation of ϵ'/ϵ, to be conservative, we do not use this bound.

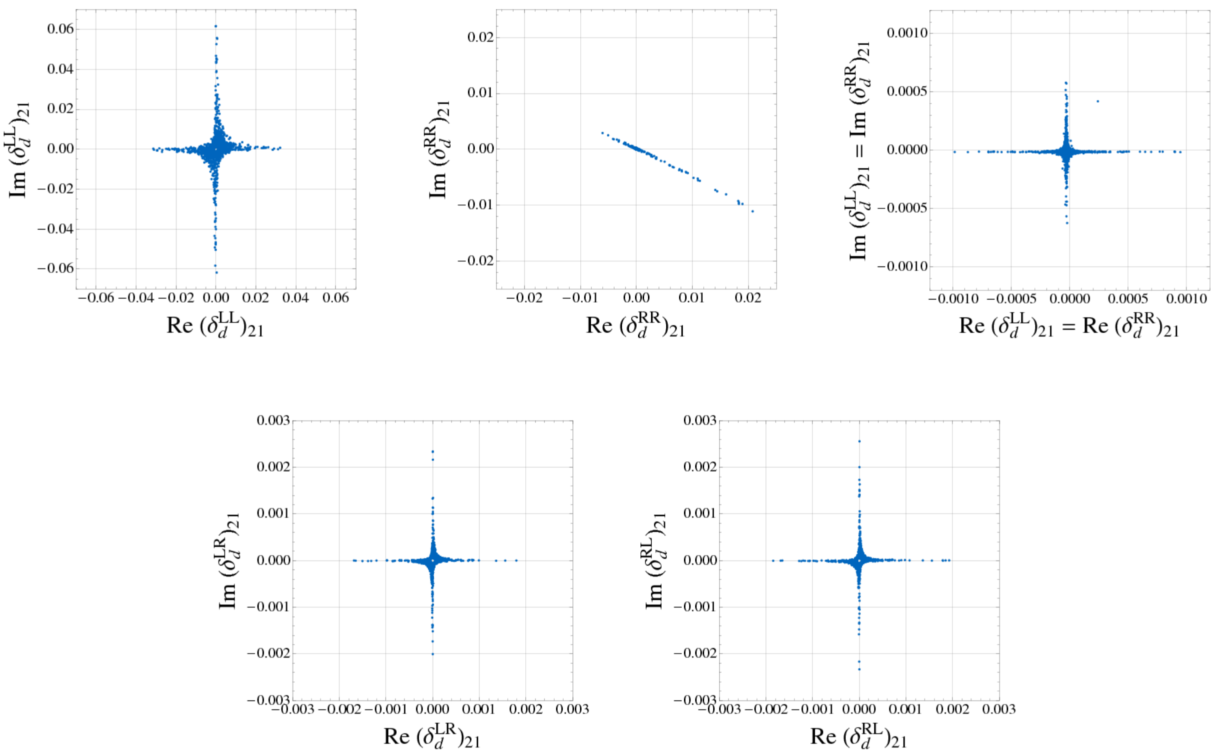

Figure 6: Bounds on the various MIs $(\delta_d^{AB})_{21}$ (with $A, B = L, R$) as obtained by imposing the experimental constraints from tabs. 1 and 6, in particular ϵ_K and ΔM_K.

Notice that the bound on the RR MI is obtained in the presence of a radiatively induced LL MI $(\delta_d^{LL})_{21} \propto V_{td}^* V_{ts}$, see (4.10). In the Kaon sector, the product $\left(\delta_d^{LL}\right)_{21}\left(\delta_d^{RR}\right)_{21}$ generates left-right operators that are enhanced by the QCD evolution, a large loop function and by the hadronic matrix element. Therefore, the bounds on RR MIs are more stringent than the ones on LL MIs. For the same reason also the constraints in the other cases $\left(\delta_d^{LL}\right)_{21} = \left(\delta_d^{RR}\right)_{21}$, $\left(\delta_d^{LR}\right)_{21}$ and $\left(\delta_d^{RL}\right)_{21}$ are particularly strong.

Similar arguments apply to the $\left(\delta_u^{AB}\right)_{21}$ with $(A, B) = (L, R)$ where we make use of the recent experimental measurement of $D^0 - \bar{D}^0$ mixing. The corresponding bounds on $\left(\delta_u^{AB}\right)_{21}$ are based on $|(M_{12}^D)_{\rm SUSY}| < 0.02$ ps^{-1} [220] and shown in fig. 7.

Concerning the bounds on $\left(\delta_u^{LL}\right)_{21}$ (see the upper left plot of fig. 7), one would naively expect that they are almost the same as the bounds found for $\left(\delta_d^{LL}\right)_{21}$, after the constraints from ϵ_K and ΔM_K are imposed. In fact, the $SU(2)_L$ gauge symmetry implies that $(M_u^2)_{21}^{LL} = \left[V^*(M_d^2)^{LL}V^{\rm T}\right]_{21}$, hence, $(\delta_u^{LL})_{21} \simeq (\delta_d^{LL})_{21}$ for degenerate left-handed squarks of the first two generations. However, as discussed in sec. 4, within scenarios predicting non degenerate left-handed squarks the above argument is no longer true, therefore $(\delta_u^{LL})_{21} \neq (\delta_d^{LL})_{21}$ and the bounds on $(\delta_u^{LL})_{21}$ and $(\delta_d^{LL})_{21}$ apply independently. In fig. 7, we consider such a general scenario. Obviously, all the bounds on the other MIs $\left(\delta_u^{AB}\right)_{21}$ with $AB \neq LL$ are unrelated to the corresponding bounds for the down sector as no symmetry principle is at work here.

6.1.2 1-3 Sector

The measurements of ΔM_d and $S_{\psi K_S}$ constrain the modulus and the phase of the B_d mixing amplitude, respectively. The bounds on the various $\left(\delta_d^{AB}\right)_{31}$ are reported in fig. 8. The

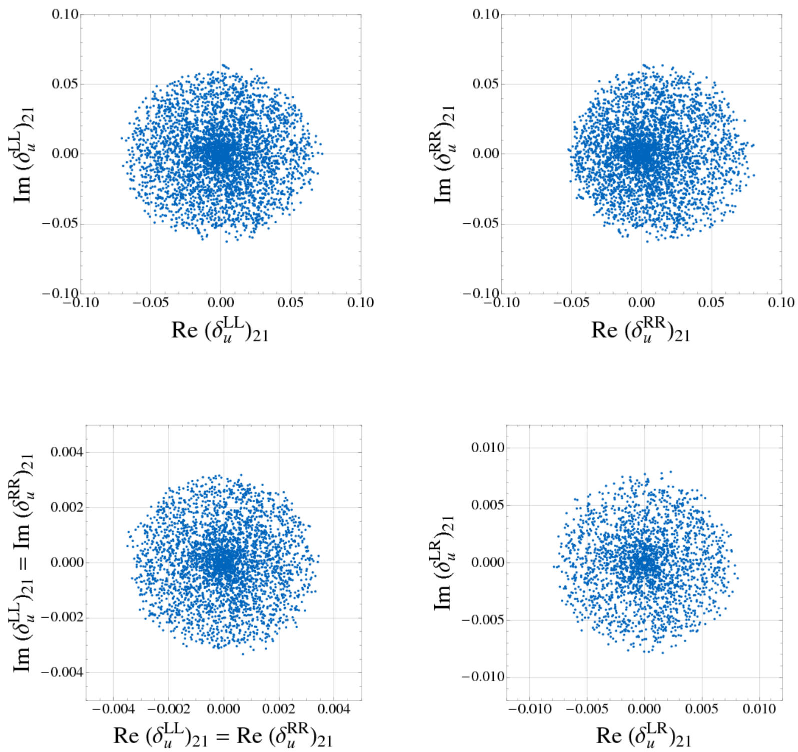

Figure 7: Bounds on the various MIs $(\delta_u^{AB})_{21}$ (with $A, B = L, R$) as obtained by imposing the experimental constraint from $D^0 - \bar{D}^0$ mixing and the constraints from tabs. 1 and 6.

constraints on $\left(\delta_d^{RR}\right)_{31}$ and $\left(\delta_d^{LL}\right)_{31}$ are different because of the contributions of the left-right operator (arising by means of the RGE induced $(\delta_d^{LL})_{31} \propto V_{tb}V_{td}^*$) that is effective in the $\left(\delta_d^{RR}\right)_{31}$ case only. The constraints in the cases $\left(\delta_d^{LL}\right)_{31} = \left(\delta_d^{RR}\right)_{31}$, $\left(\delta_d^{LR}\right)_{31}$ and $\left(\delta_d^{RL}\right)_{31}$, are particularly strong due again to the large NP contributions provided by the left-right operators that are strongly enhanced by renormalization group effects and by a large loop function.

6.1.3 2-3 Sector

In this sector, we can exploit a large number of constraints. In particular, they arise from ΔM_s and $\Delta B = 1$ branching ratios such as $b \to s\gamma$ and $b \to s\ell^+\ell^-$.

On the other hand, we do not impose the bounds from the time-dependent CP asymmetries in $B_d \to \phi K_S$ and $B_d \to \eta' K_S$ and the direct CP asymmetry in $b \to s\gamma$, given the still rather large uncertainties. In fig. 9 we show the allowed regions for the mass insertions and indicate in addition the resulting values for $S_{\psi\phi}$ with different colors. The following comments are in order:

- In the δ^{LL} case, a strong constraint arises from BR$(b \to s\gamma)$ as the related NP amplitude can interfere with the SM one. Regions in parameter space with a large real part of $(\delta_d^{LL})_{32}$ that would be allowed by $b \to s\gamma$ are excluded by the constraint from BR$(B \to X_s\ell^+\ell^-)$, while ΔM_s does not provide any further constraint. We observe that in the considered framework the possible values for $S_{\psi\phi}$ are rather moderate and lie in the range $-0.1 < S_{\psi\phi} < 0.1$ even for quite large values of $(\delta_d^{LL})_{32} \leq 0.1$.

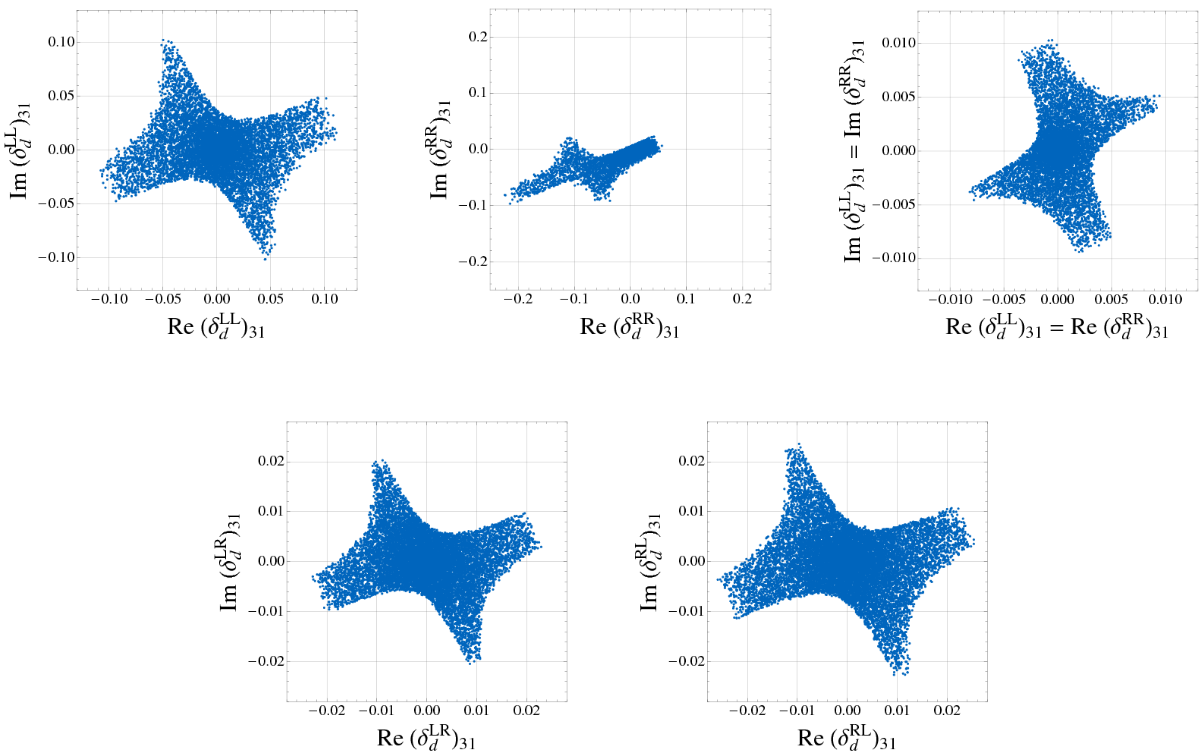

Figure 8: Bounds on the various MIs $(\delta_d^{AB})_{31}$ (with $A, B = L, R$) as obtained by imposing the experimental constraints from tabs. 1 and 6, in particular $S_{\psi K_S}$, $\cos 2\beta$ and ΔM_d.

- In the δ^{RR} case, the situation is very different compared to the δ^{LL} case as now BR$(b \to s\gamma)$ is not so much effective since the related NP amplitude (arising from right-handed currents) does not interfere with the SM one. Also BR$(B \to X_s \ell^+ \ell^-)$ is not effective for the same reason. Now, ΔM_s plays the main role in constraining $(\delta_d^{RR})_{32}$. As in the other cases, RGE induced effects generate at the low energy an effective MI $(\delta_d^{LL})_{32} \propto V_{tb}V_{ts}^*$. The product $(\delta_d^{LL})_{32}(\delta_d^{RR})_{32}$ generates left-right operators that are enhanced both by the QCD evolution and by a large loop function. Therefore, the bounds on RR MIs from ΔM_s are more stringent than the ones on LL MIs. We find that huge effects in $S_{\psi\phi}$ in the entire range from -1 to 1 are possible in this scenario.

- In the case $(\delta_d^{LL})_{32} = (\delta_d^{RR})_{32}$, very strong constraints on the MIs arise from ΔM_s due to the large contributions it receives from the left-right operator. Furthermore also BR$(b \to s\gamma)$ provides additional constraints given the rather light SUSY spectrum we consider here. Still in the remaining parameter space large effects in the B_s mixing phase in the range $-0.7 \leq S_{\psi\phi} \leq 0.7$ are possible even for $(\delta_d^{LL})_{32} = (\delta_d^{RR})_{32} \simeq 0.05$.

- Finally, in the last two scenarios with $(\delta_d^{LR})_{32}$ or $(\delta_d^{RL})_{32}$ switched on, BR$(b \to s\gamma)$ is the main constraint as the NP amplitude realizes the necessary chirality flip for the dipole $b \to s\gamma$ transition without involving the bottom mass insertion. In fact, the $b \to s\gamma$ constraint is so strong that $S_{\psi\phi}$ cannot depart significantly from the SM prediction in these cases.

In fig. 10, we show the values attained by $S_{\psi\phi}$ as a function of the modulus of different MIs, i.e. $|(\delta_d^{LL})_{32}|$ (plot on the left), $|(\delta_d^{RR})_{32}|$ (plot in the middle) and $|(\delta_d^{LL})_{32}(\delta_d^{RR})_{32}|^{1/2}$

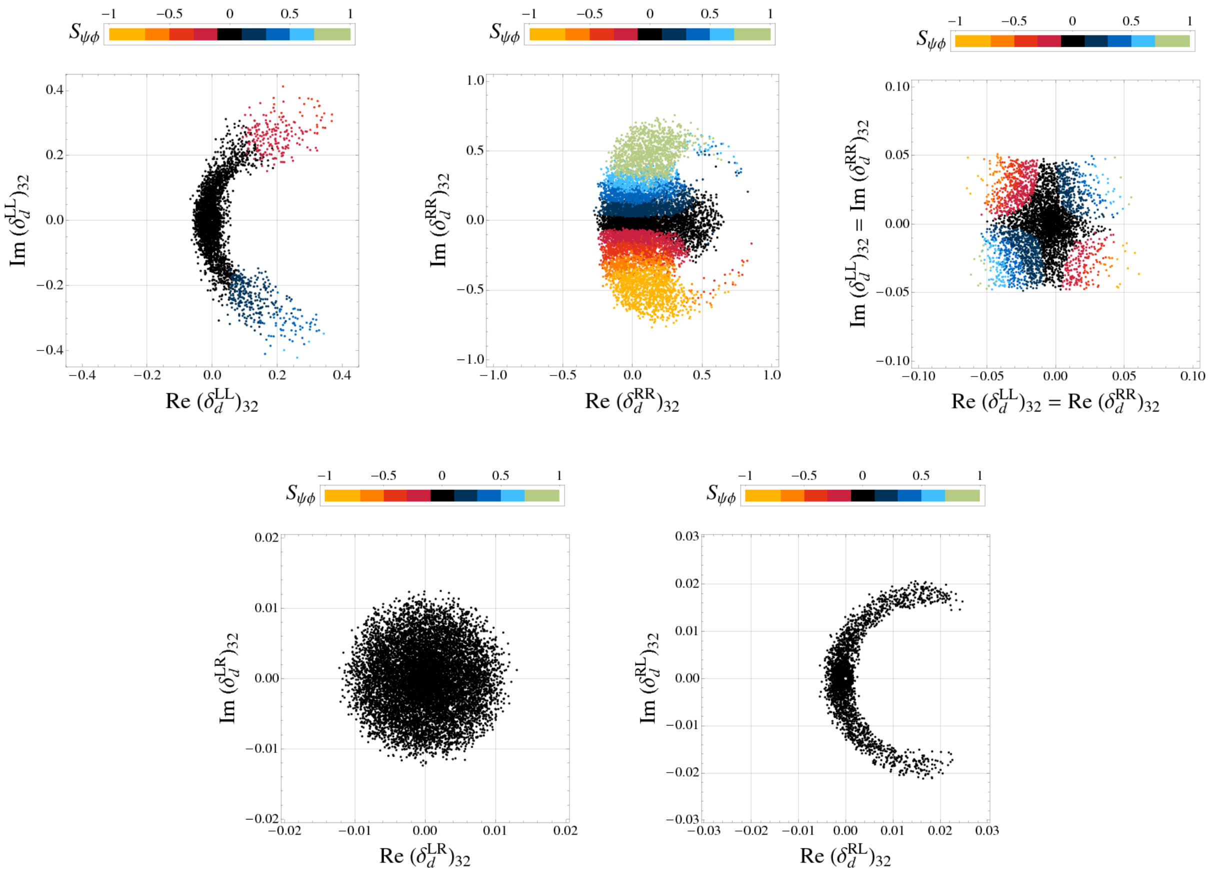

Figure 9: Bounds on the various MIs $(\delta_d^{AB})_{32}$ (with $A, B = L, R$) as obtained by imposing the experimental constraints from the $b \to s$ transitions listed in tabs. 1 and 6. The different colors indicate the resulting values for $S_{\psi\phi}$.

(plot on the right), assuming a CMSSM spectrum with the following ranges for the input parameters: $m_0 < 1$ TeV, $M_{1/2} < 1$ TeV, $|A_0| < 3m_0$, and $5 < \tan\beta < 50$.

This choice of the parameter space is different from that employed before to get the bounds on the various δs. In fact, in order to find the maximum allowed values for $S_{\psi\phi}$, it is crucial to consider the large $\tan\beta$ regime – in order to generate large Higgs mediated effects to $S_{\psi\phi}$ – and to enlarge the ranges for the SUSY mass scale – to relax the indirect constraints from observables (especially $b \to s\gamma$) decoupling faster than $S_{\psi\phi}$ with respect to the SUSY mass scale.

The plots of fig. 10 are complementary to those of fig. 9 and they show that the most natural scenario where it is possible to get large values for $S_{\psi\phi}$ even for small, CKM-like mixing angles is the third scenario where simultaneously $\delta^{LL} \neq 0$ and $\delta^{RR} \neq 0$.

6.2 Step 2: Abelian Model

In this section, we analyze the abelian flavour model by Agashe and Carone [36], presented in sec. 5, stressing, in particular, the correlations among various observables. Here and in the analysis of the other flavour models, we assume a CMSSM spectrum with the following ranges for the input parameters: $m_0 < 2$ TeV, $M_{1/2} < 1$ TeV, $|A_0| < 3m_0$, and $5 < \tan\beta < 55$. Concerning the unknown $\mathcal{O}(1)$ coefficients multiplying the off-diagonal entries in the soft

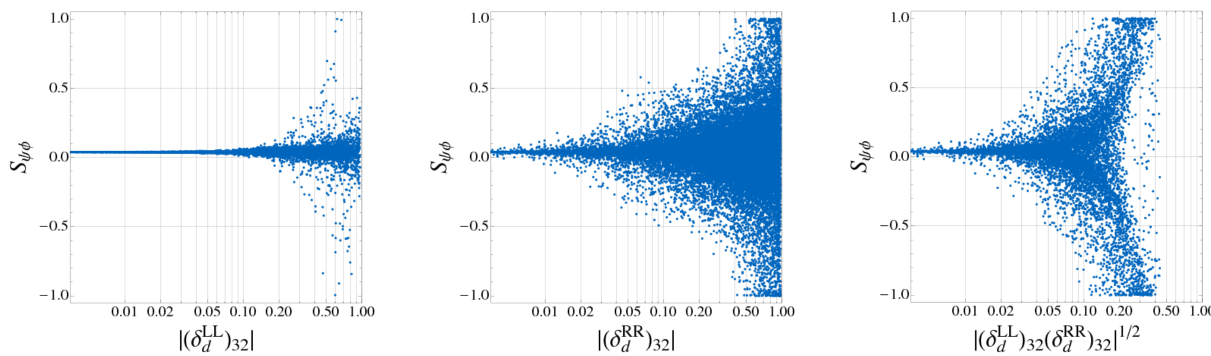

Figure 10: $S_{\psi\phi}$ vs. $|(\delta_d^{LL})_{32}|$, $|(\delta_d^{RR})_{32}|$ and $|(\delta_d^{LL})_{32}(\delta_d^{RR})_{32}|^{1/2}$, respectively. All the points fulfill the indirect constraints from flavour physics.

masses (5.12), they have been varied in the range $\pm[0.5, 2]$ in our numerical analysis.

As discussed in sec. 4, models with alignment naturally account for the tight FCNC constraints from ϵ_K and ΔM_K by construction. Consequently in this model the ϵ_K anomaly discussed in sec. 2 can only be solved by modifying the value of R_t as also $(\sin 2\beta)_{\psi K_S}$ is SM-like because of the negligibly small NP contributions to the $b \to d$ transition in this model. Yet we should remark that the latter solution implies a value for the angle α significantly below its best determined value (see fig. 2) and it is to be seen whether such a solution will remain viable. On the other hand, in contrast to ϵ_K, large effects in $D^0 - \bar{D}^0$ mixing are expected, provided the first two squark families are non-degenerate, as we expect from naturalness principles.

In our numerical analysis, concerning the squark mass matrices at the GUT scale, we impose a large splitting between the 1st and 2nd squark generation masses such that $m_{\tilde{u}_L} = 2m_{\tilde{c}_L} = 2m_0$, then the GUT scale MI is effectively $(\delta_u^{LL})_{21} \sim \lambda$. However, at the low scale, where we evaluate the SUSY contributions to the physical observables, $(\delta_u^{LL})_{21}$ is significantly smaller than λ. In fact, there is a degeneracy mechanism triggered mainly by the flavour blind $SU(3)$ interactions that restores a partial degeneracy between the 1st and 2nd generation squark masses [221, 222, 63]. In particular, while the off-diagonal entries in the squark mass matrices stay almost unaffected during the running from the GUT to the low scale (as discussed in sec. 4.4), the diagonal masses, in contrast, get strongly renormalized by the $SU(3)$ interactions: their GUT scale values $m^2_{\tilde{u}_L}(M_{GUT}) = 4m_0^2$ and $m^2_{\tilde{c}_L}(M_{GUT}) = m_0^2$ become at the low scale $m^2_{\tilde{u}_L}(M_W) \simeq 4m_0^2 + 6M^2_{1/2}$ and $m_{\tilde{c}_L}(M_W) \simeq m_0^2 + 6M^2_{1/2}$. As a result, the GUT MI $(\delta_u^{LL})_{21} \sim \lambda$ is typically reduced by one order of magnitude at the low scale and the constraints from $D^0 - \bar{D}^0$ mixing can be easily satisfied even for squark masses of a few hundred GeV. This is in contrast with the results of a low energy approach were $(\delta_u^{LL})_{21} \sim \lambda$ holds at the low scale implying a lower bound on the squark masses of around 2 TeV [220, 223].

In fig. 11, we show the resulting predictions for several observables as functions of $S_{\psi\phi}$. In all the plots, the black points satisfy the constraints of tab. 6 while the orange points correspond to negative NP effects in $\Delta M_d/\Delta M_s$ at the level of $15\% - 25\%$ times the SM one, able to solve the UT tension.

In the first row of fig. 11, we show, from left to right, the allowed values for $B_s \to \mu^+\mu^-$ vs. $S_{\psi\phi}$, $S_{\phi K_S}$ vs. $S_{\psi\phi}$ and $A^s_{\rm SL}$ vs. $S_{\psi\phi}$, respectively. In particular, fig. 11 shows that large values for $S_{\psi\phi}$ in the range $-1 \lesssim S_{\psi\phi} \lesssim +1$ are still allowed while being compatible with all the constraints such as $D^0 - \bar{D}^0$ mixing, BR$(b \to s\gamma)$, $R_{\Delta M}$ and ϵ_K. Interestingly, the first

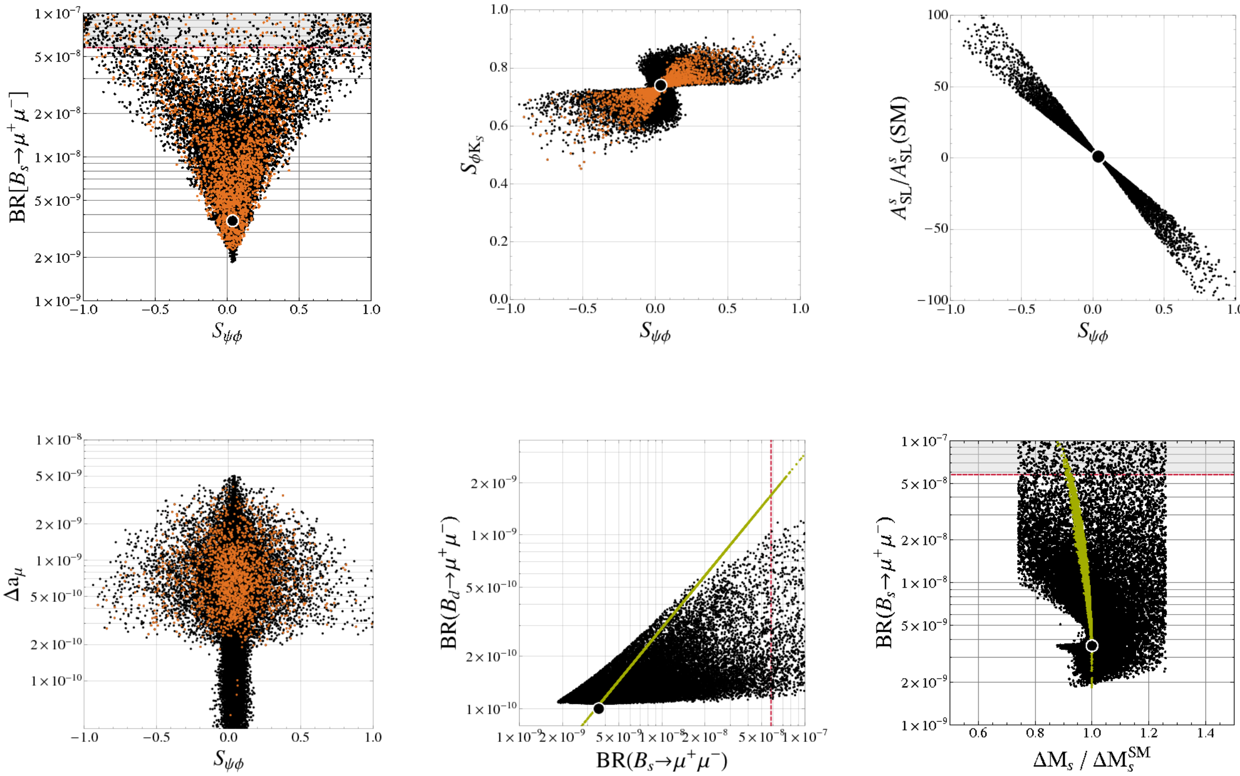

Figure 11: Predictions for various observables vs. $S_{\psi\phi}$ in the AC model. Orange points correspond to negative NP contributions to $\Delta M_d/\Delta M_s$ at the level of $15\% - 25\%$ times the SM one, able to solve the UT tension. The green points in the plot of BR$(B_s \to \mu^+\mu^-)$ vs. BR$(B_d \to \mu^+\mu^-)$ and $\Delta M_s/\Delta M_s^{\rm SM}$ vs. BR$(B_s \to \mu^+\mu^-)$ show the correlation of these observables in the MFV MSSM.

plot shows that large effects in $S_{\psi\phi}$ predict a lower bound on BR$(B_s \to \mu^+\mu^-)$ at the level of BR$(B_s \to \mu^+\mu^-) > 10^{-8}$ for $|S_{\psi\phi}| \geq 0.3$ (the converse is obviously not true). The correlation between $S_{\psi\phi}$ and BR$(B_s \to \mu^+\mu^-)$ signals that the double Higgs penguin contributions (3.21) are responsible for the large effects in $S_{\psi\phi}$ that we find in this model.

Moreover, the correlation between $S_{\psi\phi}$ and $S_{\phi K_S}$ shown in the second plot indicates that both asymmetries can simultaneously depart significantly from the SM expectations although an explanation for the $B_d \to \phi K_S$ anomaly would unambiguously imply negative values for $S_{\psi\phi}$, in contrast with the present data, in particular when the UT tensions are to be solved in this model. However, even in this case $S_{\phi K_S}$ can be at most suppressed down to 0.55.

The shape of the correlation between $S_{\psi\phi}$ and $S_{\phi K_S}$, i.e. the fact that a positive (negative) $S_{\psi\phi}$ implies an enhancement (suppression) of $S_{\phi K_S}$ with respect to its SM prediction can also be understood analytically. In the considered model, the NP effects in $S_{\phi K_S}$ are dominantly induced by the Wilson coefficient $\tilde{C}_8$ given in (3.28). As we consider only the case of a real and positive μ parameter, the sign and phase of $\tilde{C}_8$ and therefore also of the NP contribution to $S_{\phi K_S}$ is fixed by $\left(\delta_d^{RR}\right)_{32}$. Concerning $S_{\psi\phi}$, the dominant NP contribution to the mixing amplitude M_{12}^s is induced by the double Higgs penguin contribution (3.21). In particular we find that in most parts of the parameter space the largest contribution comes from a double penguin with one gluino and one Higgsino loop (see the diagram in the middle of fig. 4). The corresponding analytical expression is stated in the second line of (3.21). As both the trilinear coupling A_t and the loop functions h_1 and h_3 have a fixed sign in almost the entire parameter

space considered by us, the sign and phase of the NP contribution to M_{12}^s and hence to $S_{\psi\phi}$ is again determined by $\left(\delta_d^{RR}\right)_{32}$ and the correlation in the second plot of fig. 11 emerges.[22]

As the CDF and D0 data clearly favour $S_{\psi\phi}$ to be positive, we conclude that from the point of view of the AC model

- Either $0 \leq S_{\psi\phi} \leq 0.15$, $S_{\phi K_S} \geq 0.60$ and the UT tensions will go away, or
- $S_{\psi\phi}$ can be as large as 1, the UT tension is solved in this model but $S_{\phi K_S}$ will eventually turn out to be SM-like.

The third plot confirms the model-independent correlation between $S_{\psi\phi}$ and $A_{\rm SL}^s$ [108, 109] discussed in sec. 2.4, and shows that the dileptonic asymmetry $A_{\rm SL}^s$ normalized to its SM value can lie in the range $-100 \lesssim A_{\rm SL}^s/(A_{\rm SL}^s)_{\rm SM} \lesssim 100$ for $-1 \lesssim S_{\psi\phi} \lesssim 1$.

In the second row of the plot, from left to right, we show Δa_μ vs. $S_{\psi\phi}$, $B_d \to \mu^+\mu^-$ vs. $B_s \to \mu^+\mu^-$ and $B_s \to \mu^+\mu^-$ vs. $\Delta M_s/(\Delta M_s)_{\rm SM}$, respectively. Interestingly, there are many points accounting for large (non-standard) values for $S_{\psi\phi}$ while providing a natural explanation of the $(g-2)_\mu$ anomaly. Moreover, the AC model can predict very striking deviations from the MFV SUSY expectations for ${\rm BR}(B_d \to \mu^+\mu^-)/{\rm BR}(B_s \to \mu^+\mu^-)$ and ${\rm BR}(B_s \to \mu^+\mu^-)/\Delta M_s/(\Delta M_s)_{\rm SM}$. Hence, the above two ratios represent very clean and powerful observables to test the MFV hypothesis. In particular, as the AC model predicts new flavour structures only in the $b \to s$ sector, it turns out that only $B_s \to \mu^+\mu^-$ can depart from the MFV predictions. More specifically, the ratio ${\rm BR}(B_d \to \mu^+\mu^-)/{\rm BR}(B_s \to \mu^+\mu^-)$ is dominantly below its MFV prediction and can be much smaller than the latter.

Moreover, within a MFV framework, the current experimental constraints from ${\rm BR}(B_s \to \mu^+\mu^-)$ already imply a very small NP room in $\Delta M_s/(\Delta M_s)_{\rm SM}$, typically at a level smaller than 10%. In contrast, the AC model can predict quite sizable effects in $\Delta M_s/(\Delta M_s)_{\rm SM}$, as it is evident from fig. 11, which might saturate the $R_{\Delta M}$ constraints.

Further, even if not shown in fig. 11, the CP asymmetry in $b \to s\gamma$ is SM-like as it is basically not sensitive to right-handed currents.

In this model, NP contributions to $K \to \pi\nu\bar{\nu}$ decays are very strongly suppressed and the resulting branching ratios are SM-like. Consequently, if future experiments on these decays will show large departures from the SM expectations, the AC model will be ruled out.

Concerning the CP asymmetries in $B \to K^*\mu^+\mu^-$, we have found only small effects, at most at the percent level, after imposing all the indirect constraints, especially those from $D^0 - \overline{D}^0$ mixing.

Finally, we point out that in the AC model, as well as in many other abelian flavour models, large effects for the neutron EDM are also expected. In fact, the peculiar flavour structure of the abelian flavour models – predicting large mixing angles in the 12 up-squark sector – leads to the following order of magnitude value for the up-quark EDM d_u (see (3.65))

$$\left|\left(\frac{d_u}{e}\right)_{\tilde{g}}\right| \approx 10^{-26}\left(\frac{2\text{TeV}}{\tilde{m}}\right)^2 \frac{\left|{\rm Im}\left[(\delta_u^{LL})_{12}(\delta_u^{RR})_{21}\right]\right|}{\lambda^4}\,, \tag{6.1}$$

where we have assumed a degenerate SUSY spectrum, for simplicity. A similar expression holds for the up-quark CEDM too. Since $d_n \sim d_u$ (3.72), we conclude that $\mathcal{O}(1)$ phases for

[22] We note that if the dominant contribution to M_{12}^s came from gluino boxes (3.11) or from double penguins with two gluino loops (first line of (3.21)), with $\left(\delta_d^{LL}\right)_{32}$ induced radiatively through RG effects, the correlation between $S_{\psi\phi}$ and $S_{\phi K_S}$ would have the opposite sign.

$(\delta_u^{RR})_{12}$ (ϕ_{uR}) of abelian flavour models lead to a d_n close to its current experimental upper bound.

Analogously, CPV effects in $D^0 - \overline{D}^0$ mixing receive the dominant contributions by $\mathrm{Im}\left[(\delta_u^{LL})_{12}(\delta_u^{RR})_{12}\right]$. Hence, large CPV effects in $D^0 - \overline{D}^0$ mixing would imply experimentally visible values for the neutron EDM by means of the up-quark EDM.

Further, in the AC model, large CPV effects in B_s systems unambiguously imply a very large strange quark EDM. In particular, one can find that (see (3.64))

$$\left|\left(\frac{d_s}{e}\right)_{\tilde{g}}\right| \approx 10^{-23} \times \left(\frac{2\mathrm{TeV}}{\tilde{m}}\right)^2 \frac{\left|\mathrm{Im}\left[(\delta_d^{LL})_{23}(\delta_d^{RR})_{32}\right]\right|}{\lambda^2} \left(\frac{\tan\beta}{50}\right), \tag{6.2}$$

hence, the current experimental bounds on d_n already tell us that either the strange quark contributions to d_n have to be very small, with a proportionality coefficient smaller than 10^{-3}, or that $\mathcal{O}(1)$ CPV phases for $(\delta_d^{LL})_{32}$ (ϕ_{dL}) and/or $(\delta_d^{RR})_{32}$ (ϕ_{dR}) are not allowed (unless $\phi_{dL} = \phi_{dR}$). In the former case, large CPV effects in B_s systems are still allowed while they are excluded in the latter case (unless $\phi_{dL} = \phi_{dR}$). In this respect, a reliable knowledge of the order of magnitude for the strange quark contributions to d_n, by means of lattice QCD techniques, would be of the utmost importance to probe or to falsify flavour models with large RH currents in the 2-3 sector embedded in a SUSY framework.

In summary the striking predictions of the AC model in case the $S_{\psi\phi}$ anomaly will be confirmed by more accurate data are:

- The enhancement of $\mathrm{BR}(B_s \to \mu^+\mu^-)$ above 10^{-8},
- $\Delta a_\mu \approx 10^{-9}$, thereby providing a natural explanation of the $(g-2)_\mu$ anomaly.
- $\mathrm{BR}(B_d \to \mu^+\mu^-)/\mathrm{BR}(B_s \to \mu^+\mu^-)$ and $\mathrm{BR}(B_s \to \mu^+\mu^-)/\Delta M_s$ possibly very different from the MFV expectations with the first ratio dominantly smaller than its MFV value. Note however that $\mathrm{BR}(B_d \to \mu^+\mu^-)$ can reach values by a factor of 10 larger than in the SM.
- $S_{\phi K_S} \approx S_{\psi K_S}$
- Simultaneously UT tensions can be solved through the shift in $\Delta M_d/\Delta M_s$ at the prize of a rather low $\alpha \approx 75°$.
- Large effects in $D^0 - \bar{D}^0$ mixing but very small effects in $K^0 - \bar{K}^0$ mixing.
- Large values for the neutron EDM – very close to the current experimental bound – generated either by the up-quark (C)EDM or by the strange-quark (C)EDM. In the former case, visible CPV effects in $D^0 - \bar{D}^0$ mixing are also expected while they are not necessarily implied in the latter case. A correlated study of several hadronic EDMs, with different sensitivity to the up-quark (C)EDM and the strange-quark (C)EDM, would provide a precious tool to unveil the peculiar source of CPV that is generating the neutron EDM.

6.3 Step 3: Non-abelian $SU(3)$ Models

We now turn to the analysis of another very interesting flavour model, the model by Ross and collaborators (RVV) [51], or more specifically its particular version RVV2 recently discussed in [62]. It is based on the $SU(3)$ flavour symmetry, as was presented already in sec. 5. As already stressed in previous sections, the symmetry properties of non-abelian flavour models naturally account for degenerate squarks of the first two generations (at least) solving thereby the flavour problem related to the experimental constraints from ϵ_K and ΔM_K. As we will see, quite large – but still experimentally allowed effects in ϵ_K – can arise. Thus, in contrast to the AC model, the first solution to the UT tensions, through NP contribution to ϵ_K, becomes viable. Concerning the phenomenology of the up sector, the RVV model [51] and its RVV2 version predict very small (most likely untestable) effects in the $D^0 - \bar{D}^0$ mixing observables. These are probably the most peculiar features of non-abelian flavour models compared to the abelian ones with alignment, where the NP effects in ϵ_K are completely negligible by construction while large effects in $D^0 - \bar{D}^0$ mixing are unavoidable.

On the other hand, similarly to the AC model, also the RVV2 model exhibits large RH currents. Hence $S_{\psi\phi}$ can be large so that the analysis can be done along the lines of the one done for the AC model making the comparison of both models very transparent.

A very interesting aspect of the RVV model (as well as its RVV2 version) is that it is embedded in a SUSY GUT SO(10) model so that correlations among flavour violating processes in the lepton and quark sectors naturally occur making additional tests of this model possible.

As a second non-abelian model, we also consider the $SU(3)$ model proposed by Antusch et al. [52] (AKM model), already introduced in sec. 5. An interesting feature of the AKM model, that is in contrast to the RVV2 model, is the presence of a leading $\mathcal{O}(1)$ CPV phase only in the 23 RR sector but not in the 12 and 13 sectors. This will turn out to be crucial to generate CPV effects in the B_s mixing amplitude. Moreover, in the RVV2 model it turns out that $(\delta_d^{RR})_{23} \simeq \bar{\varepsilon}$, while in the AKM model we have $(\delta_d^{RR})_{23} \simeq \bar{\varepsilon}^2$ with $\bar{\varepsilon} \simeq 0.15$. Hence, we expect larger CPV effects in the RVV2 than in the AKM models. We stress that, even if both models arise from an underlying $SU(3)$ flavour symmetry, their low energy predictions can be quite different as their soft sectors, that cannot be set uniquely by the flavour symmetry, are different.

6.3.1 RVV2 Model: Results in the Hadronic and Leptonic Sectors

In fig. 12, we show the predictions of the RVV2 model for several observables as functions of $S_{\psi\phi}$ in analogy to fig. 11 for the abelian flavour model.

Our numerical results are obtained by implementing the flavour structures reported in sec. 5 assuming a CMSSM spectrum and scanning the unknown $\mathcal{O}(1)$ coefficients in the range $\pm[0.5, 2]$.

Large values for $S_{\psi\phi}$ up to $-0.7 \lesssim S_{\psi\phi} \lesssim 0.7$ are allowed while being compatible with all the constraints, in particular from $\mathrm{BR}(b \to s\gamma)$, $R_{\Delta M}$ and ϵ_K.

One of the most prominent differences between the RVV2 and the AC models is the loss of correlation between $S_{\psi\phi}$ and $\mathrm{BR}(B_s \to \mu^+\mu^-)$, although both observables can differ spectacularly from their SM predictions. In particular, in the AC model, the Higgs mediated effects were the only contributions able to generate large (non-standard) values for $S_{\psi\phi}$, after imposing the indirect constraints, especially from $b \to s\gamma$ and $D^0 - \overline{D}^0$ mixing. As a result,

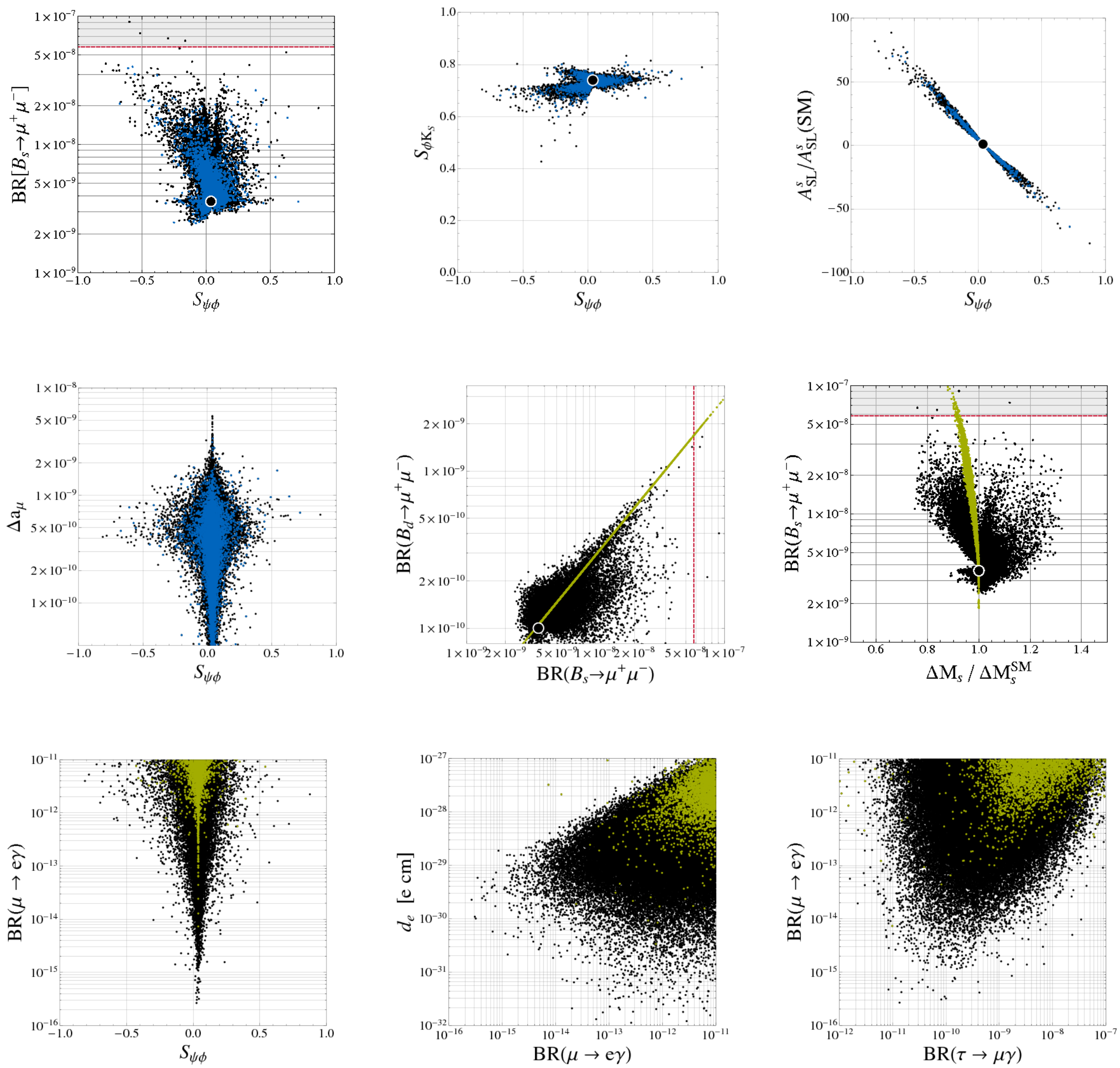

Figure 12: Predictions of the RVV2 model both in the hadronic and leptonic sectors. In the first two rows we show the predictions for various observables vs. $S_{\psi\phi}$. The blue points correspond to positive NP effects in ϵ_K such that $1.2 < \epsilon_K/(\epsilon_K)_{\rm SM} < 1.3$ and $\Delta M_d/\Delta M_s$ is SM-like. The green points in the plots of $\mathrm{BR}(B_s \to \mu^+\mu^-)$ vs. $\mathrm{BR}(B_d \to \mu^+\mu^-)$ and $\Delta M_s/\Delta M_s^{\rm SM}$ vs. $\mathrm{BR}(B_s \to \mu^+\mu^-)$ show the correlation of these observables in the MFV MSSM. The last row refers to the predictions for leptonic observables. The green points explain the $(g-2)_\mu$ anomaly at the 95% C.L., i.e. $\Delta a_\mu > 1 \times 10^{-9}$.

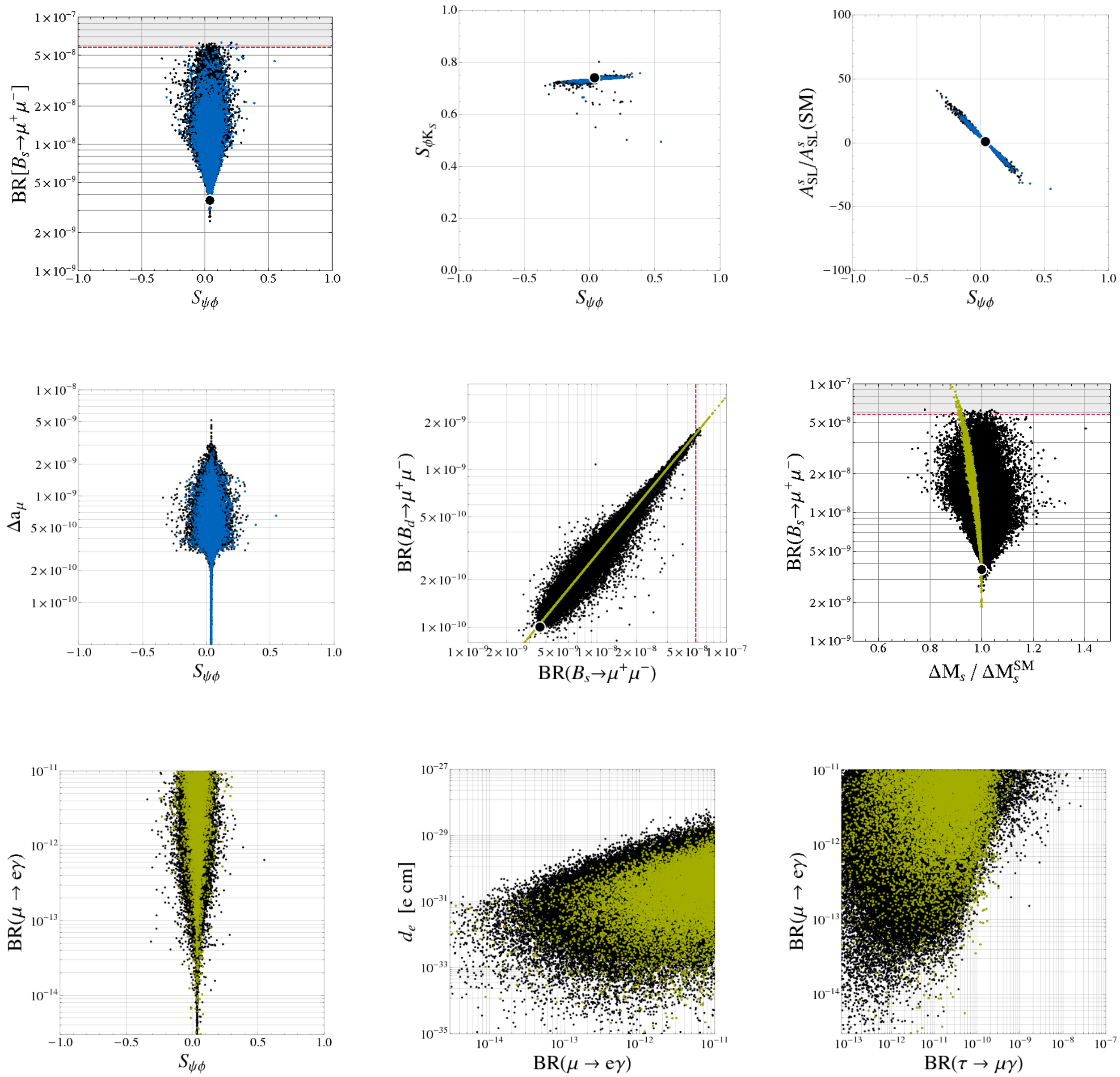

Figure 13: Predictions of the AKM model both in the hadronic and leptonic sectors. In the first two rows we show the predictions for various observables vs. $S_{\psi\phi}$. The blue points correspond to positive NP effects in ϵ_K such that $1.2 < \epsilon_K/(\epsilon_K)_{\mathrm{SM}} < 1.3$ and $\Delta M_d/\Delta M_s$ is SM-like. The green points in the plots of $\mathrm{BR}(B_s \to \mu^+\mu^-)$ vs. $\mathrm{BR}(B_d \to \mu^+\mu^-)$ and $\Delta M_s/\Delta M_s^{\mathrm{SM}}$ vs. $\mathrm{BR}(B_s \to \mu^+\mu^-)$ show the correlation of these observables in the MFV MSSM. The last row refers to the predictions for leptonic observables. The green points explain the $(g-2)_\mu$ anomaly at the 95% C.L., i.e. $\Delta a_\mu > 1 \times 10^{-9}$.

$S_{\psi\phi}$ was correlated with $B_s \to \mu^+\mu^-$ as the latter can also receive large SUSY effects only through the Higgs sector.

In the RVV2 model, the absence of the $D^0-\overline{D}^0$ constraints, as well as the more complicated flavour structure of the model (as for instance the presence of left-handed currents carrying new sources of CPV) destroy the above correlation as shown in the first plot of fig. 12.

The correlation between $S_{\psi\phi}$ and $S_{\phi K_S}$ reveals that $S_{\psi\phi}$, but probably not $S_{\phi K_S}$, can significantly depart from its SM expectation. Still, similarly to the AC model, negative NP values for $S_{\phi K_S}$, as suggested experimentally, imply negative values for $S_{\psi\phi}$, in contrast to the Tevatron results.

Moreover, even if the RVV2 model predicts sizable left-handed currents with order one CPV phases, the CP asymmetry in $b \to s\gamma$, as well as the asymmetries in $B \to K^*\ell^+\ell^-$ turn out to be almost SM-like after imposing all the indirect constraints.

In all the plots, all the points satisfy the constraints of tabs. 1 and 6 while the blue points correspond to a positive NP effect in ϵ_K such that $1.2 < \epsilon_K/(\epsilon_K)_{\rm SM} < 1.3$ and $\Delta M_d/\Delta M_s$ SM-like, allowing to solve the UT tension discussed in sec. 2. However, it is interesting to observe that a simultaneous solution to the $S_{\psi\phi}$, $(g-2)_\mu$ and ϵ_K anomalies is not very likely in this model, which constitutes an important test for this model. Similarly to the AC model the pattern of deviations from the SM predictions for $B_{s,d} \to \mu^+\mu^-$ and ΔM_s can differ spectacularly from MFV expectations. In particular, as in the AC model, the ratio $\mathrm{BR}(B_d \to \mu^+\mu^-)/\mathrm{BR}(B_s \to \mu^+\mu^-)$ is dominantly below its MFV prediction and can be much smaller than the latter.

On general grounds, we can conclude that the predictions of the AC and RVV2 models in the hadronic sector are quite similar. The NP effects in the RVV2 model are a bit smaller than in the AC model as the size of the right-handed couplings in the latter model is larger. However, one of the most important differences in predictions of these two models regards ε_K and $D^0 - \bar{D}^0$ mixing. We stress again that the RVV2 model naturally predicts sizable effects in ε_K (able to solve the current UT tension) while predicting negligibly small effects in $D^0 - \bar{D}^0$ mixing; in the AC model exactly the opposite situation occurs.

Concerning the predictions for the hadronic EDMs, we have explicitly checked that the down-quark (C)EDM reaches interesting values – up to $\approx 10^{-26} e$ cm – while being compatible with all the constraints. Moreover, large CPV effects in B_s systems typically imply predictions for the neutron EDM within the expected future experimental resolutions $\approx 10^{-28} e$ cm. The strange-quark (C)EDM is enhanced compared to the down-quark (C)EDM by a factor of $\approx \bar{\epsilon}^{-2} \approx 50$ hence, it would be very interesting to know precisely how it enters the neutron EDM. This would be also of great interest to establish the NP room left to CPV in B_s systems under the constraints from the hadronic EDMs.

In the last row of fig. 12, we show the predictions of the RVV2 model for observables in the leptonic sector. From left to right of fig. 12, we report the correlations between $S_{\psi\phi}$ vs. $\mathrm{BR}(\mu \to e\gamma)$, $\mathrm{BR}(\mu \to e\gamma)$ vs. the electron EDM d_e and $\mathrm{BR}(\tau \to \mu\gamma)$ vs. $\mathrm{BR}(\mu \to e\gamma)$, respectively. The green points are such that $\Delta a_\mu > 1 \times 10^{-9}$, thus they explain the $(g-2)_\mu$ anomaly at the 95% C.L.

We observe that, both $\mu \to e\gamma$ and $\tau \to \mu\gamma$ are very sensitive probes of LFV in the RVV2 model and they both can turn out to be the best probes of LFV in this model. In particular, it is interesting to observe that the desire to solve the $(g-2)_\mu$ anomaly in the RVV2 model implies values of $\mathrm{BR}(\tau \to \mu\gamma)$ in the reach of LHCb and future SuperB facilities as well as $\mathrm{BR}(\mu \to e\gamma) \geq 10^{-13}$, within the MEG resolution [204].

As we can see, both $\mathrm{BR}(\ell_i \to \ell_j\gamma)$ and d_e span over many orders of magnitude. Their

behavior can be understood looking at (3.56), (3.57) and (3.69), respectively. In fact, given that $\mathrm{BR}(\ell_i \to \ell_j\gamma) \sim (t_\beta^2/\tilde{m}^4) \times |\delta_{ij}|^2$ and since t_β and $\tilde{m}$ can vary roughly by one order of magnitude in our setup while the $|\delta_{ij}|$s are defined modulo unknown coefficients in the range $\pm[0.5, 2]$, we expect $\mathrm{BR}(\ell_i \to \ell_j\gamma)$ to vary by roughly seven orders of magnitude.

Moreover, the loss of the correlation between $\mathrm{BR}(\tau \to \mu\gamma)$ and $\mathrm{BR}(\mu \to e\gamma)$ can be traced back noting that $\mathrm{BR}(\mu \to e\gamma)$ receives several contributions (of comparable size) by both δ_{21} and $(\delta_{21})_{\text{eff.}} \sim \delta_{23}\delta_{31}$ while the only relevant MIs for $\mathrm{BR}(\tau \to \mu\gamma)$ are the δ_{32} ones. Further, the impact of the MIs δ^{LR} and δ^{RL} is much more relevant for $\mathrm{BR}(\mu \to e\gamma)$ – that receives an enhancement factor $(m_\tau/m_\mu)^2$ from the amplitude generated by δ^{LR} and δ^{RL} – than for $\mathrm{BR}(\tau \to \mu\gamma)$ and this also contributes to destroy their correlation.

Concerning d_e, we note that it is bounded from above by $\mathrm{BR}(\mu \to e\gamma)$ even if their correlation is loose given their very different sensitivity to the flavor structures of the model.

In summary, the distinct patterns of flavour violation in the RVV2 model are

- Large enhancements of $S_{\psi\phi}$ and $\mathrm{BR}(B_{s,d} \to \mu^+\mu^-)$ but not in a correlated manner as in the abelian AC model,
- Similarly to the AC model, $\mathrm{BR}(B_d \to \mu^+\mu^-)/\mathrm{BR}(B_s \to \mu^+\mu^-)$ and $\mathrm{BR}(B_s \to \mu^+\mu^-)/\Delta M_s$ might be very different from the MFV expectations with the first ratio dominantly smaller than its MFV value, especially for $\mathrm{BR}(B_s \to \mu^+\mu^-) \gtrsim 10^{-8}$. Also in this model, $\mathrm{BR}(B_d \to \mu^+\mu^-)$ can reach values by a factor of 10 larger than in the SM,
- Removal of the UT tension through NP contributions to ϵ_K, requiring then typically $S_{\psi\phi} \leq 0.3$ and $S_{\phi K_S} \approx S_{\psi K_S}$,
- Small effects in $D^0 - \bar{D}^0$ mixing,
- Large CPV effects in B_s systems typically imply predictions for the neutron EDM within the expected future experimental resolutions $d_n \approx 10^{-28} e$ cm,
- Large values for $-0.25 < S_{\psi\phi} < 0.25$ are still allowed even for $\mathrm{BR}(\mu \to e\gamma) \lesssim 10^{-13}$. However, the desire of an explanation for the $(g-2)_\mu$ anomaly implies that $\mathrm{BR}(\mu \to e\gamma) \gtrsim 10^{-13}$ and $|S_{\psi\phi}| \lesssim 0.25$,
- $\mathrm{BR}(\mu \to e\gamma) \geq 10^{-13}$, $d_e > 10^{-29}$ $e$cm and $\mathrm{BR}(\tau \to \mu\gamma) \geq 10^{-9}$ required by the solution of the $(g-2)_\mu$ anomaly.

6.3.2 AKM Model: Results in the Hadronic and Leptonic Sectors

In fig. 13, we show the predictions for the AKM model. As done for the other flavour models, we obtain the numerical results by implementing the flavour structures reported in sec. 5 assuming a CMSSM spectrum and scanning the unknown $\mathcal{O}(1)$ coefficients in the range $\pm[0.5, 2]$.

The main differences between the RVV2 and the AKM models can be traced back remembering the peculiar flavour structures in the soft sector of the two models. In particular, the AKM model predicts a CKM-like RH current while the corresponding mixing angle in the RVV2 model for the $b \to s$ transition is larger. This implies that in the AKM model, the effects in CPV observables are typically smaller, but still very interesting, compared to the RVV2 model. In particular, it is found that, in the AKM model $S_{\psi\phi}$ lies most likely in the range $-0.3 < S_{\psi\phi} < 0.3$ while being compatible with all the constraints. Interestingly

enough, similarly to the abelian case discussed before, large non-standard values for $S_{\psi\phi}$ would unambiguously point towards non-standard values for $\mathrm{BR}(B_s \to \mu^+\mu^-)$ as shown in the first plot of fig. 13. However, fig. 13 also shows that within this model the $S_{\phi K_S}$ anomaly cannot be accounted for. Large values for $S_{\psi\phi}$ can also be compatible with an explanation of the $(g-2)_\mu$ anomaly. Moreover, we also observe that departures from the MFV SUSY expectations for $\mathrm{BR}(B_d \to \mu^+\mu^-)/\mathrm{BR}(B_s \to \mu^+\mu^-)$ and $\mathrm{BR}(B_s \to \mu^+\mu^-)/\Delta M_s/(\Delta M_s)_{\mathrm{SM}}$(in both directions with respect to the SM predictions) are also expected in the AKM model, even if the ratio $\mathrm{BR}(B_d \to \mu^+\mu^-)/\mathrm{BR}(B_s \to \mu^+\mu^-)$ stays much closer to the MFV value of roughly 1/33 [224, 9].

Passing to the hadronic EDMs, we observe that, even if the AKM does not contain leading CPV phases in the 13 sector, the down-quark (C)EDM is always generated by means of the CKM phase, in the presence of RH MIs (see sec. 3.3.1). We have explicitly checked that the down-quark (C)EDM might reach values up to $\approx 10^{-28} e$ cm after imposing all the constraints. As a result, the constraints from the hadronic EDMs are well under control. However, large CPV effects in B_s systems would likely imply predictions for the hadronic EDMs within the expected future experimental resolutions $\approx 10^{-28} e$ cm. The strange-quark (C)EDM is enhanced compared to the down-quark (C)EDM by a factor of $\approx \bar{\epsilon}^{-2} \approx 50$, as in the RVV2 model. Once again, we stress that it would be of crucial importance to know how the strange-quark (C)EDM enters the hadronic EDMs in order to establish which are the CPV signals we can still expect in B_s systems.

In the last row of fig. 13, we show the predictions of the AKM model for observables in the leptonic sector as done for the RVV2 model in fig. 12. In particular, both $\mu \to e\gamma$ and $\tau \to \mu\gamma$ are sensitive probes of LFV in the AKM model. However, in contrast to the RVV2 model, $\mu \to e\gamma$ will represent the best probe of LFV in this model, especially after the MEG sensitivity will be fully exploited. In fact, it turns out that when $\mathrm{BR}(\mu \to e\gamma) \approx 10^{-13}$ then $\mathrm{BR}(\tau \to \mu\gamma) \leq 10^{-10}$, far from the SuperB reach.

Moreover, the predictions for the electron EDM in the AKM model are well below those of the RVV2 model. In fact, in the RVV2 model, the two largest contributions to d_e are proportional to either $\mathrm{Im}(\delta_\ell^{LR})_{13}(\delta_\ell^{RR})_{31}$ or $\mathrm{Im}(\delta_\ell^{LL})_{13}(\delta_\ell^{RR})_{31}$ with $(\delta_\ell^{RR})_{31}$ carrying a leading $\mathcal{O}(1)$ CPV phase. In contrast, in the AKM model, the first non vanishing contribution to d_e is generated at the third order in the MI expansion by means of the combination $\mathrm{Im}(\delta_\ell^{LR})_{13}(\delta_\ell^{RR})_{32}(\delta_\ell^{RR})_{21}$ as $(\delta_\ell^{RR})_{32}$ is the only MI containing an $\mathcal{O}(1)$ CPV phase. Hence, there is a higher order suppression in terms of small mixing angles in the AKM model compared to the RVV2 model.

An order of magnitude for the upper bound on d_e, compatible with the constraints from $\mathrm{BR}(\mu \to e\gamma)$, can be obtained considering a degenerate SUSY spectrum and assuming that the dominant contributions to $\mathrm{BR}(\mu \to e\gamma)$ come from $(\delta_\ell^{RL})_{21}$ and $(\delta_\ell^{LR})_{21}$.

Taking the specific expressions for the MIs arising in the AKM model (5.21) and (5.22), one can easily find that

$$\frac{d_e}{e} \lesssim 10^{-29} \sqrt{\frac{\mathrm{BR}(\mu \to e\gamma)}{10^{-11}}} \sin\Psi \; e\,\mathrm{cm}\,, \tag{6.3}$$

as is fully confirmed numerically by fig. 13.

Still, visible values for d_e can be reached in the AKM model; in particular, it turns out that $d_e \lesssim 10^{-29}(10^{-30})$ $e$cm for $\mathrm{BR}(\mu \to e\gamma) \approx 10^{-11}(10^{-13})$.

Finally, we note that, for $\mathrm{BR}(\mu \to e\gamma) \lesssim 10^{-13}$, only values for $S_{\psi\phi}$ at the level of $|S_{\psi\phi}| < 0.15$ are still possible if one wants to be fully compatible with an explanation for the

$(g-2)_\mu$ anomaly.

Therefore, the disentangling of the RVV2 and the AKM models might be problematic from a low-energy point of view, even if not impossible. Clearly the knowledge of some SUSY parameter, as the value for $\tan\beta$ and the charged Higgs mass, for instance, would be of outmost importance to make access to the flavour structure of the flavour model at work.

In summary, several of the predictions in the AKM model are similar to the ones found in the RVV2 model, but the following most significant differences should be noted:

- $|S_{\psi\phi}|$ can reach values up to $|S_{\psi\phi}| \lesssim 0.3$, values that are fully consistent with an explanation of the UT tension through NP contributions to ϵ_K
- $S_{\psi\phi} \geq 0.2$ uniquely implies $\mathrm{BR}(B_s \to \mu^+\mu^-) \geq 10^{-8}$.
- $\mathrm{BR}(B_d \to \mu^+\mu^-)/\mathrm{BR}(B_s \to \mu^+\mu^-)$ departs less from MFV expectation than in the AC and RVV2 models and can be both larger and smaller relative to its MFV value.
- A non standard $S_{\psi\phi}$ typically implies $d_n \approx 10^{-28} e$ cm that is within the expected future experimental resolutions.
- $\mathrm{BR}(\tau \to \mu\gamma)$ is likely out of the reach of SuperB machines, in particular, $\mathrm{BR}(\tau \to \mu\gamma) \lesssim (10^{-8}, 10^{-9}, 10^{-10})$ when $\mathrm{BR}(\mu \to e\gamma) \lesssim (10^{-11}, 10^{-12}, 10^{-13})$, respectively.
- $d_e \lesssim 10^{-29}(10^{-30})$ $e$cm for $\mathrm{BR}(\mu \to e\gamma) \lesssim 10^{-11}(10^{-13})$ where $\mathrm{BR}(\mu \to e\gamma) \gtrsim 10^{-13}$ is required by the solution of the $(g-2)_\mu$ anomaly.

6.4 Step 4: Flavour Model with Purely Left-handed Currents

Another typical flavour structure for the soft sector emerging in many abelian and non-abelian flavour models are purely left-handed currents with CKM-like mixing angles [42, 63].

Based on the flavour structures given in (5.23) and scanning the unknown $\mathcal{O}(1)$ coefficients in the range $\pm[0.5, 2]$, we present in fig. 14 the numerical results of our study of the non-abelian model of [42].

As already discussed in sec. 5, in the abelian case, non-standard and testable NP effects can be generated only in observables related to $D^0 - \overline{D}^0$ mixing hence, in the following, we focus on the non-abelian case.

The first upper plot refers to the correlation between $A_{\mathrm{CP}}(b \to s\gamma)$ vs. $S_{\phi K_S}$. We find that $-0.2 \lesssim S_{\phi K_S} \lesssim 1$ and $-6\% \lesssim A_{\mathrm{CP}}(b \to s\gamma) \lesssim 6\%$. Interestingly, it turns out unambiguously that positive (negative) NP contributions for $S_{\phi K_S}$ are associated with negative (positive) NP effects in $A_{\mathrm{CP}}(b \to s\gamma)$.

This correlation can also be understood analytically. While the NP contributions to $S_{\phi K_S}$ arise dominantly from the Wilson coefficient C_8, the CP asymmetry $A_{\mathrm{CP}}(b \to s\gamma)$ crucially depends on the relative size of the imaginary parts of C_7 and C_8, see (3.29). In the considered model, gluino loops typically give $C_7^{\tilde{g}} < C_8^{\tilde{g}}$ (3.27), while Wino loops lead to the opposite situation, i.e. $C_7^{\tilde{W}} > C_8^{\tilde{W}}$ (3.26). In fact the correlation that we find corresponds to the latter case, implying that Wino contributions dominate over gluino ones in large parts of the parameter space, since Winos are typically a factor 3 lighter than gluinos.

In the second upper plot we show that $S_{\eta' K_S}$ turns out to be highly correlated with $S_{\phi K_S}$, as they both receive the dominant NP contribution (that is larger in the $S_{\phi K_S}$ case) from the chromomagnetic Wilson coefficient C_8. Moreover, a solution of the $S_{\phi K_S}$ anomaly can also

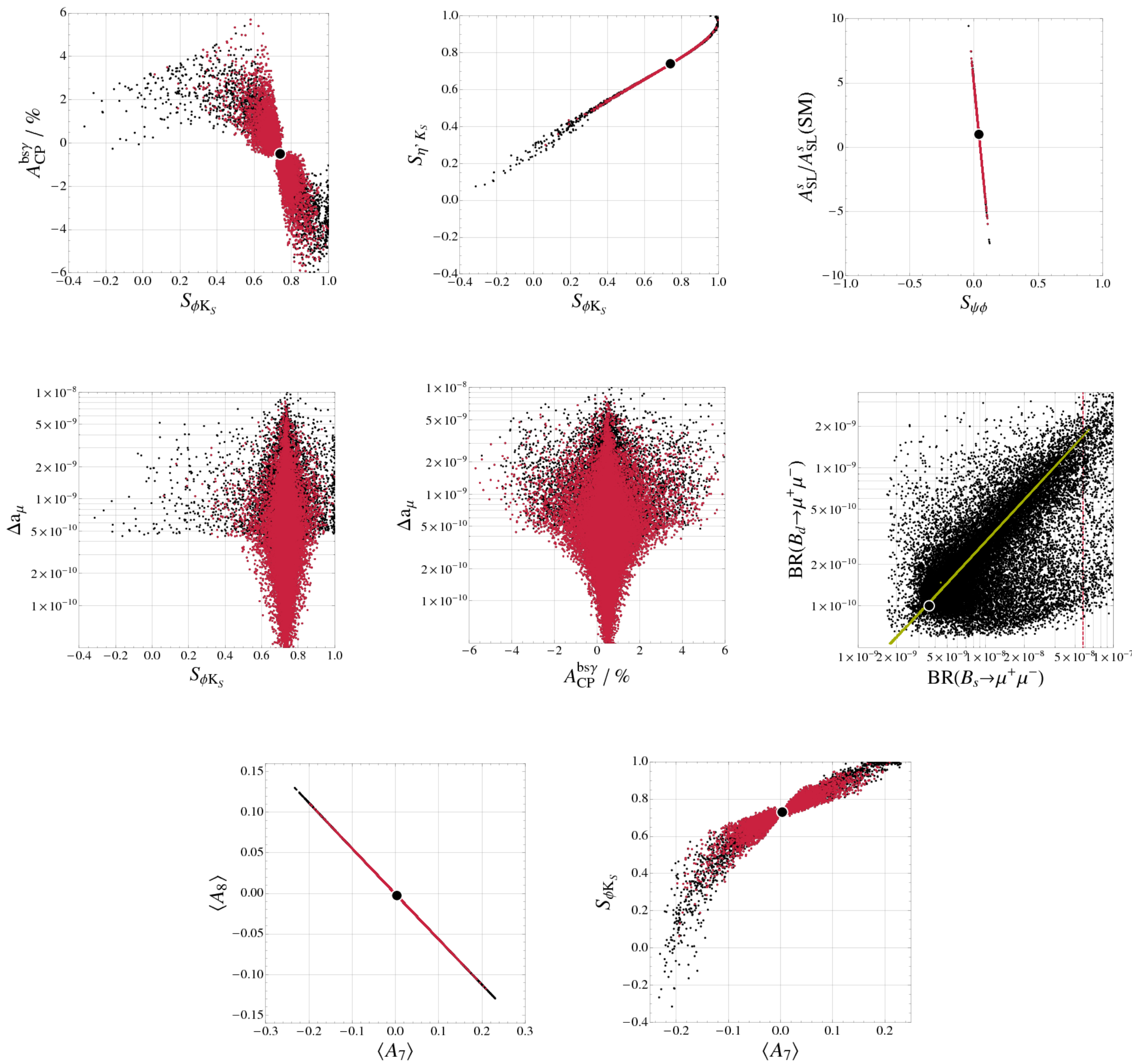

Figure 14: Predictions for various low energy processes induced by $b \to s$ transitions in the non-abelian flavour model predicting pure, CKM-like, left-handed flavour mixing angles in the soft sector [42]. In all the plots, all the black points satisfy the constraints of tab. 6 while the red ones additionally satisfy $\mathrm{BR}(B_s \to \mu^+\mu^-) < 6 \times 10^{-9}$. The green points in the plots of $\mathrm{BR}(B_s \to \mu^+\mu^-)$ vs. $\mathrm{BR}(B_d \to \mu^+\mu^-)$ show the correlation of these observables in the MFV MSSM.

lead to the solution of the $(g-2)_\mu$ anomaly and large values for the direct CP asymmetry $A_{\rm CP}(b \to s\gamma)$ are typically associated with large values for $(g-2)_\mu$. The departures of $S_{\psi\phi}$ from the SM expectations $(S_{\psi\phi})_{\rm SM} \approx 0.036$ are quite small, in the range $0 \lesssim S_{\psi\phi} \lesssim 0.1$, as expected from our model-independent analysis. The corresponding attained values for the semileptonic asymmetry $A^s_{\rm SL}$ normalized to the SM value lie in the range $-6 \lesssim A^s_{\rm SL}/(A^s_{\rm SL})_{\rm SM} \lesssim 6$, hence, NP effects could be still experimentally visible in $A^s_{\rm SL}$. Yet the confirmation of the large values of $S_{\psi\phi}$ observed by CDF and D0 will be a serious problem for this kind of models with purely left-handed currents. From fig. 14 we also show that models with purely left-handed currents can predict very large deviations (in both directions) from the MFV SUSY expectations for $\mathrm{BR}(B_d \to \mu^+\mu^-)/\mathrm{BR}(B_s \to \mu^+\mu^-)$. In particular, in contrast to the models considered so far, the ratio in question can also be significantly larger than in the MFV models and $\mathrm{BR}(B_d \to \mu^+\mu^-)$ can reach values as high as 2×10^{-9}, while staying consistent with the bound on $\mathrm{BR}(B_s \to \mu^+\mu^-)$.

Finally, in the last row of fig. 14, we show the correlations involving the CP asymmetries in $B \to K^*\mu^+\mu^-$, $\langle A_7\rangle$ vs. $\langle A_8\rangle$ and $\langle A_7\rangle$ vs $S_{\phi K_S}$. We find a very stringent correlation between $\langle A_7\rangle$ and $\langle A_8\rangle$ with the NP effect in $\langle A_7\rangle$ being a factor of two larger and with opposite sign with respect to $\langle A_8\rangle$. This strong correlation is due to the fact that, in the considered framework, effects in both $\langle A_7\rangle$ and $\langle A_8\rangle$ are almost exclusively induced by the NP contributions to C_7. Moreover, we also find a clean correlation between $\langle A_7\rangle$ and $S_{\phi K_S}$ with $-0.2 \lesssim \langle A_7\rangle \lesssim -0.1$ in the region accounting for the $S_{\phi K_S}$ anomaly.

Concerning the hadronic EDMs, the main difference between models with purely LH currents with respect to models containing RH currents is that in the former case the quark (C)EDMs turn out to be proportional to the external light quark masses. As a result, the down- and up-quark (C)EDMs generated by flavour effects are suppressed by small flavour mixing angles while not being enhanced by the heaviest quark masses, hence, the hadronic EDMs are safely under control. Assuming CKM-like MIs, $\tilde{m} = 500\,\mathrm{GeV}$ and $\tan\beta = 10$, d_d/e and d^c_d are of order $\sim 10^{-28}$ cm. The strange quark (C)EDM might reach interesting values as it is enhanced, compared to d_d/e and d^c_d, by a factor of $(m_s/m_d) \times \lambda^{-2} \approx 400$. However, it is still not possible to draw any clear-cut conclusion due to the uncertainties relating d_s to physical hadronic EDMs.

In summary, the most striking predictions of the models with purely LH currents as opposed to models with large RH currents are

- the ability to explain the $S_{\phi K_S}$ anomaly with simultaneous possible explanation of the $(g-2)_\mu$ anomaly and significantly enhanced direct CP asymmetry in $b \to s\gamma$,
- SM-like $S_{\psi\phi}$,
- in the considered δLL model, the possibility of very large deviations for $\mathrm{BR}(B_d \to \mu^+\mu^-)/\mathrm{BR}(B_s \to \mu^+\mu^-)$ in both directions compared to its MFV value, with $\mathrm{BR}(B_d \to \mu^+\mu^-)$ and $\mathrm{BR}(B_s \to \mu^+\mu^-)$ reaching values as high as 2×10^{-9} and 6×10^{-8}, respectively,
- Small NP effects in $\Delta F = 2$ processes, like ϵ_K, $S_{\psi K_s}$ and $\Delta M_d/\Delta M_s$. Therefore difficulty in addressing the UT tension.

6.5 Step 5: Comparison with the FBMSSM and the MFV MSSM

Finally, we want to recall the results for the FBMSSM [68], to discuss the general MFV framework and to make a comparison with the models with left-handed CKM-like currents discussed in step 4.

In [68], it was found that the best probes of the FBMSSM are the EDMs of the electron (d_e) and the neutron (d_n), as well as flavour changing and CP violating processes in B systems, like the CP asymmetries in $b \to s\gamma$ and $B \to \phi(\eta')K_S$, i.e. $A_{\rm CP}(b \to s\gamma)$ and $S_{\phi(\eta')K_S}$, respectively. The non-standard values for $S_{\phi(\eta')K_S}$, measured at the B factories, can find a natural explanation within the FBMSSM with the effect being typically by a factor of 1.5 larger in $S_{\phi K_S}$ in agreement with the pattern observed in the data.

Interestingly, it was found that the desire of reproducing the observed low values of $S_{\phi K_S}$ and $S_{\eta' K_S}$ implies:

- a lower bounds on the electron and neutron EDMs $d_{e,n} \gtrsim 10^{-28}\, e\,\mathrm{cm}$,
- a positive and sizable (non-standard) $A_{\rm CP}(b \to s\gamma)$ asymmetry in the ballpark of $1\% - 5\%$,
- small NP effects in $S_{\psi K_S}$ and $\Delta M_d/\Delta M_s$ so that in the FBMSSM these observables can be used to extract β and $|V_{td}|$,
- $|\epsilon_K|$ is enhanced over its SM value at most at a level of $\lesssim 15\%$,
- very small effects in $S_{\psi\phi}$ which could, however, be still visible through the semileptonic asymmetry $A^s_{\rm SL}$,
- a natural explanation of the Δa_μ anomaly under the mild assumption that the slepton masses are not much heavier than the squark masses (this is true in almost all the known models of SUSY breaking).

The question we want to address now is, to which extent this pattern of effects gets modified within the framework of the MFV MSSM. In particular we will analyse if the richer flavour and CP violating structure of the MFV MSSM allows to generate sizeable effects in $S_{\psi\phi}$.

As discussed in sec. 3.1, within a MFV MSSM scenario, the charginos and the charged Higgses can induce the FCNC amplitude $M_{12}^{(M)}$ by means of C_1 and $\tilde{C}_3$, with the chargino box contributions to $\tilde{C}_3$ given in (3.7) being the only non-negligible contributions sensitive to the new phases.

Moreover, as mentioned in sec. 5, the additional terms in the LL soft masses in the MFV MSSM lead to potentially complex MIs

$$(\delta_d^{LL})_{3i} \simeq (b_1 + b_3 y_b^2) V_{ti} \ , \tag{6.4}$$

that will lead to gluino contributions to $\Delta F = 2$ processes by means of the Wilson coefficient C_1 given in (3.9).

In fig. 15, we show the predictions for $S_{\psi\phi}$ vs. $\tan\beta$ in a MFV MSSM scenario taking into account the SUSY contributions listed above. As we can see, potentially sizable effects to $S_{\psi\phi}$ would be possible only in the very large $\tan\beta$ regime (light blue points); however, in this case the constraints from both $\mathrm{BR}(B_s \to \mu^+\mu^-)$ and $\mathrm{BR}(b \to s\gamma)$ become very powerful

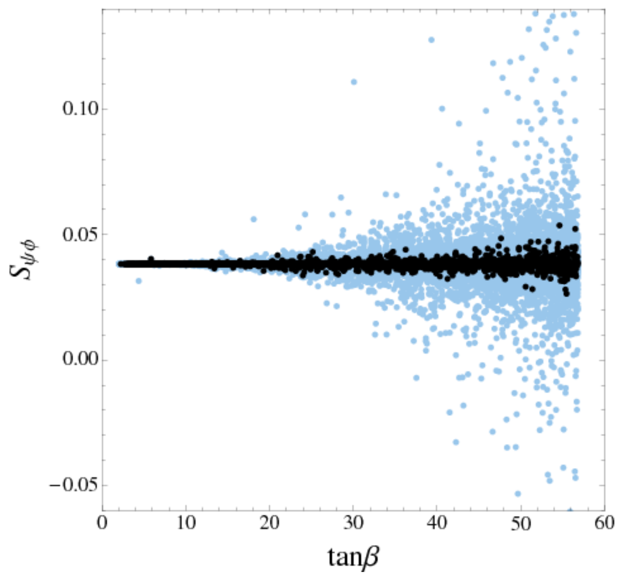

Figure 15: $S_{\psi\phi}$ vs. $\tan\beta$ in the MFV scenario. Light blue points do not satisfy the B-physics constraints while the black ones do.

and they prevent any visible effect in $S_{\psi\phi}$ (black points). This confirms and strengthens the general finding of [68] that within SUSY MFV scenarios, large NP contributions can only be expected in $\Delta B = 1$ transitions.

The models with left-handed CKM-like currents discussed in step 4 share many similarities with the FBMSSM and the MFV MSSM. In particular, all the correlations among B-physics asymmetries are almost the same in these scenarios and also the size of the effects are comparable. As argued in [68], the $(g-2)_\mu$ anomaly is naturally solved once we account for the non-standard value for $S_{\phi K_S}$; this claim has been fully confirmed in the present work where we deal with a concrete SUSY breaking scenario, that is a SUGRA scenario.

The major difference discriminating these scenarios regards their predictions for the leptonic and hadronic EDMs. Within the FBMSSM, we predicted $d_{e,n} \gtrsim 10^{-28}\, e\,\mathrm{cm}$ while solving the $S_{\phi K_S}$ anomaly. On the other hand, within the general class of models with pure left-handed CKM-like currents, such a lower bound is significantly relaxed. In fact, in this latter case, the source of CP violation is assumed to come from flavour effects and the resulting EDMs are suppressed by small flavour mixing angles. This suppression cannot be compensated by enhancement factors, as the heavy-light Yukawa ratios, as it happens in presence of RH currents.

Hence, a potential discovery of some of the above CP asymmetries with those peculiar correlations without any NP signal in $d_{e,n}$ at the level of $d_{e,n} < 10^{-28}\, e\,\mathrm{cm}$ would most likely rule out the FBMSSM and favour non-MFV models with purely left-handed currents.

7 Comparison with Other Models

7.1 Comparison with the LHT and RS Models

In the present paper we have discussed several specific supersymmetric models that exhibit different patterns of flavour and CP violation. In this section we would like to compare briefly these patterns with the ones found in the extensive analyses of flavour violation in the Littlest Higgs model with T-parity (LHT) [17, 72, 73, 75, 76, 77] and in a Randall-Sundrum (RS) Model with custodial protection and with a Kaluza-Klein (KK) scale in the reach of the LHC [15, 16].

Let us first recall that the LHT and RS models contain new sources of flavour and CP violation but while in the LHT model the operator structure in the effective weak Hamiltonians is the same as in the SM [17, 72, 73], in the RS model new operators are present [15, 16]. In particular the left-right operators contributing to ϵ_K imply some fine tuning of the parameters in order to keep ϵ_K under control if one wants to have the KK scale in the reach of the LHC [15]. Analogous tunings, albeit not as serious, are necessary in the RS model, in order to be in agreement with the experimental bounds on $\text{BR}(B \to X_s\gamma)$ [225], $\text{BR}(\mu \to e\gamma)$ [226, 227, 228] and EDMs [229, 230], that are all dominated by dipole operators. Also contributions to ϵ'/ϵ can be large [231].

On the other hand in the LHT model $\text{BR}(B \to X_s\gamma)$ and EDMs are fully under control [17] as NP contributions to the Wilson coefficients of dipole operators are small. Still the branching ratio for the decay $\mu \to e\gamma$ can reach the present upper bound [73, 76] and sizable contributions to ϵ'/ϵ are possible [74]

We now compare the predictions of the LHT and RS models with the ones of the supersymmetric models analyzed in the present paper. To this end we confine our discussion to four very interesting channels: $S_{\psi\phi}$, $B_s \to \mu^+\mu^-$, $K^+ \to \pi^+\nu\bar{\nu}$ and $\mu \to e\gamma$ that are best suited for the distinction of supersymmetric models from LHT and RS models.

- First $S_{\psi\phi}$ can be large in LHT, RS, AC, RVV2 and AKM models, however with the following hierarchy for the maximal possible values

$$(S_{\psi\phi})^{\max}_{\text{LHT}} \approx (S_{\psi\phi})^{\max}_{\text{AKM}} < (S_{\psi\phi})^{\max}_{\text{RVV2}} < (S_{\psi\phi})^{\max}_{\text{RS}} \approx (S_{\psi\phi})^{\max}_{\text{AC}} \tag{7.1}$$

  with $(S_{\psi\phi})^{\max}_{\text{LHT}} \approx 0.3$ and $(S_{\psi\phi})^{\max}_{\text{AC}} \simeq 1$ [23].

  Instead the values of $S_{\psi\phi}$ in the δLL model, in the FBMSSM and the MFV MSSM are SM-like.

- While $\text{BR}(B_s \to \mu^+\mu^-)$ in all supersymmetric models discussed by us can be as large as the present experimental upper bound, the enhancements of $\text{BR}(B_s \to \mu^+\mu^-)$ in the RS and LHT models do not exceed 10% and 30%, respectively.

- The opposite pattern is found for $K^+ \to \pi^+\nu\bar{\nu}$ decays. In all the supersymmetric flavour models discussed by us, $\text{BR}(K^+ \to \pi^+\nu\bar{\nu})$ is basically SM-like. On the other hand in the RS and LHT models $\text{BR}(K^+ \to \pi^+\nu\bar{\nu})$ can be enhanced by as much as a factor 1.5 and 2.5, respectively.

[23] In the LHT model, $S_{\psi\phi}$ can be significant in spite of the purely left-handed structure of the flavour violating currents because the $b \to s\gamma$ and $B_s \to \mu^+\mu^-$ constraints are easier satisfied than in the δLL model.

- Of particular interest will be the impact of a measurement of $S_{\psi\phi}$ much larger than the SM value:

  1. On one hand this would exclude the δLL, FBMSSM and MFV MSSM models.
  2. On the other hand in the AC and AKM models it would imply a lower bound on $\mathrm{BR}(B_s \to \mu^+\mu^-)$ significantly higher than possible values in the LHT and RS models and consequently the measurement of $\mathrm{BR}(B_s \to \mu^+\mu^-)$ could distinguish these two classes of models. In the RVV2 model large values of the branching ratio in question are possible but not necessarily implied by the anomalously large value of $S_{\psi\phi}$.
  3. In the case of $K^+ \to \pi^+\nu\bar{\nu}$, a measurement of a sizable $S_{\psi\phi}$ precludes significant enhancements of $\mathrm{BR}(K^+ \to \pi^+\nu\bar{\nu})$ in RS and LHT models. Consequently in such a scenario it will be difficult to distinguish these two models from the supersymmetric ones, just taking into account the decay $K^+ \to \pi^+\nu\bar{\nu}$. On the other hand, the measurement of $\mathrm{BR}(K^+ \to \pi^+\nu\bar{\nu})$ much larger than the SM value would favour RS and LHT models to all the supersymmetric flavour models discussed by us if $S_{\psi\phi}$ is SM-like but would rule out also the RS and LHT models if $S_{\psi\phi}$ is large.

- Finally let us recall that while the supersymmetric models and LHT models can reach the experimental bound for $\mathrm{BR}(\mu \to e\gamma)$ [73, 76, 77], the ratios $\mathrm{BR}(\mu \to 3e)/\mathrm{BR}(\mu \to e\gamma)$ and $\mathrm{BR}(\tau \to 3\mu)/\mathrm{BR}(\tau \to e\gamma)$ are in supersymmetric models roughly by one order of magnitude smaller than in the LHT model.

In summary, we observe that already the combination of $S_{\psi\phi}$, $\mathrm{BR}(B_s \to \mu^+\mu^-)$ and $\mathrm{BR}(K^+ \to \pi^+\nu\bar{\nu})$ should be able to distinguish between the AC, RVV2, AKM, LHT and RS models unless all these three observables are found SM-like. The distinction between (AC,RVV2,AKM) and (LHT,RS) models can easily be made with the help of $\mathrm{BR}(B_s \to \mu^+\mu^-)$ and $\mathrm{BR}(K^+ \to \pi^+\nu\bar{\nu})$ only but the inclusion in this test of $S_{\psi\phi}$ will be very helpful. The distinction between the AC and RVV2 models has been discussed in the previous sections while the one between LHT and RS in [16, 77]. Here the correlation between $K_L \to \pi^0\nu\bar{\nu}$ and $K^+ \to \pi^+\nu\bar{\nu}$ markedly different in both models and the hierarchy in (7.1) could play important roles.

7.2 DNA-Flavour Test of New Physics Models

We have seen in the previous sections and in sec. 7.1 that the patterns of flavour violation found in various extensions of the SM differed from model to model, thereby allowing in the future to find out which of the models considered by us, if any, can survive the future measurements. Undoubtedly, the correlations between various observables that are often characteristic for a given model will be of the utmost importance in these tests.

In tab. 8, we show a summary of the potential size of deviations from the SM results allowed for a large number of observables considered in the text, when all existing constraints from other observables not listed there are taken into account. We distinguish among:

- large effects (three *red* stars),
- moderate but still visible effects (two *blue* stars),

	AC	RVV2	AKM	δLL	FBMSSM	LHT	RS
$D^0 - \bar{D}^0$	★★★	★	★	★	★	★★★	?
ϵ_K	★	★★★	★★★	★	★	★★	★★★
$S_{\psi\phi}$	★★★	★★★	★★★	★	★	★★★	★★★
$S_{\phi K_S}$	★★★	★★	★	★★★	★★★	★	?
$A_{\text{CP}}(B \to X_s\gamma)$	★	★	★	★★★	★★★	★	?
$A_{7,8}(B \to K^*\mu^+\mu^-)$	★	★	★	★★★	★★★	★★	?
$A_9(B \to K^*\mu^+\mu^-)$	★	★	★	★	★	★	?
$B \to K^{(*)}\nu\bar{\nu}$	★	★	★	★	★	★	★
$B_s \to \mu^+\mu^-$	★★★	★★★	★★★	★★★	★★★	★	★
$K^+ \to \pi^+\nu\bar{\nu}$	★	★	★	★	★	★★★	★★★
$K_L \to \pi^0\nu\bar{\nu}$	★	★	★	★	★	★★★	★★★
$\mu \to e\gamma$	★★★	★★★	★★★	★★★	★★★	★★★	★★★
$\tau \to \mu\gamma$	★★★	★★★	★	★★★	★★★	★★★	★★★
$\mu + N \to e + N$	★★★	★★★	★★★	★★★	★★★	★★★	★★★
d_n	★★★	★★★	★★★	★★	★★★	★	★★★
d_e	★★★	★★★	★★	★	★★★	★	★★★
$(g-2)_\mu$	★★★	★★★	★★	★★★	★★★	★	?

Table 8: "DNA" of flavour physics effects for the most interesting observables in a selection of SUSY and non-SUSY models ★★★ signals large effects, ★★ visible but small effects and ★ implies that the given model does not predict sizable effects in that observable.

- vanishingly small effects (one *black* star).

This table can be considered as the collection of the DNA's for various models. These DNA's will be modified as new experimental data will be availabe and in certain cases we will be able to declare certain models to be disfavoured or even ruled out.

In constructing the table we did not take into account possible correlations among the observables listed there. We have seen that in some models, it is not possible to obtain large effects simultaneously for certain pairs or sets of observables and consequently future measurements of a few observables considered in tab. 8 will have an impact on the patterns shown in this DNA table. It will be interesting to monitor the changes in this table when the future experiments will provide new results.

8 Flavour vs. LHC Data

In sec. 6, we have performed a correlated analysis of low-energy predictions, arising in SUSY flavour models, for a complete set of flavour observables with the aim of outlining clear patterns of deviation from the SM predictions.

In the following, we will try to address the question of the synergy and interplay existing between direct and indirect NP searches.

For instance, one relevant question could be: which is the expected SUSY spectrum at the LHC in case sizable indirect NP effects will be detected in some flavour channels at the upcoming experimental facilities? Vice versa, if the LHC will measure the masses of some SUSY particles (within a given accuracy), which additional information could we obtain from some non-standard effects in flavour observables?

To answer the above questions, we analyze the flavour physics predictions of the flavour models discussed in sec. 6 with respect to the expected spectrum at the LHC.

In fig. 16, we show the planes for the lightest stop mass ($m_{\tilde{t}_1}$) vs. the lightest chargino mass ($m_{\tilde{\chi}_1}$) as well as the $M_H - \tan\beta$ planes. The first two rows of fig. 16 correspond to the AC model [36] (plots on the left), the RVV2 model [51] (plots in the middle) and the AKM model [52] (plots on the right), respectively. The different colors show the possible values for $S_{\psi\phi}$ in these models as indicated in the overall bar. The last lower plots correspond to models with pure left-handed currents with CKM-like mixing angles [42] and the different colors indicate the attained values for $S_{\phi K_S}$.

An interesting feature emerging from fig. 16 is that, in the case of the AC, RVV2 and AKM models, large effects in $S_{\psi\phi}$ are possible – and indeed even favoured – for a quite heavy soft SUSY spectrum, even beyond the LHC reach. However, this is not an evasion of the decoupling theorem but, instead, a confirmation of the dominance of the Higgs mediated effects in $S_{\psi\phi}$. In fact, since the effective FCNC couplings of the Higges with the SM fermions arise from dimension-4 operators, they do not decouple with the soft SUSY scale. Clearly, the double Higgs penguin contributions generating $S_{\psi\phi}$ decouple with the mass of the heavy Higgs sector, as confirmed by the second row of fig. 16, in agreement with the decoupling theorem. Moreover, $S_{\psi\phi}$ attains the maximum values for heavy soft masses since the most stringent indirect constraints arising from BR($b \to s\gamma$) and ϵ_K, decoupling with the soft SUSY sector, are relaxed in this case.

Hence, there exist regions of the SUSY parameter space at the border or even beyond the LHC reach where we can expect clear non-standard signals in flavour processes. In these regions, flavour phenomena, and thus the indirect search, represent the most powerful tool to shed light on NP in case of SUSY. In such a case, where we will obtain only an improved upper bound on the scale of SUSY masses, the study of the correlations among flavour observables, departing from their SM expectations, would be the only tool at our disposal to unveil the nature of the NP theory that is operating.

An opposite behaviour, compared to the AC, RVV2 and AKM models, is shown by the δLL model (last row of fig. 16) where the double Higgs penguins do not play a significant role and the flavour observables decouple with the soft SUSY masses.

Large – non-standard – effects in flavour observables necessarily imply, in this case, a SUSY spectrum within the LHC reach. Hence, combining the information on the spectrum from the LHC with the information from the low-energy flavour processes, we would be able, to some extent, to measure the mixing angle regulating the flavour transition. Such an achievement would represent a crucial step forward towards the reconstruction of the

underlying flavour symmetry at work. The described situation represents one clear example of the synergy and interplay of direct and indirect NP searches.

9 Summary

The coming years will witness tremendous progress at the high energy frontier accomplished primarily at the LHC, where the available energy will be increased by one order of magnitude. Equivalently, for the first time we will be able to resolve directly distances well below 10^{-18} m, that have been explored so far. Parallel to these developments, important advances are expected at the high precision frontier through the improved B_s-physics experiments at the Tevatron and in particular LHCb at CERN. At later stages in the coming decade these efforts will be strengthened by new rare K experiments at J-PARC, the NA62 collaboration at CERN and possibly Project X at Fermilab as well as Belle-II at KEK and the planned Super$B$ facility in Rome. The latter two will also provide new insights into the FCNC processes in the D meson system and in charged lepton decays.

While the main goal at the high energy frontier is the discovery of new particles and the determination of their masses, the main goal of flavour physics is the search for the footprints of these new particles in rare processes and the determination of their couplings. As the latter exploration of very short distance scales is indirect, only measurements of a large number of observables and the study of correlations between them in a given extension of the SM and in particular of patterns of flavour violation characteristic for a given model can allow us to identify the correct NP scenario.

In the present paper, we have performed an extensive study of processes governed by $b \to s$ transitions and of their correlations with processes governed by $b \to d$ transitions, $s \to d$ transitions, $D^0 - \bar{D}^0$ oscillations, lepton flavour violating decays, electric dipole moments and $(g-2)_\mu$. To this end, we have considered a number of supersymmetric flavour models that on one hand aim at the explanation of the observed hierarchical fermion masses and mixings and on the other hand provide natural suppression of FCNC transitions. In particular we have analyzed the following representative scenarios:

i) dominance of right-handed currents (abelian model by Agashe and Carone [36]),

ii) comparable left- and right-handed currents with CKM-like mixing angles represented by the special version (RVV2) of the non abelian $SU(3)$ model by Ross, Velasco and Vives [51] as discussed recently in [62] and the model by Antusch, King and Malinsky (AKM) [52],

iii) dominance of left-handed currents in non-abelian models [42].

In the choice of these three classes of flavour models, we were guided by our model independent analysis, as these three scenarios predicting quite different patterns of flavour violation should give a good representation of most SUSY flavour models discussed in the literature.

The distinct patterns of flavour violation found in each scenario have been listed in detail in sec. 6 and the corresponding plots can be found in figures 11–14.

The main messages from our analysis of the models in question are as follows:

- Supersymmetric models with right-handed currents (AC, RVV2, AKM) and those with left-handed currents can be globally distinguished by the values of the CP-asymmetries

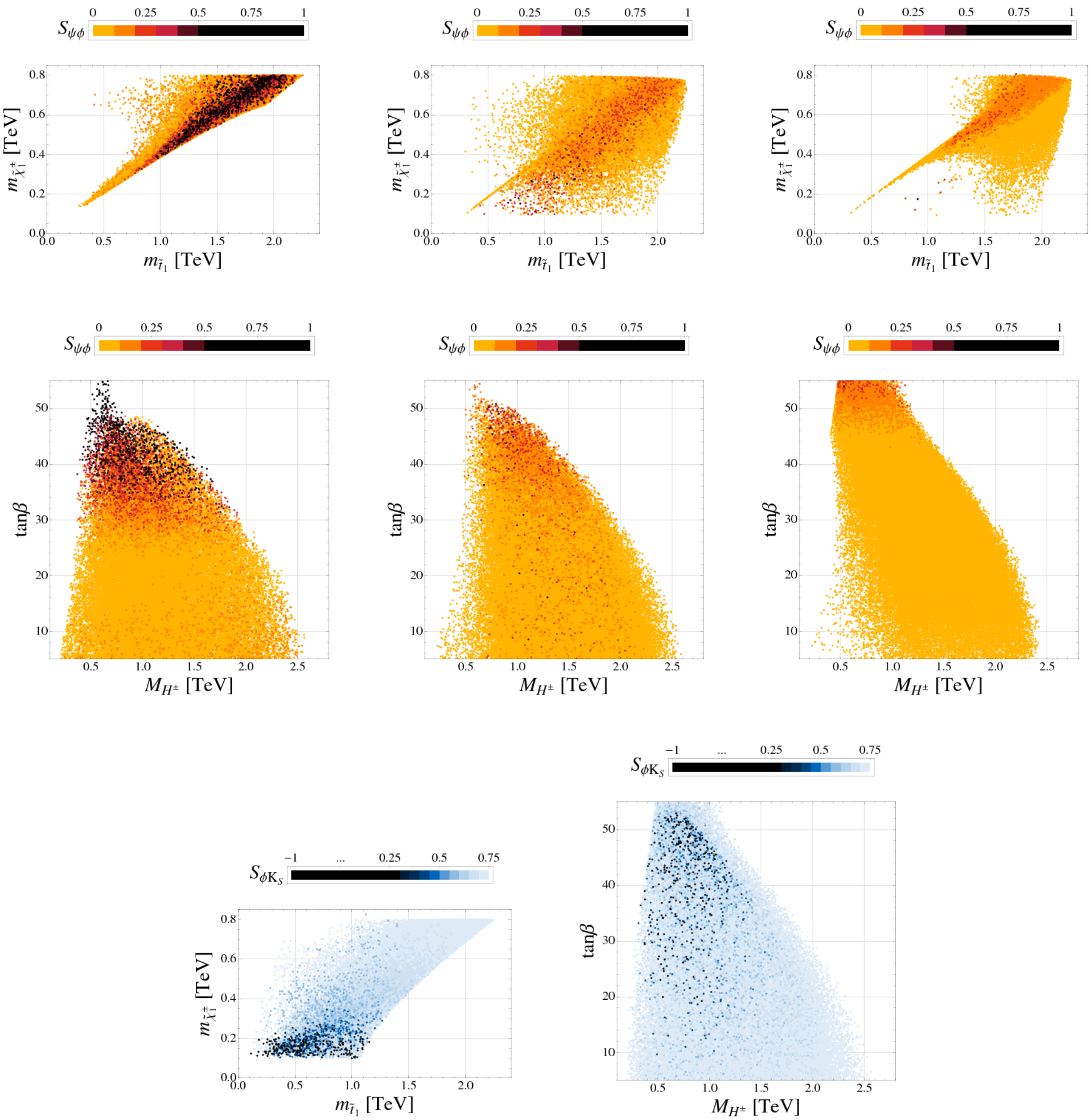

Figure 16: The plane of the lightest stop mass ($m_{\tilde{t}_1}$) vs. the lightest chargino mass ($m_{\tilde{\chi}_1}$) as well as the $M_H - \tan\beta$ planes. The first two rows of fig. 16 correspond to the AC model [36] (plots on the left), the RVV2 model [51] (plots in the middle) and the AKM model [52] (plots on the right), respectively. The different colors show the possible values for $S_{\psi\phi}$ in these models as indicated in the overall bar. The last lower plots correspond to models with pure left-handed currents with CKM-like mixing angles [42] and the different colors indicate the attained values for $S_{\phi K_S}$.

$S_{\psi\phi}$ and $S_{\phi K_S}$ with the following important result: none of the models considered by us can simultaneously solve the $S_{\psi\phi}$ and $S_{\phi K_S}$ anomalies observed in the data. In the models with RH currents, $S_{\psi\phi}$ can naturally be much larger than its SM value, while $S_{\phi K_S}$ remains either SM-like or its correlation with $S_{\psi\phi}$ is inconsistent with the data. On the contrary, in the models with LH currents, $S_{\psi\phi}$ remains SM-like, while the $S_{\phi K_S}$ anomaly can easily be solved. Thus, already future precise measurements of $S_{\psi\phi}$ and $S_{\phi K_S}$ will select one of these two classes of models, if any.

- The desire to explain the $S_{\psi\phi}$ anomaly within the models with RH currents unambiguously implies, in the case of the AC and the AKM models, values of $\mathrm{BR}(B_s \to \mu^+\mu^-)$ as high as several 10^{-8}, while in the RVV2 model, such values are also possible but not necessarily implied by the large value of $S_{\psi\phi}$. Interestingly enough, in all these models large values of $S_{\psi\phi}$ can also explain the $(g-2)_\mu$ anomaly. Moreover, in the AC and RVV2 models, the ratios $\mathrm{BR}(B_d \to \mu^+\mu^-)/\mathrm{BR}(B_s \to \mu^+\mu^-)$ and $\mathrm{BR}(B_d \to \mu^+\mu^-)/\Delta M_s$ can significantly differ from the MFV prediction, providing a splendid opportunity to shed light on new sources of flavour violation beyond the CKM ones. Further, $\mathrm{BR}(B_d \to \mu^+\mu^-)/\mathrm{BR}(B_s \to \mu^+\mu^-)$ is predicted to be dominantly smaller than its MFV value especially for $\mathrm{BR}(B_s \to \mu^+\mu^-) \gtrsim 10^{-8}$. Values of $\mathrm{BR}(B_d \to \mu^+\mu^-)$ as high as 1×10^{-9} are still possible in these models.

- The hadronic EDMs represent very sensitive probes of SUSY flavour models with right-handed currents. In the AC model, large values for the neutron EDM might be easily generated by both the up- and strange-quark (C)EDM. In the former case, visible CPV effects in $D^0 - \bar{D}^0$ mixing are also expected while in the latter case large CPV effects in B_s systems are unavoidable. The RVV2 and AKM models predict values for the down-quark (C)EDM and, hence for the neutron EDM, above the $\approx 10^{-28}\,e$cm level when a large – non-standard – $S_{\psi\phi}$ is generated. All the above models predict a large strange-quark (C)EDM, hence, a reliable knowledge of its contribution to the hadronic EDMs, by means of lattice QCD techniques, would be of the utmost importance to probe or to falsify flavour models embedded in a SUSY framework.

- In the RVV2 and AKM models, the desire to explain the $(g-2)_\mu$ anomaly implies that $\mathrm{BR}(\mu \to e\gamma) \gtrsim 10^{-13}$, in the reach of the MEG experiment, and $d_e > 10^{-29}\,e$cm ($d_e \lesssim 10^{-30}\,e$cm) in the RVV2 (AKM) model is predicted. Moreover, in the case of the RVV2 model, $\mathrm{BR}(\tau \to \mu\gamma) \gtrsim 10^{-9}$ is then in the reach of Super-B machines, while $\tau \to \mu\gamma$ remains most likely beyond the Super-B reach in the case of the AKM model. The explanation of the $(g-2)_\mu$ anomaly, combined with non-standard values for $S_{\psi\phi}$, would imply $\mathrm{BR}(\mu \to e\gamma) \gtrsim 10^{-12}$ in both the RVV2 and AKM models.

- Finally, while the abelian AC model resolves the present UT tension through the modification of the ratio $\Delta M_d/\Delta M_s$, the non-abelian flavour models RVV2 and AKM provide the solution through NP contributions to ϵ_K. Moreover, while the AC model predicts sizable NP contributions to $D^0 - \bar{D}^0$ mixing, such contributions are negligibly small in the RVV2 and AKM models.

- In the supersymmetric models with LH currents only, the desire to explain the $S_{\phi K_S}$ anomaly unambiguously implies that the direct CP asymmetry in $b \to s\gamma$ is much larger than its SM value. This is in contrast to the models with RH currents where this

asymmetry remains SM-like. Also the solution to the $(g-2)_\mu$ anomaly can be easily accounted for.

- Interestingly, also in the LH-current-models –that are in many aspects similar to MFV models–, the ratio $\mathrm{BR}(B_d \to \mu^+\mu^-)/\mathrm{BR}(B_s \to \mu^+\mu^-)$ can not only deviate significantly from its MFV value, but in contrast to the models with RH currents considered by us can also be much larger than the latter value. Consequently, values for $\mathrm{BR}(B_d \to \mu^+\mu^-)$ as high as 2×10^{-9} are still possible while being consistent with the bounds on all other observables, in particular the one on $\mathrm{BR}(B_s \to \mu^+\mu^-)$. Also interesting correlations between $S_{\phi K_S}$ and CP asymmetries in $B \to K^*\ell^+\ell^-$ are found.

- The FBMSSM as well as the MFV MSSM bear several similarities to the models with LH currents only. In particular, in all these models, $S_{\psi\phi}$ is basically SM like. The FBMSSM and the MFV MSSM differ however from the δLL model especially in their predictions of the EDMs. In the FBMSSM and the MFV MSSM, large effects in CP violating $\Delta F = 1$ observables naturally imply values for the EDMs close to the current experimental limits. In the δLL model, on the other hand, the EDMs can be easily well under control.

This summary of our most important results already shows that the simultaneous study of various flavour violating processes can allow us to distinguish various NP scenarios. More results can be found in the numerous figures presented by us.

We have also presented a comprehensive model-independent analysis of the MSSM with general sources of flavour and CP violation that goes in several aspects, listed at the beginning of our paper, beyond many analyses found in the literature. The bounds on the mass insertions $(\delta^{AB}_{u,d})_{i,j}$ can be found in figures 6–9. Any version of the MSSM based on a SUGRA spectrum has to satisfy them. Beyond our MSSM analysis, we have also emphasized the usefulness of the $R_b - \gamma$ plane in exhibiting transparently various tensions in present UT analyses.

It will be exciting to monitor upcoming results from Tevatron and the LHC on $S_{\psi\phi}$ and $B_s \to \mu^+\mu^-$. Already these two measurements will be capable of excluding some of the models considered by us and distinguish them from the LHT and RS model with custodial protection in which $S_{\psi\phi}$ can be large but $B_{s,d} \to \mu^+\mu^-$ remain SM-like. Further observables analyzed by us will help to identify more precisely the correct extension of the SM. In particular, while the branching ratios for $K \to \pi\nu\bar{\nu}$ decays in the supersymmetric models considered by us remain SM-like, they can be significantly enhanced in the LHT and RS models.

A DNA-Flavour Test proposed by us should give still a deeper insight into the patterns of flavour violation in various scenarios, in particular when it is considered simultaneously with various correlations present in concrete models. The interplay of these efforts with the direct searches for NP will be most exciting.

In conclusion, the above physics cases are representative of the richness which is present in flavour physics once we assume flavour models embedded within a gravity mediated SUSY breaking framework. It could be that, at the end, flavour physics is one of the very few tools we have to understand from low-energy physics whether nature possesses supersymmetry at the root of its symmetries, or whether other scenarios like LHT or RS are realized in nature.

Acknowledgments

We would like to thank M. Blanke for discussions and especially J. Jones-Perez and O. Vives for many informative correspondences about the RVV2 model [62].

This work has been supported in part by the Cluster of Excellence "Origin and Structure of the Universe", the Deutsche Forschungsgemeinschaft (DFG) under contract BU 706/2-1 and the German Bundesministerium für Bildung und Forschung under contract 05HT6WOA. WA acknowledges support by the Graduiertenkolleg GRK 1054 of DFG. SG acknowledges support by the European Community's Marie Curie Research Training Network under contract MRTN-CT-2006-035505 ["HEP-TOOLS"].

A Explicit Expressions for the Loop Functions

Loop Functions for the $\Delta F = 2$ Mixing Amplitudes

$$g_1^{(1)}(x) = -\frac{11+144x+27x^2-2x^3}{108(1-x)^4} - \frac{x(13+17x)}{18(1-x)^5}\log x\ , \tag{A.1}$$

$$g_1^{(2)}(x) = \frac{33+665x+237x^2-39x^3+4x^4}{216(1-x)^5} + \frac{x(26+49x)}{18(1-x)^6}\log x\ , \tag{A.2}$$

$$g_1^{(3)}(x) = -\frac{66+1835x+1005x^2-255x^3+55x^4-6x^5}{1080(1-x)^6} - \frac{x(13+32x)}{18(1-x)^7}\log x\ , \tag{A.3}$$

$$g_4^{(1)}(x) = \frac{2-99x-54x^2+7x^3}{18(1-x)^4} - \frac{x(5+19x)}{3(1-x)^5}\log x\ , \tag{A.4}$$

$$g_4^{(2)}(x) = -\frac{3-212x-192x^2+48x^3-7x^4}{18(1-x)^5} + \frac{10x(1+5x)}{3(1-x)^6}\log x\ , \tag{A.5}$$

$$g_4^{(3)}(x) = \frac{12-1117x-1452x^2+528x^3-152x^4+21x^5}{180(1-x)^6} - \frac{x(5+31x)}{3(1-x)^7}\log x\ , \tag{A.6}$$

$$g_5^{(1)}(x) = -\frac{10+117x+18x^2-x^3}{54(1-x)^4} - \frac{x(11+13x)}{9(1-x)^5}\log x\ , \tag{A.7}$$

$$g_5^{(2)}(x) = \frac{15+272x+84x^2-12x^3+x^4}{54(1-x)^5} + \frac{2x(11+19x)}{9(1-x)^6}\log x\ , \tag{A.8}$$

$$g_5^{(3)}(x) = -\frac{60+1507x+732x^2-168x^3+32x^4-3x^5}{540(1-x)^6} - \frac{x(11+25x)}{9(1-x)^7}\log x\ , \tag{A.9}$$

$$h_1(x) = \frac{4(1+x)}{3(1-x)^2} + \frac{8x}{3(1-x)^3}\log x\ , \tag{A.10}$$

$$h_2(x) = -\frac{4(2+5x-x^2)}{9(1-x)^3} - \frac{8x}{3(1-x)^4}\log x\ , \tag{A.11}$$

$$h_3(x) = -\frac{1}{2(1-x)} - \frac{x}{2(1-x)^2}\log x\ , \tag{A.12}$$

$$h_4(x,y) = -\frac{1}{(1-x)(1-y)} + \frac{x}{(1-x)^2(y-x)}\log x + \frac{y}{(1-y)^2(x-y)}\log y\ , \tag{A.13}$$

$$f_1(x) = -\frac{x+1}{4(1-x)^2} - \frac{x}{2(1-x)^3}\log x \ , \tag{A.14}$$

$$f_3(x) = \frac{x^2-6x-17}{6(1-x)^4} - \frac{3x+1}{(1-x)^5}\log x \ , \tag{A.15}$$

$$f(x) = \frac{1}{1-x} + \frac{x}{(1-x)^2}\log x \ . \tag{A.16}$$

Loop Functions for $b \to s\gamma$

$$h_7(x) = -\frac{5x^2-3x}{12(1-x)^2} - \frac{3x^2-2x}{6(1-x)^3}\log x \ , \tag{A.17}$$

$$h_8(x) = -\frac{x^2-3x}{4(1-x)^2} + \frac{x}{2(1-x)^3}\log x \ , \tag{A.18}$$

$$f_7^{(2)}(x) = -\frac{13-7x}{24(1-x)^3} - \frac{3+2x-2x^2}{12(1-x)^4}\log x \ , \tag{A.19}$$

$$f_8^{(2)}(x) = \frac{1+5x}{8(1-x)^3} + \frac{x(2+x)}{4(1-x)^4}\log x \ , \tag{A.20}$$

$$f_{7,8}^{(1)}(x,y) = \frac{2}{x-y}\left(f_{7,8}^2(x) - f_{7,8}^2(y)\right) \ , \tag{A.21}$$

$$g_7^{(1)}(x) = -\frac{2(1+5x)}{9(1-x)^3} - \frac{4x(2+x)}{9(1-x)^4}\log x \ , \tag{A.22}$$

$$g_7^{(2)}(x) = -\frac{2(1+10x+x^2)}{9(1-x)^4} - \frac{4x(1+x)}{3(1-x)^5}\log x \ , \tag{A.23}$$

$$g_8^{(1)}(x) = \frac{11+x}{3(1-x)^3} + \frac{9+16x-x^2}{6(1-x)^4}\log x \ , \tag{A.24}$$

$$g_8^{(2)}(x) = \frac{53+44x-x^2}{12(1-x)^4} + \frac{3+11x+2x^2}{2(1-x)^5}\log x \ . \tag{A.25}$$

Loop Functions for $\ell_i \to \ell_j\gamma$

$$f_{2n}(x) = (-5x^2+4x+1+2x(x+2)\log x)/(4(1-x)^4) \ , \tag{A.26}$$

$$f_{3n}(x) = (1+9x-9x^2-x^3+6x(x+1)\log x)/(3(1-x)^5) \ , \tag{A.27}$$

$$f_{2c}(x) = (-x^2-4x+5+2(2x+1)\log x)/(2(1-x)^4) \ . \tag{A.28}$$

Loop Functions for the EDMs

$$f_{\tilde{g}}^d(x) = \left\{ -\frac{4}{9} f_0^{(3)}(x), -\frac{1}{6} f_0^{(3)}(x) + \frac{3}{2} f_1^{(3)}(x) \right\} , \tag{A.29}$$

$$f_{\tilde{g}}^u(x) = \left\{ \frac{8}{9} f_0^{(3)}(x), -\frac{1}{6} f_0^{(3)}(x) + \frac{3}{2} f_1^{(3)}(x) \right\} , \tag{A.30}$$

$$f_{H^\pm}(z) = \left\{ -f_0^{(0)}(z) + \frac{2}{3} f_1^{(0)}(z),\ f_1^{(0)}(z) \right\} , \tag{A.31}$$

$$f_{\tilde{H}^\pm}(y) = \left\{ \frac{2}{3} f_0^{(1)}(y) - f_1^{(1)}(y),\ f_0^{(1)}(y) \right\} , \tag{A.32}$$

$$g_{\tilde{H}^\pm}(x) = \left\{ \frac{2}{3} f_0^{(2)}(x) - f_1^{(2)}(x),\ f_0^{(2)}(x) \right\} , \tag{A.33}$$

$$\begin{aligned}
f_0^{(0)}(x) &= \frac{1 - x^2 + 2x \log x}{(1-x)^3} , \\
f_0^{(1)}(x) &= \frac{-1 - 4x + 5x^2 - 2x(x+2) \log x}{(1-x)^4} , \\
f_0^{(2)}(x) &= \frac{1 + 9x - 9x^2 - x^3 + 6x(x+1) \log x}{(1-x)^5} , \\
f_0^{(3)}(x) &= \frac{-3 - 44x + 36x^2 + 12x^3 - x^4 - 12x(3x+2) \log x}{3(1-x)^6} , \\
f_1^{(0)}(x) &= \frac{3 - 4x + x^2 + 2 \log x}{(1-x)^3} , \\
f_1^{(1)}(x) &= \frac{-5 + 4x + x^2 - 2(1+2x) \log x}{(1-x)^4} , \\
f_1^{(2)}(x) &= \frac{2(3 - 3x^2 + (1 + 4x + x^2) \log x)}{(1-x)^5} , \\
f_1^{(3)}(x) &= 2\ \frac{-10 - 9x + 18x^2 + x^3 - 3(1 + 6x + 3x^2) \log x}{3(1-x)^6} .
\end{aligned} \tag{A.34}$$

SM Loop Functions

$$S_0(x) = \frac{4x - 11x^2 + x^3}{4(1-x)^2} - \frac{3x^3 \log x}{2(1-x)^3} , \tag{A.35}$$

$$Y_0(x) = \frac{x}{8} \left(\frac{x-4}{x-1} + \frac{3x}{(x-1)^2} \log x \right) , \tag{A.36}$$

$$S_0(x_c, x_t) = x_c \left(\log \frac{x_t}{x_c} - \frac{3x_c x_t}{4(1-x_t)} - \frac{3x_t^2 \log x_t}{4(1-x_t)^2} \right) . \tag{A.37}$$

B MSSM parameter convention

Throughout sec. 3 we adopted the convention of [113] for squark matrices and trilinear terms. In tab. 9 we show a dictionary between this convention and the "SUSY Les Houches Accord 2" (SLHA 2) convention in [232].

SLHA 2 [232]	[113]
$\hat{T}_U, \hat{T}_D, \hat{T}_E$	$-A_u^T, +A_d^T, +A_l^T$
$\hat{m}^2_{\tilde{Q}}, \hat{m}^2_{\tilde{L}}$	m^2_Q, m^2_L
$\hat{m}^2_{\tilde{u}}, \hat{m}^2_{\tilde{d}}, \hat{m}^2_{\tilde{e}}$	$(m^2_U)^T, (m^2_D)^T, (m^2_R)^T$
$\mathcal{M}^2_{\tilde{u}}, \mathcal{M}^2_{\tilde{d}}$	$(\mathcal{M}^2_U)^T, (\mathcal{M}^2_D)^T$

Table 9: Dictionary between the SLHA 2 convention of [232] and the convention of [113]. Note that A_t and A_b used in sec. 3 are defined as $m_t A_t = \frac{v_2}{\sqrt{2}} (A_u)_{33}$ and $m_b A_b = \frac{v_1}{\sqrt{2}} (A_d)_{33}$.

References

[1] **Heavy Flavor Averaging Group** Collaboration, E. Barberio *et al.*, "Averages of $b-$hadron and $c-$hadron Properties at the End of 2007," `arXiv:0808.1297 [hep-ex]`.

[2] M. Artuso *et al.*, "B, D and K decays," *Eur. Phys. J.* **C57** (2008) 309–492, `arXiv:0801.1833 [hep-ph]`.

[3] A. J. Buras, P. Gambino, M. Gorbahn, S. Jager, and L. Silvestrini, "Universal unitarity triangle and physics beyond the standard model," *Phys. Lett.* **B500** (2001) 161–167, `arXiv:hep-ph/0007085`.

[4] A. J. Buras, "Minimal flavor violation," *Acta Phys. Polon.* **B34** (2003) 5615–5668, `arXiv:hep-ph/0310208`.

[5] G. D'Ambrosio, G. F. Giudice, G. Isidori, and A. Strumia, "Minimal flavour violation: An effective field theory approach," *Nucl. Phys.* **B645** (2002) 155–187, `arXiv:hep-ph/0207036`.

[6] R. S. Chivukula and H. Georgi, "Composite Technicolor Standard Model," *Phys. Lett.* **B188** (1987) 99.

[7] L. J. Hall and L. Randall, "Weak scale effective supersymmetry," *Phys. Rev. Lett.* **65** (1990) 2939–2942.

[8] **UTfit** Collaboration, M. Bona *et al.*, "Model-independent constraints on $\Delta F = 2$ operators and the scale of new physics," *JHEP* **03** (2008) 049, `arXiv:0707.0636 [hep-ph]`.

[9] T. Hurth, G. Isidori, J. F. Kamenik, and F. Mescia, "Constraints on New Physics in MFV models: a model- independent analysis of $\Delta F = 1$ processes," *Nucl. Phys.* **B808** (2009) 326–346, arXiv:0807.5039 [hep-ph].

[10] T. Moroi, "CP violation in $B_d \to \phi K_S$ in SUSY GUT with right- handed neutrinos," *Phys. Lett.* **B493** (2000) 366–374, arXiv:hep-ph/0007328.

[11] D. Chang, A. Masiero, and H. Murayama, "Neutrino mixing and large CP violation in B physics," *Phys. Rev.* **D67** (2003) 075013, arXiv:hep-ph/0205111.

[12] R. Harnik, D. T. Larson, H. Murayama, and A. Pierce, "Atmospheric neutrinos can make beauty strange," *Phys. Rev.* **D69** (2004) 094024, arXiv:hep-ph/0212180.

[13] M. Ciuchini, E. Franco, A. Masiero, and L. Silvestrini, "$b \to s$ transitions: A new frontier for indirect SUSY searches," *Phys. Rev.* **D67** (2003) 075016, arXiv:hep-ph/0212397.

[14] J. Foster, K.-i. Okumura, and L. Roszkowski, "Probing the flavour structure of supersymmetry breaking with rare B-processes: A beyond leading order analysis," *JHEP* **08** (2005) 094, arXiv:hep-ph/0506146.

[15] M. Blanke, A. J. Buras, B. Duling, S. Gori, and A. Weiler, "$\Delta F = 2$ Observables and Fine-Tuning in a Warped Extra Dimension with Custodial Protection," *JHEP* **03** (2009) 001, arXiv:0809.1073 [hep-ph].

[16] M. Blanke, A. J. Buras, B. Duling, K. Gemmler, and S. Gori, "Rare K and B Decays in a Warped Extra Dimension with Custodial Protection," *JHEP* **03** (2009) 108, arXiv:0812.3803 [hep-ph].

[17] M. Blanke *et al.*, "Particle antiparticle mixing, ϵ_K, $\Delta(\Gamma(q))$, $A_{\rm SL}(q)$, $A_{\rm CP}(B_d \to \psi K_S)$, $A_{\rm CP}(B_s \to \psi\phi)$ and $B \to X_{s,d}\gamma$ in the littlest Higgs model with T-parity," *JHEP* **12** (2006) 003, arXiv:hep-ph/0605214.

[18] V. Barger *et al.*, "$b \to s$ Transitions in Family-dependent $U(1)'$ Models," arXiv:0906.3745 [hep-ph].

[19] **CDF** Collaboration, T. Aaltonen *et al.*, "First Flavor-Tagged Determination of Bounds on Mixing- Induced CP Violation in $B_s^0 \to J/\psi\phi$ Decays," *Phys. Rev. Lett.* **100** (2008) 161802, arXiv:0712.2397 [hep-ex].

[20] **D0** Collaboration, V. M. Abazov *et al.*, "Measurement of B_s^0 mixing parameters from the flavor-tagged decay $B_s^0 \to J/\psi\phi$," *Phys. Rev. Lett.* **101** (2008) 241801, arXiv:0802.2255 [hep-ex].

[21] **UTfit** Collaboration, M. Bona *et al.*, "First Evidence of New Physics in $b \leftrightarrow s$ Transitions," arXiv:0803.0659 [hep-ph].

[22] A. Lenz and U. Nierste, "Theoretical update of $B_s - \bar{B}_s$ mixing," *JHEP* **06** (2007) 072, arXiv:hep-ph/0612167.

[23] Y. Nir and N. Seiberg, "Should squarks be degenerate?," *Phys. Lett.* **B309** (1993) 337–343, arXiv:hep-ph/9304307.

[24] J. R. Ellis, G. K. Leontaris, and J. Rizos, "Implications of anomalous $U(1)$ symmetry in unified models: The flipped $SU(5) \times U(1)$ paradigm," *JHEP* **05** (2000) 001, `arXiv:hep-ph/0002263`.

[25] A. S. Joshipura, R. D. Vaidya, and S. K. Vempati, "$U(1)$ symmetry and R parity violation," *Phys. Rev.* **D62** (2000) 093020, `arXiv:hep-ph/0006138`.

[26] N. Maekawa, "Neutrino masses, anomalous $U(1)$ gauge symmetry and doublet-triplet splitting," *Prog. Theor. Phys.* **106** (2001) 401–418, `arXiv:hep-ph/0104200`.

[27] M. Kakizaki and M. Yamaguchi, "$U(1)$ flavor symmetry and proton decay in supersymmetric standard model," *JHEP* **06** (2002) 032, `arXiv:hep-ph/0203192`.

[28] K. S. Babu, I. Gogoladze, and K. Wang, "Natural R-parity, mu-term, and fermion mass hierarchy from discrete gauge symmetries," *Nucl. Phys.* **B660** (2003) 322–342, `arXiv:hep-ph/0212245`.

[29] I. Jack, D. R. T. Jones, and R. Wild, "Yukawa textures and the mu-term," *Phys. Lett.* **B580** (2004) 72–78, `arXiv:hep-ph/0309165`.

[30] H. K. Dreiner, H. Murayama, and M. Thormeier, "Anomalous flavor $U(1)_X$ for everything," *Nucl. Phys.* **B729** (2005) 278–316, `arXiv:hep-ph/0312012`.

[31] Z. Berezhiani and Z. Tavartkiladze, "Anomalous $U(1)$ symmetry and missing doublet $SU(5)$ model," *Phys. Lett.* **B396** (1997) 150–160, `arXiv:hep-ph/9611277`.

[32] K. Choi, E. J. Chun, and H. D. Kim, "Supersymmetry hierarchy problems and anomalous horizontal $U(1)$ symmetry," *Phys. Lett.* **B394** (1997) 89–98, `arXiv:hep-ph/9611293`.

[33] C. D. Froggatt, M. Gibson, and H. B. Nielsen, "Neutrino masses and mixings from an anomaly free $SMG \times U(1)^2$ model," *Phys. Lett.* **B446** (1999) 256–266, `arXiv:hep-ph/9811265`.

[34] Q. Shafi and Z. Tavartkiladze, "Neutrino mixings and fermion masses in supersymmetric $SU(5)$," *Phys. Lett.* **B451** (1999) 129–135, `arXiv:hep-ph/9901243`.

[35] G. K. Leontaris and J. Rizos, "New fermion mass textures from anomalous $U(1)$ symmetries with baryon and lepton number conservation," *Nucl. Phys.* **B567** (2000) 32–60, `arXiv:hep-ph/9909206`.

[36] K. Agashe and C. D. Carone, "Supersymmetric flavor models and the $B \to \phi K_S$ anomaly," *Phys. Rev.* **D68** (2003) 035017, `arXiv:hep-ph/0304229`.

[37] E. Dudas, S. Pokorski, and C. A. Savoy, "Soft scalar masses in supergravity with horizontal $U(1)_X$ gauge symmetry," *Phys. Lett.* **B369** (1996) 255–261, `arXiv:hep-ph/9509410`.

[38] Z. Berezhiani and A. Rossi, "Predictive grand unified textures for quark and neutrino masses and mixings," *Nucl. Phys.* **B594** (2001) 113–168, `arXiv:hep-ph/0003084`.

[39] R. G. Roberts, A. Romanino, G. G. Ross, and L. Velasco-Sevilla, "Precision test of a Fermion mass texture," *Nucl. Phys.* **B615** (2001) 358–384, `arXiv:hep-ph/0104088`.

[40] M.-C. Chen and K. T. Mahanthappa, "Fermion masses and mixing and CP-violation in $SO(10)$ models with family symmetries," *Int. J. Mod. Phys.* **A18** (2003) 5819–5888, `arXiv:hep-ph/0305088`.

[41] A. Pomarol and D. Tommasini, "Horizontal symmetries for the supersymmetric flavor problem," *Nucl. Phys.* **B466** (1996) 3–24, `arXiv:hep-ph/9507462`.

[42] L. J. Hall and H. Murayama, "A Geometry of the generations," *Phys. Rev. Lett.* **75** (1995) 3985–3988, `arXiv:hep-ph/9508296`.

[43] C. D. Carone, L. J. Hall, and H. Murayama, "A Supersymmetric Theory of Flavor and R Parity," *Phys. Rev.* **D54** (1996) 2328–2339, `arXiv:hep-ph/9602364`.

[44] R. Barbieri, L. J. Hall, S. Raby, and A. Romanino, "Unified theories with $U(2)$ flavor symmetry," *Nucl. Phys.* **B493** (1997) 3–26, `arXiv:hep-ph/9610449`.

[45] R. Dermisek and S. Raby, "Fermion masses and neutrino oscillations in $SO(10)$ SUSY GUT with $D(3) \times U(1)$ family symmetry," *Phys. Rev.* **D62** (2000) 015007, `arXiv:hep-ph/9911275`.

[46] T. Blazek, S. Raby, and K. Tobe, "Neutrino oscillations in an $SO(10)$ SUSY GUT with $U(2) \times U(1)^n$ family symmetry," *Phys. Rev.* **D62** (2000) 055001, `arXiv:hep-ph/9912482`.

[47] R. Barbieri, G. R. Dvali, and L. J. Hall, "Predictions From A $U(2)$ Flavour Symmetry In Supersymmetric Theories," *Phys. Lett.* **B377** (1996) 76–82, `arXiv:hep-ph/9512388`.

[48] R. Barbieri, L. J. Hall, and A. Romanino, "Consequences of a $U(2)$ flavour symmetry," *Phys. Lett.* **B401** (1997) 47–53, `arXiv:hep-ph/9702315`.

[49] S. F. King and G. G. Ross, "Fermion masses and mixing angles from $SU(3)$ family symmetry," *Phys. Lett.* **B520** (2001) 243–253, `arXiv:hep-ph/0108112`.

[50] S. F. King and G. G. Ross, "Fermion masses and mixing angles from $SU(3)$ family symmetry and unification," *Phys. Lett.* **B574** (2003) 239–252, `arXiv:hep-ph/0307190`.

[51] G. G. Ross, L. Velasco-Sevilla, and O. Vives, "Spontaneous CP violation and non-Abelian family symmetry in SUSY," *Nucl. Phys.* **B692** (2004) 50–82, `arXiv:hep-ph/0401064`.

[52] S. Antusch, S. F. King, and M. Malinsky, "Solving the SUSY Flavour and CP Problems with $SU(3)$ Family Symmetry," *JHEP* **06** (2008) 068, `arXiv:0708.1282 [hep-ph]`.

[53] M. Ciuchini *et al.*, "Soft SUSY breaking grand unification: Leptons versus quarks on the flavor playground," *Nucl. Phys.* **B783** (2007) 112–142, `arXiv:hep-ph/0702144`.

[54] J. Hisano and Y. Shimizu, "CP Violation in B_s Mixing in the SUSY SU(5) GUT with Right-handed Neutrinos," *Phys. Lett.* **B669** (2008) 301, `arXiv:0805.3327 [hep-ph]`.

[55] P. Ko, J.-h. Park, and M. Yamaguchi, "Sflavor mixing map viewed from a high scale in supersymmetric SU(5)," *JHEP* **11** (2008) 051, `arXiv:0809.2784 [hep-ph]`.

[56] B. Dutta and Y. Mimura, "Penguin Contribution to the Phase of $B_s - \bar{B}_s$ Mixing and $B_s \to \mu\mu$ in Grand Unified Theories," *Phys. Lett.* **B677** (2009) 164–171, `arXiv:0902.0016 [hep-ph]`.

[57] S. Trine, S. Westhoff, and S. Wiesenfeldt, "Probing Yukawa Unification with K and B Mixing," `arXiv:0904.0378 [hep-ph]`.

[58] P. Ball, S. Khalil, and E. Kou, "B_s^0 - $\bar{B}_s^0$ mixing and the $B_s \to J/\psi\phi$ asymmetry in supersymmetric models," *Phys. Rev.* **D69** (2004) 115011, `arXiv:hep-ph/0311361`.

[59] J. Foster, K.-i. Okumura, and L. Roszkowski, "Current and future limits on general flavour violation in $b \to s$ transitions in minimal supersymmetry," *JHEP* **03** (2006) 044, `arXiv:hep-ph/0510422`.

[60] T. Goto, Y. Okada, T. Shindou, and M. Tanaka, "Patterns of flavor signals in supersymmetric models," *Phys. Rev.* **D77** (2008) 095010, `arXiv:0711.2935 [hep-ph]`.

[61] F. Gabbiani, E. Gabrielli, A. Masiero, and L. Silvestrini, "A complete analysis of FCNC and CP constraints in general SUSY extensions of the standard model," *Nucl. Phys.* **B477** (1996) 321–352, `arXiv:hep-ph/9604387`.

[62] L. Calibbi *et al.*, "FCNC and CP Violation Observables in a SU(3)-flavoured MSSM," `arXiv:0907.4069 [hep-ph]`.

[63] Y. Nir and G. Raz, "Quark squark alignment revisited," *Phys. Rev.* **D66** (2002) 035007, `arXiv:hep-ph/0206064`.

[64] S. Baek and P. Ko, "Probing SUSY-induced CP violations at B factories," *Phys. Rev. Lett.* **83** (1999) 488–491, `arXiv:hep-ph/9812229`.

[65] S. Baek and P. Ko, "Effects of supersymmetric CP violating phases on $B \to X_s \ell^+ \ell^-$ and ϵ_K," *Phys. Lett.* **B462** (1999) 95–102, `arXiv:hep-ph/9904283`.

[66] A. Bartl *et al.*, "General flavor blind MSSM and CP violation," *Phys. Rev.* **D64** (2001) 076009, `arXiv:hep-ph/0103324`.

[67] J. R. Ellis, J. S. Lee, and A. Pilaftsis, "*B*-Meson Observables in the Maximally CP-Violating MSSM with Minimal Flavour Violation," *Phys. Rev.* **D76** (2007) 115011, `arXiv:0708.2079 [hep-ph]`.

[68] W. Altmannshofer, A. J. Buras, and P. Paradisi, "Low Energy Probes of CP Violation in a Flavor Blind MSSM," *Phys. Lett.* **B669** (2008) 239–245, `arXiv:0808.0707 [hep-ph]`.

[69] G. Colangelo, E. Nikolidakis, and C. Smith, "Supersymmetric models with minimal flavour violation and their running," *Eur. Phys. J.* **C59** (2009) 75–98, `arXiv:0807.0801 [hep-ph]`.

[70] L. Mercolli and C. Smith, "EDM constraints on flavored CP-violating phases," *Nucl. Phys.* **B817** (2009) 1–24, `arXiv:0902.1949 [hep-ph]`.

[71] P. Paradisi and D. M. Straub, "The SUSY CP Problem and the MFV Principle," `arXiv:0906.4551 [hep-ph]`.

[72] M. Blanke *et al.*, "Rare and CP-violating K and B decays in the Littlest Higgs model with T-parity," *JHEP* **01** (2007) 066, `arXiv:hep-ph/0610298`.

[73] M. Blanke, A. J. Buras, B. Duling, A. Poschenrieder, and C. Tarantino, "Charged Lepton Flavour Violation and $(g-2)_\mu$ in the Littlest Higgs Model with T-Parity: a clear Distinction from Supersymmetry," *JHEP* **05** (2007) 013, `arXiv:hep-ph/0702136`.

[74] M. Blanke, A. J. Buras, S. Recksiegel, C. Tarantino, and S. Uhlig, "Correlations between ϵ'/ϵ and rare K decays in the littlest Higgs model with T-parity," *JHEP* **06** (2007) 082, `arXiv:0704.3329 [hep-ph]`.

[75] T. Goto, Y. Okada, and Y. Yamamoto, "Ultraviolet divergences of flavor changing amplitudes in the littlest Higgs model with T-parity," *Phys. Lett.* **B670** (2009) 378–382, `arXiv:0809.4753 [hep-ph]`.

[76] F. del Aguila, J. I. Illana, and M. D. Jenkins, "Precise limits from lepton flavour violating processes on the Littlest Higgs model with T-parity," `arXiv:0811.2891 [hep-ph]`.

[77] M. Blanke, A. J. Buras, B. Duling, S. Recksiegel, and C. Tarantino, "FCNC Processes in the Littlest Higgs Model with T-Parity: a 2009 Look," `arXiv:0906.5454 [hep-ph]`.

[78] A. Crivellin, "Effects of right-handed charged currents on the determinations of $|V_{ub}|$ and $|V_{cb}|$," `arXiv:0907.2461 [hep-ph]`.

[79] T. Goto, N. Kitazawa, Y. Okada, and M. Tanaka, "Model independent analysis of $B\bar{B}$ mixing and CP violation in B decays," *Phys. Rev.* **D53** (1996) 6662–6665, `arXiv:hep-ph/9506311`.

[80] M. Blanke, A. J. Buras, D. Guadagnoli, and C. Tarantino, "Minimal Flavour Violation Waiting for Precise Measurements of ΔM_s, $S_{\psi\phi}$, $A^s_{\rm SL}$, $|V_{ub}|$, γ and $B^0_{s,d} \to \mu^+\mu^-$," *JHEP* **10** (2006) 003, `arXiv:hep-ph/0604057`.

[81] **Particle Data Group** Collaboration, C. Amsler *et al.*, "Review of particle physics," *Phys. Lett.* **B667** (2008) 1.

[82] **CDF** Collaboration, A. Abulencia *et al.*, "Observation of $B^0_s - \bar{B}^0_s$ oscillations," *Phys. Rev. Lett.* **97** (2006) 242003, `arXiv:hep-ex/0609040`.

[83] **UTfit** Collaboration, M. Bona *et al.*, "The UTfit collaboration report on the status of the unitarity triangle beyond the standard model. I: Model- independent analysis and minimal flavour violation," *JHEP* **03** (2006) 080, arXiv:hep-ph/0509219.

[84] A. J. Buras, M. Jamin, and P. H. Weisz, "Leading and next-to-leading QCD corrections to ε_K parameter and $B^0 - \bar{B}^0$ mixing in the presence of a heavy top quark," *Nucl. Phys.* **B347** (1990) 491–536.

[85] S. Herrlich and U. Nierste, "Enhancement of the $K_L - K_S$ mass difference by short distance QCD corrections beyond leading logarithms," *Nucl. Phys.* **B419** (1994) 292–322, arXiv:hep-ph/9310311.

[86] S. Herrlich and U. Nierste, "Indirect CP violation in the neutral kaon system beyond leading logarithms," *Phys. Rev.* **D52** (1995) 6505–6518, arXiv:hep-ph/9507262.

[87] S. Herrlich and U. Nierste, "The Complete $|\Delta S| = 2$ Hamiltonian in the Next-To-Leading Order," *Nucl. Phys.* **B476** (1996) 27–88, arXiv:hep-ph/9604330.

[88] A. J. Buras and D. Guadagnoli, "Correlations among new CP violating effects in $\Delta F = 2$ observables," *Phys. Rev.* **D78** (2008) 033005, arXiv:0805.3887 [hep-ph].

[89] C. Aubin, J. Laiho, and R. S. Van de Water, "The neutral kaon mixing parameter B_K from unquenched mixed-action lattice QCD," arXiv:0905.3947 [hep-lat].

[90] **RBC** Collaboration, D. J. Antonio *et al.*, "Neutral kaon mixing from 2+1 flavor domain wall QCD," *Phys. Rev. Lett.* **100** (2008) 032001, arXiv:hep-ph/0702042.

[91] **CKMfitter Group** Collaboration, J. Charles *et al.*, "CP violation and the CKM matrix: Assessing the impact of the asymmetric B factories," *Eur. Phys. J.* **C41** (2005) 1–131, arXiv:hep-ph/0406184.

[92] A. J. Buras and D. Guadagnoli, "On the consistency between the observed amount of CP violation in the K- and B_d-systems within minimal flavor violation," arXiv:0901.2056 [hep-ph].

[93] E. Lunghi and A. Soni, "Possible Indications of New Physics in B_d -mixing and in $\sin 2\beta$ Determinations," *Phys. Lett.* **B666** (2008) 162–165, arXiv:0803.4340 [hep-ph].

[94] E. Lunghi and A. Soni, "Hints for the scale of new CP-violating physics from B-CP anomalies," arXiv:0903.5059 [hep-ph].

[95] A. J. Buras, F. Parodi, and A. Stocchi, "The CKM matrix and the unitarity triangle: Another look," *JHEP* **01** (2003) 029, arXiv:hep-ph/0207101.

[96] W. Altmannshofer, A. J. Buras, and D. Guadagnoli, "The MFV limit of the MSSM for low $\tan\beta$: Meson mixings revisited," *JHEP* **11** (2007) 065, arXiv:hep-ph/0703200.

[97] M. Bartsch, G. Buchalla, and C. Kraus, "$B \to V_L V_L$ Decays at Next-to-Leading Order in QCD," arXiv:0810.0249 [hep-ph].

[98] **Tevatron Electroweak Working Group** Collaboration, "Combination of CDF and D0 Results on the Mass of the Top Quark," `arXiv:0903.2503 [hep-ex]`.

[99] K. G. Chetyrkin, J. H. Kuhn, and M. Steinhauser, "RunDec: A Mathematica package for running and decoupling of the strong coupling and quark masses," *Comput. Phys. Commun.* **133** (2000) 43–65, `arXiv:hep-ph/0004189`.

[100] V. Lubicz and C. Tarantino, "Flavour physics and Lattice QCD: averages of lattice inputs for the Unitarity Triangle Analysis," *Nuovo Cim.* **123B** (2008) 674–688, `arXiv:0807.4605 [hep-lat]`.

[101] K. G. Chetyrkin *et al.*, "Charm and Bottom Quark Masses: an Update," `arXiv:0907.2110 [hep-ph]`.

[102] U. Nierste, "Three Lectures on Meson Mixing and CKM phenomenology," `arXiv:0904.1869 [hep-ph]`.

[103] Http://www.lnf.infn.it/wg/vus/. Flavianet Kaon Working Group.

[104] J. Urban, F. Krauss, U. Jentschura, and G. Soff, "Next-to-leading order QCD corrections for the $B^0\bar{B}^0$ mixing with an extended Higgs sector," *Nucl. Phys.* **B523** (1998) 40–58, `arXiv:hep-ph/9710245`.

[105] D. Becirevic, V. Gimenez, G. Martinelli, M. Papinutto, and J. Reyes, "B-parameters of the complete set of matrix elements of $\Delta B = 2$ operators from the lattice," *JHEP* **04** (2002) 025, `arXiv:hep-lat/0110091`.

[106] M. Ciuchini, E. Franco, V. Lubicz, F. Mescia, and C. Tarantino, "Lifetime differences and CP violation parameters of neutral B mesons at the next-to-leading order in QCD," *JHEP* **08** (2003) 031, `arXiv:hep-ph/0308029`.

[107] M. Beneke, G. Buchalla, A. Lenz, and U. Nierste, "CP asymmetry in flavour-specific B decays beyond leading logarithms," *Phys. Lett.* **B576** (2003) 173–183, `arXiv:hep-ph/0307344`.

[108] Z. Ligeti, M. Papucci, and G. Perez, "Implications of the measurement of the $B_s^0 - \bar{B}_s^0$ mass difference," *Phys. Rev. Lett* **97** (2006) 101801, `arXiv:hep-ph/0604112`.

[109] Y. Grossman, Y. Nir, and G. Perez, "Testing New Indirect CP Violation," `arXiv:0904.0305 [hep-ph]`.

[110] **CDF** Collaboration, D. Tonelli, "Search for New Physics in the B_s^0 mixing phase," `arXiv:0810.3229 [hep-ex]`.

[111] M. Bona *et al.*, "New Physics from Flavour," `arXiv:0906.0953 [hep-ph]`.

[112] V. Tisserand, "CKM fits as of winter 2009 and sensitivity to New Physics," `arXiv:0905.1572 [hep-ph]`.

[113] J. Rosiek, "Complete set of Feynman rules for the MSSM – ERRATUM," `arXiv:hep-ph/9511250`.

[114] G. F. Giudice, M. Nardecchia, and A. Romanino, "Hierarchical Soft Terms and Flavor Physics," *Nucl. Phys.* **B813** (2009) 156, arXiv:0812.3610 [hep-ph].

[115] A. J. Buras, P. H. Chankowski, J. Rosiek, and L. Slawianowska, "$\Delta M_{d,s}, B^0_{d,s} \to \mu^+\mu^-$ and $B \to X_s\gamma$ in supersymmetry at large $\tan\beta$," *Nucl. Phys.* **B659** (2003) 3, arXiv:hep-ph/0210145.

[116] A. J. Buras, P. H. Chankowski, J. Rosiek, and L. Slawianowska, "Correlation between ΔM_s and $B^0_{s,d} \to \mu^+\mu^-$ in supersymmetry at large $\tan\beta$," *Phys. Lett.* **B546** (2002) 96–107, arXiv:hep-ph/0207241.

[117] L. J. Hall, R. Rattazzi, and U. Sarid, "The Top quark mass in supersymmetric SO(10) unification," *Phys. Rev.* **D50** (1994) 7048–7065, arXiv:hep-ph/9306309.

[118] M. S. Carena, M. Olechowski, S. Pokorski, and C. E. M. Wagner, "Electroweak symmetry breaking and bottom - top Yukawa unification," *Nucl. Phys.* **B426** (1994) 269–300, arXiv:hep-ph/9402253.

[119] G. Isidori and A. Retico, "Scalar flavor changing neutral currents in the large $\tan\beta$ limit," *JHEP* **11** (2001) 001, arXiv:hep-ph/0110121.

[120] L. Hofer, U. Nierste, and D. Scherer, "Resummation of tan-beta-enhanced supersymmetric loop corrections beyond the decoupling limit," arXiv:0907.5408 [hep-ph].

[121] A. Crivellin and U. Nierste, "Chirally enhanced corrections to FCNC processes in the generic MSSM," arXiv:0908.4404 [hep-ph].

[122] A. J. Buras, P. H. Chankowski, J. Rosiek, and L. Slawianowska, "$\Delta M_s/\Delta M_d$, $\sin 2\beta$ and the angle γ in the presence of new $\Delta F = 2$ operators," *Nucl. Phys.* **B619** (2001) 434–466, arXiv:hep-ph/0107048.

[123] A. Dedes and A. Pilaftsis, "Resummed effective Lagrangian for Higgs-mediated FCNC interactions in the CP-violating MSSM," *Phys. Rev.* **D67** (2003) 015012, arXiv:hep-ph/0209306.

[124] M. Gorbahn, S. Jager, U. Nierste, and S. Trine, "The supersymmetric Higgs sector and $B - \bar{B}$ mixing for large $\tan\beta$," arXiv:0901.2065 [hep-ph].

[125] M. Ciuchini *et al.*, "Next-to-leading order strong interaction corrections to the Delta(F) = 2 effective hamiltonian in the MSSM," *JHEP* **09** (2006) 013, arXiv:hep-ph/0606197.

[126] J. Virto, "Exact NLO strong interaction corrections to the Delta F=2 effective Hamiltonian in the MSSM," *JHEP* **11** (2009) 055, arXiv:0907.5376 [hep-ph].

[127] M. Ciuchini *et al.*, "Next-to-leading order QCD corrections to $\Delta F = 2$ effective Hamiltonians," *Nucl. Phys.* **B523** (1998) 501–525, arXiv:hep-ph/9711402.

[128] A. J. Buras, M. Misiak, and J. Urban, "Two-loop QCD anomalous dimensions of flavour-changing four-quark operators within and beyond the standard model," *Nucl. Phys.* **B586** (2000) 397–426, arXiv:hep-ph/0005183.

[129] J. Hisano, M. Nagai, and P. Paradisi, "A Complete Analysis of 'Flavored' Electric Dipole Moments in Supersymmetric Theories," `arXiv:0812.4283 [hep-ph]`.

[130] M. Wick and W. Altmannshofer, "A Reconsideration of the $b \to s\gamma$ Decay in the Minimal Flavor Violating MSSM," *AIP Conf. Proc.* **1078** (2009) 348–353, `arXiv:0810.2874 [hep-ph]`.

[131] B. Dudley and C. Kolda, "Supersymmetric Flavor-Changing Sum Rules as a Tool for $b \to s\gamma$," *Phys. Rev.* **D79** (2009) 015011, `arXiv:0805.4565 [hep-ph]`.

[132] M. Carena, A. Menon, and C. E. M. Wagner, "Minimal Flavor Violation and the Scale of Supersymmetry Breaking," *Phys. Rev.* **D79** (2009) 075025, `arXiv:0812.3594 [hep-ph]`.

[133] J. M. Soares, "CP violation in radiative b decays," *Nucl. Phys.* **B367** (1991) 575–590.

[134] A. L. Kagan and M. Neubert, "Direct CP violation in $B \to X_s\gamma$ decays as a signature of new physics," *Phys. Rev.* **D58** (1998) 094012, `arXiv:hep-ph/9803368`.

[135] A. L. Kagan and M. Neubert, "QCD anatomy of $B \to X_s\gamma$ decays," *Eur. Phys. J.* **C7** (1999) 5–27, `arXiv:hep-ph/9805303`.

[136] Y. Grossman and M. P. Worah, "CP asymmetries in B decays with new physics in decay amplitudes," *Phys. Lett.* **B395** (1997) 241–249, `arXiv:hep-ph/9612269`.

[137] G. Buchalla, A. J. Buras, and M. E. Lautenbacher, "Weak decays beyond leading logarithms," *Rev. Mod. Phys.* **68** (1996) 1125–1144, `arXiv:hep-ph/9512380`.

[138] G. Buchalla, G. Hiller, Y. Nir, and G. Raz, "The pattern of CP asymmetries in $b \to s$ transitions," *JHEP* **09** (2005) 074, `arXiv:hep-ph/0503151`.

[139] E. Gabrielli, K. Huitu, and S. Khalil, "Comparative study of CP asymmetries in supersymmetric models," *Nucl. Phys.* **B710** (2005) 139–188, `arXiv:hep-ph/0407291`.

[140] W. Altmannshofer *et al.*, "Symmetries and Asymmetries of $B \to K^*\mu^+\mu^-$ Decays in the Standard Model and Beyond," *JHEP* **01** (2009) 019, `arXiv:0811.1214 [hep-ph]`.

[141] C. Bobeth, G. Hiller, and G. Piranishvili, "CP Asymmetries in bar $B \to \bar{K}^*(\to \bar{K}\pi)\bar{\ell}\ell$ and Untagged $\bar{B}_s$, $B_s \to \phi(\to K^+K^-)\bar{\ell}\ell$ Decays at NLO," *JHEP* **07** (2008) 106, `arXiv:0805.2525 [hep-ph]`.

[142] U. Egede, T. Hurth, J. Matias, M. Ramon, and W. Reece, "New observables in the decay mode $\bar{B}_d \to \bar{K}^{*0}\ell^+\ell^-$," *JHEP* **11** (2008) 032, `arXiv:0807.2589 [hep-ph]`.

[143] **BABAR** Collaboration, B. Aubert *et al.*, "Angular Distributions in the Decays $B \to K^*\ell^+\ell^-$," *Phys. Rev.* **D79** (2009) 031102, `arXiv:0804.4412 [hep-ex]`.

[144] **BELLE** Collaboration, J. T. Wei *et al.*, "Measurement of the Differential Branching Fraction and Forward-Backword Asymmetry for $B \to K^*\ell^+\ell^-$," `arXiv:0904.0770 [hep-ex]`.

[145] E. Lunghi and J. Matias, "Huge right-handed current effects in $B \to K^*(K\pi)\ell^+\ell^-$ in supersymmetry," *JHEP* **04** (2007) 058, `arXiv:hep-ph/0612166`.

[146] **CDF** Collaboration, T. Aaltonen *et al.*, "Search for $B_s^0 \to \mu^+\mu^-$ and $B_d^0 \to \mu^+\mu^-$ decays with $2fb^{-1}$ of $p\bar{p}$ collisions," *Phys. Rev. Lett.* **100** (2008) 101802, arXiv:0712.1708 [hep-ex].

[147] **D0** Collaboration, "A new upper limit for the rare decay B($B_s^0 \to \mu^+\mu^-$) using 2 fb^{-1} of Run II data." http://www-d0.fnal.gov/Run2Physics/WWW/results/prelim/B/B48/.

[148] Talk given by G. Punzi at EPS HEP 2009 in Krakow.

[149] C. Hamzaoui, M. Pospelov, and M. Toharia, "Higgs-mediated FCNC in supersymmetric models with large $\tan\beta$," *Phys. Rev.* **D59** (1999) 095005, arXiv:hep-ph/9807350.

[150] S. R. Choudhury and N. Gaur, "Dileptonic decay of B_s meson in SUSY models with large $\tan\beta$," *Phys. Lett.* **B451** (1999) 86–92, arXiv:hep-ph/9810307.

[151] K. S. Babu and C. F. Kolda, "Higgs mediated $B^0 \to \mu^+\mu^-$ in minimal supersymmetry," *Phys. Rev. Lett.* **84** (2000) 228–231, arXiv:hep-ph/9909476.

[152] G. Buchalla and A. J. Buras, "The rare decays $K \to \pi\nu\bar{\nu}$, $B \to X\nu\bar{\nu}$ and $B \to \ell^+\ell^-$: An update," *Nucl. Phys.* **B548** (1999) 309–327, arXiv:hep-ph/9901288.

[153] W.-S. Hou, "Enhanced charged Higgs boson effects in $B^- \to \tau\bar{\nu}, \mu\bar{\nu}$ and $b \to \tau\bar{\nu} + X$," *Phys. Rev.* **D48** (1993) 2342–2344.

[154] A. G. Akeroyd and S. Recksiegel, "The effect of $H^\pm$ on $B^\pm \to \tau^\pm\nu_\tau$ and $B^\pm \to \mu^\pm\ \nu_\mu$," *J. Phys.* **G29** (2003) 2311–2317, arXiv:hep-ph/0306037.

[155] G. Isidori and P. Paradisi, "Hints of large $\tan\beta$ in flavour physics," *Phys. Lett.* **B639** (2006) 499–507, arXiv:hep-ph/0605012.

[156] **BABAR** Collaboration, B. Aubert *et al.*, "A Search for $B^+ \to \tau^+\nu$ with Hadronic B tags," *Phys. Rev.* **D77** (2008) 011107, arXiv:0708.2260 [hep-ex].

[157] K. Ikado *et al.*, "Evidence of the purely leptonic decay $B^- \to \tau^-\bar{\nu}_\tau$," *Phys. Rev. Lett.* **97** (2006) 251802, arXiv:hep-ex/0604018.

[158] **Belle** Collaboration, I. Adachi *et al.*, "Measurement of $B^- \to \tau^-\bar{\nu}_\tau$ Decay With a Semileptonic Tagging Method," arXiv:0809.3834 [hep-ex].

[159] **BABAR** Collaboration, B. Aubert *et al.*, "A Search for $B^+ \to \ell^+\nu_\ell$ Recoiling Against $B^- \to D^0\ell^-\bar{\nu}X$," arXiv:0809.4027 [hep-ex].

[160] **UTfit** Collaboration, . M. Bona *et al.*, "An Improved Standard Model Prediction Of $BR(B \to \tau\nu)$ And Its Implications For New Physics," arXiv:0908.3470 [hep-ph].

[161] M. Antonelli *et al.*, "Flavor Physics in the Quark Sector," arXiv:0907.5386 [hep-ph].

[162] J. Barenboim, P. Paradisi, O. Vives, E. Lunghi, and W. Porod, "Light charged Higgs at the beginning of the LHC era,," *JHEP* **0804** (2008) 079, arXiv:0712.3559 [hep-ph].

[163] **FlaviaNet Working Group on Kaon Decays** Collaboration, M. Antonelli *et al.*, "Precision tests of the Standard Model with leptonic and semileptonic kaon decays," arXiv:0801.1817 [hep-ph].

[164] Y. Nir and M. P. Worah, "Probing the flavor and CP structure of supersymmetric models with $K \to \pi\nu\bar{\nu}$ decays," *Phys. Lett.* **B423** (1998) 319–326, arXiv:hep-ph/9711215.

[165] A. J. Buras, A. Romanino, and L. Silvestrini, "$K \to \pi\nu\bar{\nu}$: A model independent analysis and supersymmetry," *Nucl. Phys.* **B520** (1998) 3–30, arXiv:hep-ph/9712398.

[166] G. Colangelo and G. Isidori, "Supersymmetric contributions to rare kaon decays: Beyond the single mass-insertion approximation," *JHEP* **09** (1998) 009, arXiv:hep-ph/9808487.

[167] A. J. Buras, G. Colangelo, G. Isidori, A. Romanino, and L. Silvestrini, "Connections between ϵ'/ϵ and rare kaon decays in supersymmetry," *Nucl. Phys.* **B566** (2000) 3–32, arXiv:hep-ph/9908371.

[168] G. Isidori and P. Paradisi, "Higgs-mediated $K \to \pi\nu\bar{\nu}$ in the MSSM at large $\tan\beta$," *Phys. Rev.* **D73** (2006) 055017, arXiv:hep-ph/0601094.

[169] Y. Yamada, "$b \to s\nu\bar{\nu}$ decay in the MSSM: Implication of $b \to s\gamma$ at large $\tan\beta$," *Phys. Rev.* **D77** (2008) 014025, arXiv:0709.1022 [hep-ph].

[170] W. Altmannshofer, A. J. Buras, D. M. Straub, and M. Wick, "New strategies for New Physics search in $B \to K^*\nu\bar{\nu}$, $B \to K\nu\bar{\nu}$ and $B \to X_s\nu\bar{\nu}$ decays," *JHEP* **04** (2009) 022, arXiv:0902.0160 [hep-ph].

[171] **MEG** Collaboration, H. G. Evans, "A limit for the $\mu \to e\gamma$ decay from the MEG experiment," arXiv:0908.2594 [hep-ex].

[172] P. Paradisi, "Constraints on SUSY lepton flavour violation by rare processes," *JHEP* **10** (2005) 006, arXiv:hep-ph/0505046.

[173] K. S. Babu and C. Kolda, "Higgs-mediated $\tau \to 3\mu$ in the supersymmetric seesaw model," *Phys. Rev. Lett.* **89** (2002) 241802, arXiv:hep-ph/0206310.

[174] A. Brignole and A. Rossi, "Lepton flavour violating decays of supersymmetric Higgs bosons," *Phys. Lett.* **B566** (2003) 217–225, arXiv:hep-ph/0304081.

[175] A. Brignole and A. Rossi, "Anatomy and phenomenology of $\mu\,\tau$ lepton flavour violation in the MSSM," *Nucl. Phys.* **B701** (2004) 3–53, arXiv:hep-ph/0404211.

[176] R. Kitano, M. Koike, S. Komine, and Y. Okada, "Higgs-mediated muon electron conversion process in supersymmetric seesaw model," *Phys. Lett.* **B575** (2003) 300–308, arXiv:hep-ph/0308021.

[177] E. Arganda, A. M. Curiel, M. J. Herrero, and D. Temes, "Lepton flavor violating Higgs boson decays from massive seesaw neutrinos," *Phys. Rev.* **D71** (2005) 035011, arXiv:hep-ph/0407302.

[178] E. Arganda, M. J. Herrero, and J. Portoles, "Lepton flavour violating semileptonic tau decays in constrained MSSM-seesaw scenarios," *JHEP* **06** (2008) 079, arXiv:0803.2039 [hep-ph].

[179] P. Paradisi, "Higgs-mediated $\tau \to \mu$ and $\tau \to e$ transitions in II Higgs doublet model and supersymmetry," *JHEP* **02** (2006) 050, arXiv:hep-ph/0508054.

[180] P. Paradisi, "Higgs-mediated $e \to \mu$ transitions in II Higgs doublet model and supersymmetry," *JHEP* **08** (2006) 047, arXiv:hep-ph/0601100.

[181] J. Hisano, M. Nagai, and P. Paradisi, "Electric dipole moments from flavor-changing supersymmetric soft terms," *Phys. Rev.* **D78** (2008) 075019, arXiv:0712.1285 [hep-ph].

[182] J. Hisano, M. Nagai, and P. Paradisi, "New two-loop contributions to hadronic EDMs in the MSSM," *Phys. Lett.* **B642** (2006) 510–517, arXiv:hep-ph/0606322.

[183] Z. W. Liu and H. P. Kelly, "Analysis of atomic electric dipole moment in thallium by all-order calculations in many-body perturbation theory," *Phys. Rev.* **A45** (1992) no. 7, R4210–R4213.

[184] A.-M. Martensson-Pendrill, "Calculation of P and T Violating Properties in Atoms and Molecules," *Methods in Computational Chemistry (Ed. S. Wilson)* **6** (1992) 99–156.

[185] A.-M. Martensson-Pendrill and E. Lindroth, "Limit on a P- and T-Violating Electron-Nucleon Interaction," *EPL (Europhysics Letters)* **15** (1991) no. 2, 155–160.

[186] M. Pospelov and A. Ritz, "Theta-Induced Electric Dipole Moment of the Neutron via QCD Sum Rules," *Phys. Rev. Lett.* **83** (1999) 2526–2529, arXiv:hep-ph/9904483.

[187] M. Pospelov and A. Ritz, "Neutron EDM from electric and chromoelectric dipole moments of quarks," *Phys. Rev.* **D63** (2001) 073015, arXiv:hep-ph/0010037.

[188] **Muon G-2** Collaboration, G. W. Bennett *et al.*, "Final report of the muon E821 anomalous magnetic moment measurement at BNL," *Phys. Rev.* **D73** (2006) 072003, arXiv:hep-ex/0602035.

[189] F. Jegerlehner and A. Nyffeler, "The Muon $g-2$," *Phys. Rept.* **477** (2009) 1–110, arXiv:0902.3360 [hep-ph].

[190] M. Davier *et al.*, "The Discrepancy Between τ and e^+e^- Spectral Functions Revisited and the Consequences for the Muon Magnetic Anomaly," arXiv:0906.5443 [hep-ph].

[191] M. Passera, W. J. Marciano, and A. Sirlin, "The Muon $g-2$ and the bounds on the Higgs boson mass," *Phys. Rev.* **D78** (2008) 013009, arXiv:0804.1142 [hep-ph].

[192] T. Moroi, "The Muon Anomalous Magnetic Dipole Moment in the Minimal Supersymmetric Standard Model," *Phys. Rev.* **D53** (1996) 6565–6575, arXiv:hep-ph/9512396.

[193] **LHCb** Collaboration, J. Blouw, "Time-dependent CP asymmetries in B_s decays at LHCb," `arXiv:0710.5124 [hep-ex]`.

[194] M. Bona *et al.*, "SuperB: A High-Luminosity Asymmetric e^+e^- Super Flavor Factory. Conceptual Design Report," `arXiv:0709.0451 [hep-ex]`.

[195] T. Hurth, E. Lunghi, and W. Porod, "Untagged $B \to X_{s+d}\gamma$ CP asymmetry as a probe for new physics," *Nucl. Phys.* **B704** (2005) 56–74, `arXiv:hep-ph/0312260`.

[196] M. Pospelov and A. Ritz, "Electric dipole moments as probes of new physics," *Annals Phys.* **318** (2005) 119–169, `arXiv:hep-ph/0504231`. And references therein.

[197] B. C. Regan, E. D. Commins, C. J. Schmidt, and D. DeMille, "New limit on the electron electric dipole moment," *Phys. Rev. Lett.* **88** (2002) 071805.

[198] C. A. Baker *et al.*, "An improved experimental limit on the electric dipole moment of the neutron," *Phys. Rev. Lett.* **97** (2006) 131801, `arXiv:hep-ex/0602020`.

[199] M. P. Altarelli, "LHCb status and early physics prospects," `arXiv:0907.0926 [hep-ph]`.

[200] M. Misiak *et al.*, "The first estimate of $B(\bar{B} \to X_s\gamma)$ at $O(\alpha_s^2)$," *Phys. Rev. Lett.* **98** (2007) 022002, `arXiv:hep-ph/0609232`.

[201] T. Huber, E. Lunghi, M. Misiak, and D. Wyler, "Electromagnetic logarithms in $\bar{B} \to X_s\ell^+\ell^-$," *Nucl. Phys.* **B740** (2006) 105–137, `arXiv:hep-ph/0512066`.

[202] **BABAR** Collaboration, B. Aubert *et al.*, "Measurement of the $B \to X_s\ell^+\ell^-$ branching fraction with a sum over exclusive modes," *Phys. Rev. Lett.* **93** (2004) 081802, `arXiv:hep-ex/0404006`.

[203] **Belle** Collaboration, M. Iwasaki *et al.*, "Improved measurement of the electroweak penguin process $B \to X_s\ell^+\ell^-$," *Phys. Rev.* **D72** (2005) 092005, `arXiv:hep-ex/0503044`.

[204] A. Maki, "Status of the MEG experiment," *AIP Conf. Proc.* **981** (2008) 363–365.

[205] J. Hisano, M. Nagai, P. Paradisi, and Y. Shimizu, "Waiting for $\mu \to e\gamma$ from the MEG experiment," `arXiv:0904.2080 [hep-ph]`.

[206] L. Calibbi, J. Jones-Perez, and O. Vives, "Electric dipole moments from flavoured CP violation in SUSY," *Phys. Rev.* **D78** (2008) 075007, `arXiv:0804.4620 [hep-ph]`.

[207] J. R. Ellis, J. S. Lee, and A. Pilaftsis, "Electric Dipole Moments in the MSSM Reloaded," *JHEP* **10** (2008) 049, `arXiv:0808.1819 [hep-ph]`.

[208] J. R. Ellis, J. Hisano, M. Raidal, and Y. Shimizu, "Lepton electric dipole moments in non-degenerate supersymmetric seesaw models," *Phys. Lett.* **B528** (2002) 86–96, `arXiv:hep-ph/0111324`.

[209] I. Masina, "Lepton electric dipole moments from heavy states Yukawa couplings," *Nucl. Phys.* **B671** (2003) 432–458, `arXiv:hep-ph/0304299`.

[210] Y. Farzan and M. E. Peskin, "The contribution from neutrino Yukawa couplings to lepton electric dipole moments," *Phys. Rev.* **D70** (2004) 095001, `arXiv:hep-ph/0405214`.

[211] H.-C. Cheng, J. L. Feng, and N. Polonsky, "Super-oblique corrections and non-decoupling of supersymmetry breaking," *Phys. Rev.* **D56** (1997) 6875–6884, `arXiv:hep-ph/9706438`.

[212] J. L. Feng, C. G. Lester, Y. Nir, and Y. Shadmi, "The Standard Model and Supersymmetric Flavor Puzzles at the Large Hadron Collider," *Phys. Rev.* **D77** (2008) 076002, `arXiv:0712.0674 [hep-ph]`.

[213] G. Hiller, Y. Hochberg, and Y. Nir, "Flavor Changing Processes in Supersymmetric Models with Hybrid Gauge- and Gravity-Mediation," *JHEP* **03** (2009) 115, `arXiv:0812.0511 [hep-ph]`.

[214] A. L. Kagan, G. Perez, T. Volansky, and J. Zupan, "General Minimal Flavor Violation," `arXiv:0903.1794 [hep-ph]`.

[215] T. Feldmann, M. Jung, and T. Mannel, "Sequential Flavour Symmetry Breaking," `arXiv:0906.1523 [hep-ph]`.

[216] C. D. Froggatt and H. B. Nielsen, "Hierarchy of Quark Masses, Cabibbo Angles and CP Violation," *Nucl. Phys.* **B147** (1979) 277.

[217] P. Paradisi, M. Ratz, R. Schieren, and C. Simonetto, "Running minimal flavor violation," *Phys. Lett.* **B668** (2008) 202–209, `arXiv:0805.3989 [hep-ph]`.

[218] S. P. Martin and M. T. Vaughn, "Two loop renormalization group equations for soft supersymmetry breaking couplings," *Phys. Rev.* **D50** (1994) 2282, `arXiv:hep-ph/9311340`.

[219] J. A. Casas, A. Lleyda, and C. Munoz, "Strong constraints on the parameter space of the MSSM from charge and color breaking minima," *Nucl. Phys.* **B471** (1996) 3–58, `arXiv:hep-ph/9507294`.

[220] M. Ciuchini *et al.*, "D - $\bar{D}$ mixing and new physics: General considerations and constraints on the MSSM," *Phys. Lett.* **B655** (2007) 162–166, `arXiv:hep-ph/0703204`.

[221] M. Dine, A. Kagan, and S. Samuel, "Naturalness in Supersymmetry, or raising the Supersymmetry breaking scale," *Phys. Lett.* **B243** (1990) 250–256.

[222] A. Brignole, L. E. Ibanez, and C. Munoz, "Towards a theory of soft terms for the supersymmetric Standard Model," *Nucl. Phys.* **B422** (1994) 125–171, `arXiv:hep-ph/9308271`.

[223] Y. Nir, "Lessons from BaBar and Belle measurements of $D - \bar{D}$ mixing parameters," *JHEP* **05** (2007) 102, `arXiv:hep-ph/0703235`.

[224] A. J. Buras, "Relations between $\Delta M_{s,d}$ and $B_{s,d} \to \mu\bar{\mu}$ in models with minimal flavor violation," *Phys. Lett.* **B566** (2003) 115–119, `arXiv:hep-ph/0303060`.

[225] K. Agashe, A. Azatov, and L. Zhu, "Flavor Violation Tests of Warped/Composite SM in the Two- Site Approach," *Phys. Rev.* **D79** (2009) 056006, `arXiv:0810.1016 [hep-ph]`.

[226] K. Agashe, A. E. Blechman, and F. Petriello, "Probing the Randall-Sundrum geometric origin of flavor with lepton flavor violation," *Phys. Rev.* **D74** (2006) 053011, `arXiv:hep-ph/0606021`.

[227] S. Davidson, G. Isidori, and S. Uhlig, "Solving the flavour problem with hierarchical fermion wave functions," *Phys. Lett.* **B663** (2008) 73–79, `arXiv:0711.3376 [hep-ph]`.

[228] K. Agashe, "Relaxing Constraints from Lepton Flavor Violation in 5D Flavorful Theories," `arXiv:0902.2400 [hep-ph]`.

[229] K. Agashe, G. Perez, and A. Soni, "Flavor structure of warped extra dimension models," *Phys. Rev.* **D71** (2005) 016002, `arXiv:hep-ph/0408134`.

[230] E. O. Iltan, "The effects of lepton KK modes on the lepton electric dipole moments in the Randall Sundrum scenario," *Eur. Phys. J.* **C54** (2008) 583–590, `arXiv:0708.3765 [hep-ph]`.

[231] O. Gedalia, G. Isidori, and G. Perez, "Combining Direct & Indirect Kaon CP Violation to Constrain the Warped KK Scale," `arXiv:0905.3264 [hep-ph]`.

[232] B. Allanach *et al.*, "SUSY Les Houches Accord 2," *Comp. Phys. Commun.* **180** (2009) 8–25, `arXiv:0801.0045 [hep-ph]`.